



HAL
open science

Interference management in sectored cellular networks with local multi-cell processing

Samet Gelincik

► **To cite this version:**

Samet Gelincik. Interference management in sectored cellular networks with local multi-cell processing. Networking and Internet Architecture [cs.NI]. Institut Polytechnique de Paris, 2019. English. NNT : 2019IPPAT010 . tel-02907058

HAL Id: tel-02907058

<https://theses.hal.science/tel-02907058>

Submitted on 27 Jul 2020

HAL is a multi-disciplinary open access archive for the deposit and dissemination of scientific research documents, whether they are published or not. The documents may come from teaching and research institutions in France or abroad, or from public or private research centers.

L'archive ouverte pluridisciplinaire **HAL**, est destinée au dépôt et à la diffusion de documents scientifiques de niveau recherche, publiés ou non, émanant des établissements d'enseignement et de recherche français ou étrangers, des laboratoires publics ou privés.



INSTITUT
POLYTECHNIQUE
DE PARIS

NNT : 2019IPPAT010

Thèse de doctorat



Interference Management in Sectored Cellular Networks with Local Multi-Cell Processing

Thèse de doctorat de l'Institut Polytechnique de Paris
préparée à Télécom Paris

École doctorale n°626 de l'Institut Polytechnique de Paris (ED IP Paris)
Spécialité de doctorat : Information and Communications

Thèse présentée et soutenue à Palaiseau, le 17.12.2019, par

SAMET GELINCIK

Composition du Jury :

M. Alain Sibille Professor, Telecom Paris, France	Président
M. Sheng Yang Professor, Centrale Supélec, France	Rapporteur
M. Abdellatif Zaidi, Professor, University of Paris-Est, France	Rapporteur
M. Emre Aktas Professor, Hacettepe University, Turkey	Examineur
M. Dirck Slock Professor, EUROCOM, France	Examineur
Mme, Ghaya Rekaya-Ben Othman Professor, Télécom Paris, France	Directeur de thèse
M. Ligong Wang Chargé de Recherche, ENSEA ETIS, France	Co-directeur de thèse

Contents

List of Acronyms	v
List of Symbols	vii
Notations	ix
1 Introduction	1
1.1 Literature Overview	1
1.2 Preliminaries	4
1.3 Overview of the Thesis	9
2 Benefits of Local MCP in Cooperative Sectored Cellular Networks	13
2.1 Introduction	13
2.2 Problem Definition	14
2.3 Uplink Scheme with Cooperative BSs	16
2.4 Upper Bound for the Communication Model	25
2.5 DoF without Sectorization	33
2.6 Finite SNR Analysis	36
2.7 Summary	42
3 Benefits of Local MCP in Multi-Cloud Based Sectored Cellular Networks	43
3.1 Introduction	43
3.2 Problem Definition	44
3.3 Main Results	47
3.4 Uplink Scheme with Parallelogram Clustering	49
3.5 Uplink Scheme with Hexagon Clustering	54
3.6 DoF Without Sectorization	58
3.7 Numerical Results and Discussion	59
3.8 Finite SNR Analysis	64
3.9 Summary	69

4 Local MCP with Lattice Codes in Multi-Cloud Based Sectored Cellular Networks	71
4.1 Introduction	71
4.2 Problem Definition	72
4.3 CoF for Decomposed Network	74
4.4 QCoF for Decomposed Network	77
4.5 Simulation Results	78
4.6 Summary	84
5 Conclusion	85
Appendices	89
A	91
A.1 Proof of Remark 3.1	91
A.2 Proof of Theorem 3.2	97
A.3 Proof of Corollary 3.1	97
A.4 Proof of Theorem 3.3	98
B	101
B.1 Preliminaries for Lattices	101
B.2 Basic Compute and Forward (CoF) in Real Valued Channels	103
B.3 Basic Quantized Compute and Forward (QCoF) in Real Valued Channels	106
C	111
C.1 Appendix for Chapter 4	111
Bibliography	113

List of Acronyms

3GPP	3rd Generation Partnership Project
4G	4th Generation wireless systems
5G	5th Generation wireless systems
AWGN	Additive White Gaussian Noise
BBUP	Base Band Unit Pool
BS	Base Station
CB	Coordinated Beamforming
CoF	Compute and Forward
CoMP	Coordinated Multi-Point
CRAN	Cloud Radio Access Network
DoF	Degrees of Freedom
IA	Interference Alignment
LMMSE	Linear Minimum Mean Square Error
LTE	Long Term Evolution
MAC	Multiple Access Channel
MCP	Multi-Cell Processing
M-CRAN	Multi Cloud Radio Access Networks
MIMO	Multiple Input Multiple Output
QCoF	Quantized Compute and Forward
Rx	Receiver
SIC	Successive Interference Cancellation
SNR	Signal-to-Noise Ratio
TDMA	Time Division Multiple Access
Tx	Transmitter

List of Symbols

Notation	Definition
W	User message
R	Message rate
n	Number of channel uses to send a message
n'	Time-slot index
P	Transmit power
κ	Number of cooperation rounds
μ_B	Backhaul capacity prelog
μ_F	Fronthaul capacity prelog
μ_{BBU}	BBUP Processing capacity prelog
r	BBUP-BS ratio

Notations

Sets

\mathbb{R}	The set of real numbers
\mathbb{Z}	The set of integers
\mathbb{Z}^+	The set of nonnegative integers
\mathbb{F}_p	Finite field with p elements
$\mathcal{A}, \mathcal{B}, \mathcal{C}, \dots$	Index sets
$\mathbb{A}, \mathbb{B}, \mathbb{C}, \dots$	Sets other than index sets
$ \mathcal{A} , \mathbb{A} $	Cardinality of the set
$\mathcal{A}^m, \mathbb{A}^m$	m times Cartesian product of the sets
$\{x_j\}_{j \in \mathcal{A}}$	Elements of a set \mathbb{X} indexed with $j \in \mathcal{A}$: $\{x_j : j \in \mathcal{A}, x_j \in \mathbb{X}\}$
$\mathcal{A} \setminus \mathcal{B}, \mathbb{A} \setminus \mathbb{B}$	Set difference operation

Vectors and Matrices

$\mathbf{a}, \mathbf{b}, \mathbf{c}, \dots$	Constant vectors
$\mathbf{A}, \mathbf{B}, \mathbf{C}, \dots$	Matrices
\mathbf{A}^T	Transpose of \mathbf{A}
\mathbf{I}_L	$L \times L$ identity matrix
$\ \mathbf{a}\ $	ℓ^2 -norm of \mathbf{a}
$ \mathbf{A} $	Determinant of \mathbf{A}

Random Variables and Events

pdf	Probability density function
i.i.d.	Independent and identically distributed
A, B, C, \dots	Random variables
a	Realization of random variable A or a constant
$\mathbf{A}, \mathbf{B}, \mathbf{C}, \dots$	Random vectors
\mathbf{a}	Realization of random vector \mathbf{A} or a constant vector
$\ \mathbf{A}\ $	ℓ^2 -norm of \mathbf{A}
$\mathbf{A}^{(n)}$	Time sequence of random vectors, $\mathbf{A}_1, \dots, \mathbf{A}_n$
$\Pr[\mathcal{E}]$	Probability of event \mathcal{E}
$E[\mathbf{A}]$	Expectation
$H(A)$	Entropy of the discrete random variable A
$H(A B)$	Conditional entropy of the discrete random variable A given B
$h(A)$	Entropy of continuous random variable A
$I(A; B)$	Mutual information between A and B

Lattices

Λ, Λ_0	Lattices in \mathbb{R}^n
$Q_\Lambda(\mathbf{x})$	Lattice quantizer: maps the point \mathbf{x} to the closest (in Euclidean distance) lattice point (in Λ)
$[\mathbf{x}] \bmod \Lambda$	Modulo operation or quantization error: $\mathbf{x} - Q_\Lambda(\mathbf{x})$
$\mathcal{V}_\Lambda, \mathcal{V}(\Lambda)$	Fundamental Voronoi region of Λ
$\text{Vol}(\mathcal{V}_\Lambda), \text{Vol}(\mathcal{V}(\Lambda))$	Volume of the Fundamental Voronoi region of Λ

General

$\log(\cdot)$	Logarithm in base 2
$f(x) = o(g(x))$	Little- o Landau symbol: $\lim_{x \rightarrow \infty} \frac{f(x)}{g(x)} = 0$

Chapter 1

Introduction

The data rate requirement in wireless communication due to employment of smartphones, laptops, tablets and sensors is increasing drastically. This directly poses extra-ordinary demands on precious spectral resources. To satisfy with the expected saturation on the currently used bands, modern communication systems are allowing very aggressive spatial frequency reuse and moving towards heterogenous networks of base stations (BS) covering smaller areas (small cells [3]). Evidently, such system suffer from the detrimental inter-cell interference conditions, particularly at cell edges. Therefore, it is clearly convincing that interference management is a bottleneck for current and future wireless networks [25].

1.1 Literature Overview

There are two essential ways to deal with the inter-cell interference: coordination of BSs that leads to **mitigation** of interference and cooperation of BSs leads to **exploitation** of interference [25]. BS coordination techniques require channel state information (CSI) exchange, and, hence the transmission strategies can be jointly adapted to global CSI of the network. The transmission strategies includes power control, resource allocation, coordinated beamforming (CB) and interference alignment (IA). The power control and resource allocation are mostly considered together. The increase in the total spectral efficiency of the network comes from optimizing power levels and allocated resources jointly or individually across transmitters (Tx) to lower the interference level [68, 70, 78, 80]. The CB technique can be implemented when Tx's have multiple antennas so that spatial channels of mobile users can be separated through jointly optimizing all the beamforming vectors across Tx's. If the receivers (Rx) have a single antenna, the coordination between Tx's can be performed based on mostly local CSI at Tx: this idea has been explored in [9, 81, 8, 79].

In contrast, with the adoption of multiple antennas at the Rx's, the channel between Tx and Rx becomes a multi-input multi-output (MIMO) structure: the transmission paradigm in either uplink or downlink changes completely since it become possible to align the interference in a predefined subspace at the Rx, so that it can cancel the interference. This

scheme called interference alignment (IA) [13, 40, 77] and has led to a large number of novel algorithms ([26, 50] among others) and analysis ([77, 53] among others). Information theoretical findings [13, 42, 48] have shown that coding schemes based on IA provides half of the available spectrum to each user of the network and yields significant gains regarding orthogonal access schemes, e.g., frequency-division-multiple-access (FDMA) and time-division-multiple-access (TDMA), and conventional interference management techniques such as resource allocation and CB. Nevertheless, realizing the gain promised by IA is almost impossible in practice since the IA coding schemes rely on asymptotic number of symbol expansions [13, 66] or infinite layer lattice alignment [42].

Cooperation between communication devices (BSs or mobiles) has first been considered in [73], and subsequently in many other works such as [60, 61, 33, 12, 72, 6, 11, 63, 71, 65, 58]. In the context of cellular systems, in addition to exchanging CSI, cooperation has mostly been used to create alternate communication paths (by having mobile users or dedicated terminals relay the transmit signals of adjacent mobiles, see e.g., [10, 30, 34, 15]), or to provide BSs with quantized versions of the transmit/receive signals of other BSs via backhaul links (allowing for clustered decoding, see e.g., [37, 31, 29, 63, 65, 58, 27, 76, 62, 55, 57, 56]). It is then possible for user data to be jointly processed by several BSs at both uplink and downlink, hence imitating the benefits of virtual MIMO. This framework is known as multi-cell processing (MCP) [25]. The study of MCP was started for an uplink with the works [27, 76] and for a downlink with the work [62]. The analysis in these works is based on the **full** cooperation assumption: in uplink, the received signal at the BSs are relayed to a central processor (CP) via perfect backhaul links (assumed to be of infinite capacity and error free) then the CP decodes all user messages jointly. In contrast, in downlink, the CP encodes all messages jointly and sends each transmit signal to its corresponding BS via backhaul links and each mobile user decodes the message itself. With such a full MCP through unlimited backhaul, there is no signal causing complete interference, that is, all received or transmitted signals provide useful information in decoding at the CP or mobile users. Then, interference becomes **constructive** rather than destructive. Thus, it is **exploited**.

The full MCP in uplink with limited backhaul capacity was studied in [55, 57, 56]. In these works, BSs share functions of their received signals with compress-and-forward (CF) [18, Theorem 6], where each BS first quantizes its received signal then sends the quantization codewords to the CP. Then, the CP either decodes the quantization codewords and user messages jointly, or decompress quantization codewords first and following decodes the user messages. The downlink full MCP with limited backhaul was studied in [64], where the transmit signals of BSs obtained by joint Dirty Paper Coding (DPC) [17] under individual power constraint for each BS, in which the interference is precoded in the transmitted signals, and, hence, each mobile user decodes its message itself by cancelling it.

A totally different class of coding strategies of called **compute-and-forward (CoF)**

[46] is also an attractive candidate for implementing MCP in uplink, due to its good complexity-performance tradeoff [23]. In standard CoF [46], each BS is expected to compute a linear function of lattice codewords with integer coefficients and the linear equations are sent to the CP by the BSs through backhaul links. Then the CP can decode the user messages if the integer coefficient vectors are **linearly independent**. In [47], CoF scheme implementation of full MCP for symmetric Wyner model with equal backhaul capacity for each BS outperforms conventional decode-and-forward [18, Theorem 1] and CF schemes under certain signal-to-interference-noise-ratio (SINR) regimes. In [28], under equal backhaul capacity for each BS, it is shown that CoF provides competitive performance compared to CF scheme for a general cellular network with several fold larger receivers than number of users (each Tx and Rx has single antenna). It is also shown that the CoF suffers from rank deficiency when number of receivers is equal to number of mobile users. In their recent work [5], Aguerri and Zaidi have proposed two schemes that are variants of CoF, named Quantized CoF (QCoF) and Jointly Quantized CoF (JQCoF). Both schemes employ lattice code based Wyner-Ziv (WZ) source coding [74] for compression at relays and successive interference cancellation (SIC) with lattice decoding at Rx side, which relaxes the necessity of linearly independent vectors required in standard CoF implementation.

The implementation of full MCP is quite challenging in practice due to the large computational complexity and excessive delays needed for moderately large networks. However, dividing the network into several clusters and letting them to cooperate within each cluster rather than the entire network also brings some benefit of MCP by requiring only local received signals and local CSI. We name this framework as **local** MCP, which also improves the robustness of the network to connection failures and scalability. Therefore, in large networks, local MCP avoids the disadvantages of the full MCP in exchange for achievable rates. In [37], the local MCP is proposed only for adjacent BS's for both one and two dimensional Wyner model [76]. In the latter, each BS decodes messages of its users from receive signals of adjacent cells as well as its own. It is shown that in the high signal-to-noise-ratio (SNR) gain of the two dimensional Wyner network is higher than single dimensional one due to the gain of having more receive signals for joint decoding. In [11], it is shown for one dimensional Wyner array that the spectral efficiency of cooperation in clustered BS's approaches to the spectral efficiency of full MCP even for quite moderate cluster sizes. The results also show that the gain obtained for the same cluster sizes increases with the power of inter-cell interference, which essentially increases the receive diversity and total power collected from the cluster. These two studies assume infinite backhaul links between BS's, on which, however, the benefit of cooperation tightly depends. In [63], for one dimensional **asymmetric** Wyner model, the cooperation between adjacent cells is carried out through finite capacity backhaul links. The results show that when the BSs have codebook information of interfering mobile users with its corresponding one, the high-SNR gain increases with cluster size if the backhaul capacity scales with $\log P$. Reference [71] studies the effect of transmitter and receiver cooperation in one dimensional asymmetric Wyner model

where both cooperation are limited in rate scaling with $\log P$, and number of cooperation rounds. In the coding scheme, the writers silence some of the mobile users regarding the total number of transmitter and cooperation rounds so that the network is decomposed into non-interfering clusters. Then, they perform successive interference cancellation in receiver cooperation and DPC in transmitter cooperation. The results show that increasing transmitter or receiver cooperation rates and rounds increases the high SNR gain.

Finally, we discuss briefly the **cloud-radio-access-networks (CRAN)**, that is an architecture considered for future 5G networks [4] to handle the massive increase in data traffic and the high density of users and BS. For a single-CRAN (having a single CP), the BS acts only as a relay. Moreover, the encoding/decoding functionalities are performed by a base-band-unit-pool (BBUP), which mimics the effect of a CP. Therefore, it also allows for natural implementation of full MCP. However, due to constraints of latency, connectivity, scalability and synchronization, the deployment of multi cloud-radio-access-networks (M-CRAN) is recently considered in a few works such as [49, 20]. Reference [49] studies the problem of optimization of precoding and joint compression of baseband signals across multiple clusters of BSs in downlink. It is shown that the multivariate compression based solution reduces the inter-cluster interference. The work [20] handles a distributed power minimization problem for downlink, where fronthaul capacity, CSI error, quality of service and BS power are taken into account. The mentioned work propose a distributed iterative solution that achieves the performance of the case all BSs connected to a single BBUP.

1.2 Preliminaries

1.2.1 Sectorized Cellular Network Model

Consider the hexagonal cell in Figure 1.1. As is standard in current 4G communication systems[54], we assume that each cell is divided into three separate regions, which we call sector later on. The BS employs M antennas for each sector, by which it provides directional radiation pattern for each of them. We assume that radiation pattern of side lobes is negligible. This requires that the communication process in different sectors of the same BS does not interfere with each other neither uplink nor downlink. We follow the convention of the current 4G standards [54] that makes use of orthogonal multiple access. Therefore, we consider single mobile user per sector. Each mobile user has the same number of antenna M with the ensemble of sector antennas.

In a large network of sectorized hexagonal cells, due to the shadowing effect and distance-dependent pathloss, which is intrinsic for wireless communication systems [41], and directivity of sector antenna beams, we assume a **local interference model**, where the observed interference by any Rx in a sector (either mobile user or sector antennas) is generated by Tx's located in adjacent sectors (either sector antennas or mobile user). The assumption that we made is reminiscent of well-known Wyner's hexagonal network model

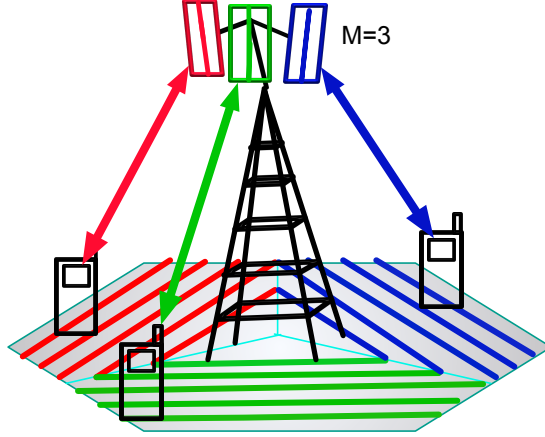


Figure 1.1: A sectored hexagonal cell with single user per sector

[76], where, due to the lack of sectorization, any Rx in a BS observes interference from Txs in six adjacent cells. For interference there is a **symmetric** relation in our model, i.e., if the Tx in sector u creates interference to the Rx in sector v , the Tx in sector v creates interference to the Rx in sector u . A figurative representation of the sectored cellular model is shown in Figure 1.2, where each circle represents a mobile user and sector antenna pair. The explained framework leads to the interference pattern seen in the figure, where each solid line between circles refers to the symmetric interference between Tx-Rx pairs.

Let $\mathcal{N} = \{1, \dots, N\}$ be index set of cells in the network. We denote each BS with the index of cell in which it is located, e.g., BS j denotes the BS in the j^{th} cell. Let $\mathcal{T} = \{1, \dots, 3N\}$ be index set of sectors of the network. We denote each transmitter and receiver with the index of sector in which they are located, e.g., Tx/Rx u denotes the Tx/Rx in u^{th} sector. Throughout this manuscript, we are interested in uplink communications, hence, we refer to **Tx** as mobile user and we refer to **Rx** as sector antennas. Throughout the manuscript, we will use these terms interchangeably. Then, the observed signal at the Rx $u \in \mathcal{T}$ is given by the following discrete-time input-output relation:

$$\mathbf{y}_{u,n'} = \sum_{v \in \mathcal{T}_u} \mathbf{H}_{u,v} \mathbf{x}_{v,n'} + \mathbf{z}_{u,n'}, \quad n' \in \{1, \dots, n\}, \quad (1.1)$$

where

- n denotes the number of total channel uses to send a message;
- \mathcal{T}_u denotes the index set of mobile users whose transmitted signal is observed by receiver u (including mobile user u),

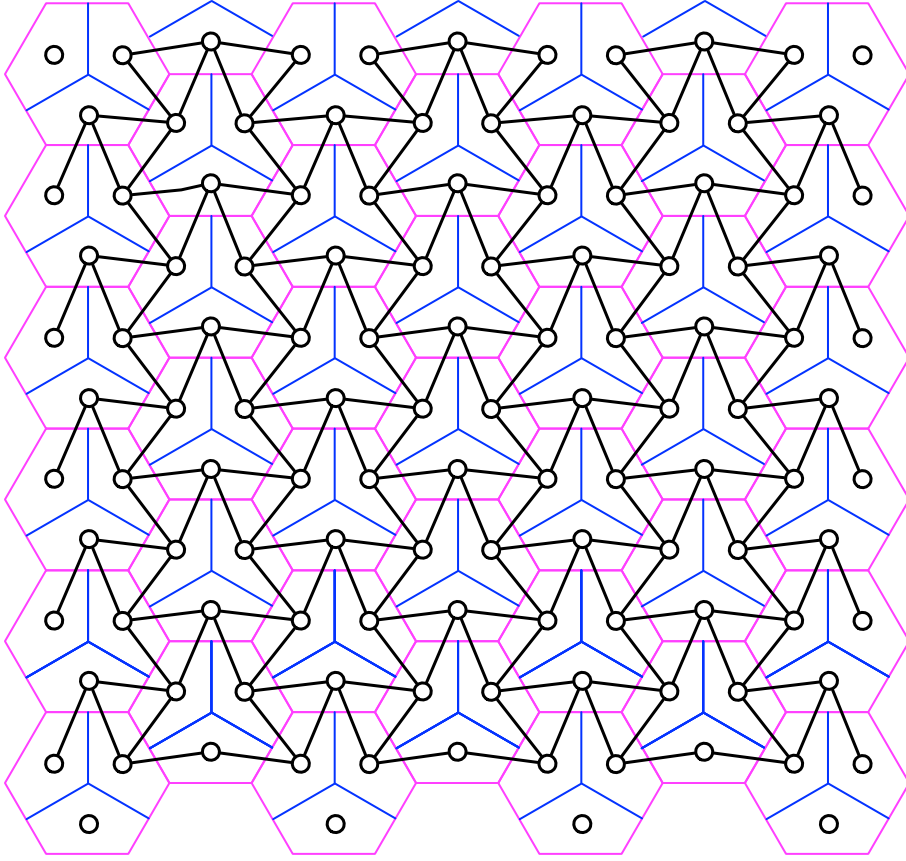


Figure 1.2: Sectored cellular model. Purple hexagonal regions depict the various cells and the blue lines determine their sectorizations. Each circle depicts a mobile-user and sector antenna pair, where both of them are equipped with M antennas.

- $\mathbf{x}_{v,n'}$ denotes the M -dimensional time- n' signal sent by mobile user v , satisfying the average power constraint $\frac{1}{n} \sum_{n'=1}^n \|\mathbf{x}_{v,n'}\|^2 \leq P$;
- $\mathbf{z}_{u,n'}$ denotes the M -dimensional i.i.d. standard Gaussian¹ noise vector corrupting the time- n' signal at Rx u ; it is independent of all other noise vectors;
- and $\mathbf{H}_{u,v}$ denotes an M -by- M dimensional random matrix with entries that are independently drawn according to a standard Gaussian distribution that models the channel from mobile user v to the Rx u .

We assume **quasi-static**² fading channel model, i.e., channel coefficients are randomly drawn but stay constant over the n channel uses employed for the transmission of a message.

¹By [35, Section 19], the standard Gaussian is defined as a zero-mean Gaussian random variable with unit variance.

²The term “quasi-static” is widely used in the communication literature (see, e.g., [24], [69, Section 5.4.1]).

In other words, the transmission duration of a codeword is assumed shorter than the coherence time of the channel.

In our model, beside referring to average transmitter power, P also refers to average receive signal-to-noise ratio (SNR) at a single sector antenna since the channel coefficients and channel noise are with unit variance.

1.2.2 DoF for Cellular Networks

The concept of **degrees-of-freedom** (DoF), which is also known as multiplexing gain, was introduced as a measure of performance gain in **information rate** obtained from employing multiple transmit and receive antennas for point to point communications instead of single transmit and receive antenna in the field of space time coding [24], [67]. Essentially, the DoF is the number of **independent** point-to-point additive white Gaussian noise (AWGN) channel that are created by using multiple transmit and receive antenna at high SNR.

For multiple-input multiple-output (MIMO) channel, under the assumption of quasi-static fading with capacity achieving codes, the conventional DoF definition for real valued channel is given by [38] as:

$$\text{DoF} = \lim_{P \rightarrow \infty} \frac{R(P)}{\frac{1}{2} \cdot \log P}, \quad (1.2)$$

where $R(P)$ is the achievable rate and P is the average SNR per receive antenna. However, for realistic SNR values, the finite SNR DoF, DoF_f , is given by [43] as the ratio of $R(P)$ to the capacity of point-to-point AWGN channel at SNR level P with receiver antenna array gain:

$$\text{DoF}_f = \frac{R(P)}{\frac{1}{2} \cdot \log(1 + MP)}, \quad (1.3)$$

where M is the number of receive antennas.

In the context of cellular communications, which is inherently interference limited network, any kind of metric yielding the number of point-to-point AWGN channel basically provides information about number of interference free channels that can be provided. Hence, for any cellular network model, the per-user DoF indexes the interference management capability at high-SNR

Let $\{\mathcal{C}(P)\}$ be a family of codes corresponding to the proposed network model at each SNR level P . Then, the per-user DoF is given as:

$$\text{DoF} = \lim_{P \rightarrow \infty} \frac{\sum_{u \in \mathcal{T}} R_u(P)}{|\mathcal{T}| \cdot \frac{1}{2} \log P} \quad (1.4)$$

where $R_u(P)$ is the achievable rate for user $u \in \mathcal{T}$.

1.2.3 A Basic CRAN

BS provide mainly two functions: baseband processing and radio functionalities. Baseband processing functions are encoding/decoding, modulation/demodulation, fast Fourier transform and radio resource allocation etc.[14]. Radio functionalities are transmission/reception of signals, power amplification, digital up/down conversion and analog-to-digital/digital-to-analog converter etc. [14]. In traditional architecture, these capabilities are integrated into a BS and that kind of architecture was employed in 1G and 2G. However, starting from 3G, another type of BS architecture has been introduced, in which baseband processing and radio functionalities are partitioned to independent entities called base-band-unit (BBU) and remote-radio-head (RRH), respectively. Hence, in this new architecture, the BS functions as RRH and the BS provides interface to a fiber or microwave [14], and therefore a BS and a BBU can be separated several km's.

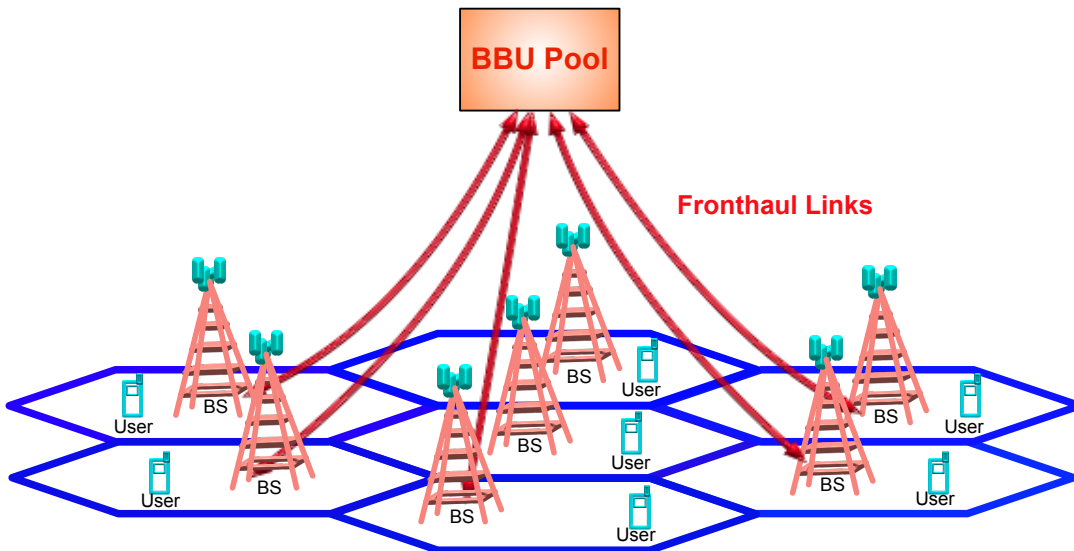


Figure 1.3: Basic CRAN

The **cloud radio access network** (CRAN) is a novel system architecture which was first introduced by [1], see Figure 1.3 for an illustration. In a CRAN, each BS still functions as RRH but baseband processing of BS's are performed at a central place called **BBU pool** (BBUP) or **cloud** that functions as a CP. The communication between a BS and BBUP is carried out by bidirectional communication channel called **fronthaul** link and it can be realized by several technologies such as optical fiber [14, 7], microwave communications [14, 51] and millimeter wave communications [82, 52].

The C-RAN architecture provides a number of benefits to current and future wireless systems: the centralized BBUP yields efficient usage of baseband processing resources, reduces power consumption and cost of BS deployment and operation. It also provides more flexibility in network upgrades and adaptability to non-uniform traffic. Furthermore, advanced LTE features such as **joint processing** coordinated multi point (CoMP) [2],

which is equivalent to **local** MCP, can be implemented.

1.3 Overview of the Thesis

This thesis focuses on investigating the benefits of local MCP in interference management at uplink for sectorized cellular networks under different communications model. The network model of sectorized cellular network is introduced in Section 1.2.1, where each hexagonal cell is divided into 3 sectors and interference at sector antennas is observed from only adjacent users of sectors. The main objective of this thesis is to propose clustering methods and coding schemes that provides high per-user DoF gain and average sum-rates for the communication models under consideration.

In Chapter 2, we investigate the achievable DoF per-user and sum-rate in sectorized cellular networks when BSs can cooperate at most κ cooperation rounds, where κ takes into account the complexity and delay constraint imposed by the system, over backhaul links of capacities $C_B = \mu_B \cdot \frac{1}{2} \log P$, with P denoting the transmit power. Both lower and upper bound are derived. The lower bound is based on practically implementable beamforming and adapts the way BSs cooperate to the sectorization of the cells. It improves over the naive approach that ignores this sectorization. The upper bound is information-theoretic and holds for all possible coding schemes, including ergodic interference alignment whose practical implementation currently seems out of reach. Lower and upper bounds show that both the complexity constraint imposed by limiting the number of interaction rounds κ and the backhaul capacity, indeed limits the largest achievable DoF. In particular, irrespective of the backhaul capacity C_B , the per-user DoF cannot exceed a threshold which depends on κ .

In Chapter 3, we investigate achievable the per-user DoF and sum-rate in multi-cloud based sectorized cellular networks (M-CRAN). The network consists of N BSs and $K \leq N$ BBUPs. In the network, the computing units, i.e., BBUPs, have limited **processing capacity**, $C_{BBU} = \mu_{BBU} \cdot \frac{1}{2} \log P$. The communication between BSs and BBUPs occurs by means of finite-capacity fronthaul links, $C_F = \mu_F \cdot \frac{1}{2} \log P$. We propose two different achievability schemes that are based on dividing network into non-interfering clusters that are called p-clusters and h-clusters, respectively. The BBUP-BS ratio, $r = K/N$, determines minimum number of users/sectors in a cluster. The lower bound on per-user DoF parametrized by processing capacity prelog μ_{BBU} , fronthaul capacity prelog μ_F and the ratio $r = K/N$. The upper bound is obtained through cut-set argument. It is shown that upper bound are attained for several cases. The achievability gap decreases with the BBUP-BS ratio r for $\mu_F \leq 2M$ irrespective of μ_{BBU} . We show that for $\mu_F \leq 2M$ the p-clustering can achieve at least the same performance as h-clustering irrespective of other parameters. However, for $\mu_F > 2M$, h-clustering mostly provides higher DoF gain than p-clustering if C_{BBU} is high enough since it provides higher joint processing gain due to the clustering geometry.

In Chapter 4, we investigate the achievable sum-rate by utilizing lattice codes for uplink in M-CRAN. We decompose the cellular network into interfering but non-overlapping clusters. We employ compute-and-forward (CoF) and quantized-CoF (QCoF) for each cluster by allowing each sector to treat out-of-cluster as noise. CoF may perform poorly due to rank deficiency of the integer coefficient matrix. This is solved using QCoF [5], which shows highly favorable performance in terms of average sum-rate. To reduce implementation complexity of nested lattices, we investigate the effect of employing a lower number of nested lattices than number of users, i.e., some users employ the same lattice code. The sum rate degradation of QCoF due to using fewer nested lattices is not significant especially if the fronthaul capacity is scarce. We show that QCoF with reduced number of nested lattices outperforms CoF even employing the same lattice codebook for all cluster users while CoF employs different codebook for each user of the cluster.

List of Publications

International Conferences

- C1.** : S. Gelincik, M. Wigger and L. Wang, "DoF in Sectorized Cellular Systems with BS Cooperation under a Complexity Constraint", *in proc. of 15th International Symposium on Wireless Communication Systems (ISWCS)*, Lisbon (Portugal), August 2018.
- C2.** : S. Gelincik and G. Rekaya Ben-Othman, "DoF in Sectorized Cellular Systems with C-RAN", *in proc. IEEE Wireless Communications and Networking Conference*, Marrakesh (Morocco), April 2019,
- C3.** : S. Gelincik and G. Rekaya Ben-Othman, "Lattice codes for Sectorized Cellular Networks with C-RAN", *submitted to IEEE Conference on Communications*, July 2020
Dublin, Ireland

Peer Reviewed Journals

- J1.** : S. Gelincik, M. Wigger and L. Wang, "Benefits of Local Cooperation in Sectorized Cellular Networks", *submitted to the IEEE Trans. on Communications*, October 2019.
- J2.** : S. Gelincik and G. Rekaya Ben-Othman, "DoF in Multi-Cloud Based Sectorized Cellular Networks", *to be submitted to EURASIP J. on Wireless Communications and Networking*.

Patent Filings

- P1.** : M. Wigger, S. Gelincik and L. Wang, "Cell Sector Clustering for Joint Decoding of Messages," submitted to European Patent Office, April 13 2018, patent application PCT/EP2018/059535.
-

Chapter 2

Benefits of Local MCP in Cooperative Sectorized Cellular Networks

2.1 Introduction

In this chapter, we are interested in characterizing the largest **degrees-of-freedom** (DoF) per-user and the achievable sum-rate **in uplink** when the local multi-cell processing (MCP) is constrained through limited backhaul capacity, $C_B = \mu_B \cdot \frac{1}{2} \log P$, and the number of cooperation rounds, κ , between base stations (BS). The lower bound on DoF is based on **deactivating** some of the mobile users in a way that the network decomposes into **non-interfering** clusters. Then, backhaul links between BSs is used to collect quantized versions of the received signals of such a cluster at a single BS called **master** BS or **master** cell. Subsequently, the master BS jointly decodes all the clusters' receive signal and then distributes the decoded messages over the backhaul links to their intended BSs. The maximum number of allowed BS cooperation rounds κ limits the size of the clusters since each sector in the cluster needs to be reachable in $\kappa/2$ hops from the given master BS. This ensures that this BS can learn all the receive signals in the cluster and inform all the cluster's BSs about their decoded messages in κ rounds. The decoding in our scheme is thus reminiscent of **clustered decoding** as performed in [31, 29]. The main contribution of our scheme is the specific way we build the clusters. We find a way to decompose the network into separate clusters by only deactivating the users in single sectors of the cells between two clusters. However, in the naive approach, all users of the borders cells between adjacent clusters are deactivated.

The lower bound is given in function of backhaul capacity prelog μ_B and maximum cooperation rounds κ . It shows that DoF $M/2$ is achievable in the sectorized hexagonal cellular network without interference alignment and with only two BS cooperation rounds and a backhaul prelog of $M/6$. However, the naive approach would need $M/3$ backhaul

prelog to achieve $M/2$ DoF in the transmission from the mobile users to the BSs. Generally, the new lower bound improves over this naive approach in all parameter regimes.

The upper bound presented in this chapter is information-theoretic and allows for any coding scheme. The bound shows that for small backhaul capacities, the DoF of the proposed scheme is close to optimal and that irrespective of the capacities of the backhaul links, for finite κ , the DoF is bounded away from M when the number of cells $N \rightarrow \infty$.

The finite signal-to-noise ratio (SNR) analysis show that, in sum rate performance, the proposed scheme outperforms the scheme with no deactivated users, where the network is divided into non-overlapping but interfering clusters regarding parameter κ , except at low-SNR if the backhaul capacity is high enough. For practical considerations, it is also deduced that the small delay parameters achieves higher sum-rate than larger ones if the backhaul capacity is not high enough to communicate the data generated in larger clusters.

In Section 2.2, we present the communication model. In Section 2.3, we present the achievability scheme. Section 2.4 is devoted to the converse proof. In Section 2.5, we present achievability results for non-sectored cooperative cellular systems. In Section 2.6, we proceed the finite SNR analysis for the presented scheme and present numerical evaluations. Summary is given in Section 2.7.

2.2 Problem Definition

2.2.1 Communication Model with Backhaul Cooperation

Consider the uplink communication over the cellular network described in Section 1.2.1 where each mobile user $u \in \mathcal{T}$ wishes to send an independent message W_u , that is uniformly distributed over $\{1, \dots, \lfloor 2^{nR_u} \rfloor\}$, to the single BS in its cell. Communication takes place in two phases. In a first phase, each mobile user u applies an encoding function

$$f_u^{(n)}: \{1, \dots, \lfloor 2^{nR_u} \rfloor\} \rightarrow \mathbb{R}^{M \times n}, \quad (2.1)$$

to its message W_u and sends the n resulting vectors $\mathbf{X}_u^{(n)} := (\mathbf{X}_{u,1}, \dots, \mathbf{X}_{u,n})$ as its inputs over the network. Each encoding function $f_u^{(n)}$ has to be chosen so that the input vectors satisfy an average input power constraint P :

$$\frac{1}{n} \sum_{n'=1}^n \|\mathbf{X}_{u,n'}\|^2 \leq P \quad \text{with probability 1.} \quad (2.2)$$

The subsequent second communication phase starts after each BS $j \in \{1, \dots, N\}$ has observed all outputs at the antennas in each of the three sectors of the cell. The second phase takes place over the backhaul links connecting adjacent BSs. It is assumed to be noise-free but rate-limited and can be interactive. However, to limit complexity and latency of the backhaul communications, we constrain the interaction with **maximum** κ rounds, for a positive integer κ .

For each $j \in \mathcal{N}$, let $\mathbf{Y}_j^{(3n)}$ denote all the wireless signals observed at the $3M$ antennas of BS j :

$$\mathbf{Y}_j^{(3n)} := (\mathbf{Y}_{u_{j,1}}^{(n)}, \mathbf{Y}_{u_{j,2}}^{(n)}, \mathbf{Y}_{u_{j,3}}^{(n)}), \quad (2.3)$$

where $u_{j,1}$, $u_{j,2}$ and $u_{j,3}$ denote the three sectors in BS j . In the k^{th} cooperation round, $k \in \{1, \dots, \kappa\}$, each BS j calculates the message $V_{j \rightarrow i}^k$ that it sends to a neighboring BS i as:

$$V_{j \rightarrow i}^k = \psi_{j \rightarrow i}^{k,(n)}(\mathbf{Y}_j, \mathbf{V}_{\text{to } j}^{k-1}), \quad (2.4)$$

for some cooperation functions $\{\psi_{j \rightarrow i}^{k,(n)}\}$ on appropriate domains. Here, $\mathbf{V}_{\text{to } j}^{k-1}$ denotes the $6 \cdot (k-1)$ cooperation messages BS j has received from its 6 neighboring BSs during the first $k-1$ cooperation rounds:

$$\mathbf{V}_{\text{to } j}^{k-1} := \{V_{i \rightarrow j}^{k'} : \text{BS } i \text{ adjacent to BS } j \text{ and } k' = 1, \dots, k-1\}. \quad (2.5)$$

The cooperation functions have to be chosen so that for each pair of neighbouring BSs $i, j \in \mathcal{N}^2$ the total information a BS j sends over the backhaul link to BS i does not exceed the total information transmission allowed by the backhaul links

$$\sum_{k=1}^{\kappa} H(V_{j \rightarrow i}^k) \leq n \cdot C_B, \quad (2.6)$$

where

$$C_B = \mu_B \cdot \frac{1}{2} \log P \quad (2.7)$$

and μ_B is **backhaul capacity prelog**, which is a nonnegative constant.

Once the BS-cooperation phase is terminated, each BS $j \in \mathcal{N}$ proceeds to decode the three messages sent by the mobiles in the three sectors of its cell. To this end, for each sector u in its cell, it applies a decoding function h_u on the corresponding domains to produce the message estimates

$$\hat{W}_u := h_u^{(n)}(\mathbf{Y}_j^{(3n)}, \mathbf{V}_{\text{to } j}^{\kappa}). \quad (2.8)$$

An error occurs in the communication unless, for every sector $u \in \mathcal{T}$:

$$\hat{W}_u = W_u. \quad (2.9)$$

2.2.2 Capacity and Degrees of Freedom

A rate-tuple $\{R_u\}_{u \in \mathcal{T}}$ is said **achievable**, if for every $\epsilon > 0$ and sufficiently large block-lengths n , there exist encoding, cooperation, and decoding functions $\{f_u^{(n)}\}$, $\{\psi_{j,i}^{k,(n)}\}$, and $\{h_u^{(n)}\}$, such that

$$Pr \left[\bigcup_{u \in \mathcal{T}} \{\hat{W}_u \neq W_u\} \right] \leq \epsilon. \quad (2.10)$$

The **capacity region** $\mathcal{C}(P, \mu_B, \kappa)$ is defined as the closure of the set of all achievable rate-tuples, and the **sum-capacity** $C_\Sigma(P, \mu_B, \kappa)$ is given as

$$C_\Sigma(P, \mu_B, \kappa) := \sup_{\{R_u\}_{u \in \mathcal{T}} \in \mathcal{C}(P, \mu_B, \kappa)} \sum_{u \in \mathcal{T}} R_u. \quad (2.11)$$

In the high SNR regime, the quantity of interest is the **DoF**.

Definition 2.1 (Per-user DoF). *For any given $\mu_B \geq 0$ and $\kappa > 0$, the DoF is given as*

$$\text{DoF}(\mu_B, \kappa) := \lim_{N \rightarrow \infty} \lim_{P \rightarrow \infty} \frac{C_\Sigma(P, \mu_B, \kappa)}{|\mathcal{T}| \cdot \frac{1}{2} \log P}. \quad (2.12)$$

2.3 Uplink Scheme with Cooperative BSs

The main contribution of this chapter is a new uplink communication scheme with BS cooperation. In this scheme, some of the mobile users are deactivated, i.e., transmit no messages, and the other mobile users use multi-antenna Gaussian codebooks to send their own messages. However, to attain fairness among users, different versions with different sets of deactivated mobile users can be time-shared. As we will see, the deactivation process divides the network into isolated hexagonal-like clusters, for short called **h-clusters**. Receiving BSs quantize their output signals and send the resulting quantization messages to specific BSs, which we refer as **master** BSs or **master** cells the h-cluster under consideration. Then, each master BS jointly decodes the subset of messages corresponding to the quantized output signals it received. After this decoding step, the master BSs send back the decoded messages to the BSs to which the messages are actually intended.

The details of the h-clustering scheme are as described in the following, where the positive integer t denotes the single parameter of the scheme. To this end, we choose the master cells so that they build a regular grid of equilateral triangles where the three master cells forming each of the triangles are lying $2t$ cell-hops apart from each other. The distance between two cells here is defined as the minimum number of cell-hops needed to get from one cell to the other.

As we will see, the proposed scheme takes place over $2t$ cooperation rounds, and thus one is allowed to choose any

$$t \in \left\{ 1, \dots, \left\lfloor \frac{\kappa}{2} \right\rfloor \right\}. \quad (2.13)$$

For simplicity, we first present the scheme in the special case $t = 2$. The general case is treated later.

2.3.1 Special case $t = 2$

Consider the network in Figure 2.1, where the magenta cells indicate the master cells. We refer to cells that are adjacent to master cells as layer-“1” cells, and the cells that are

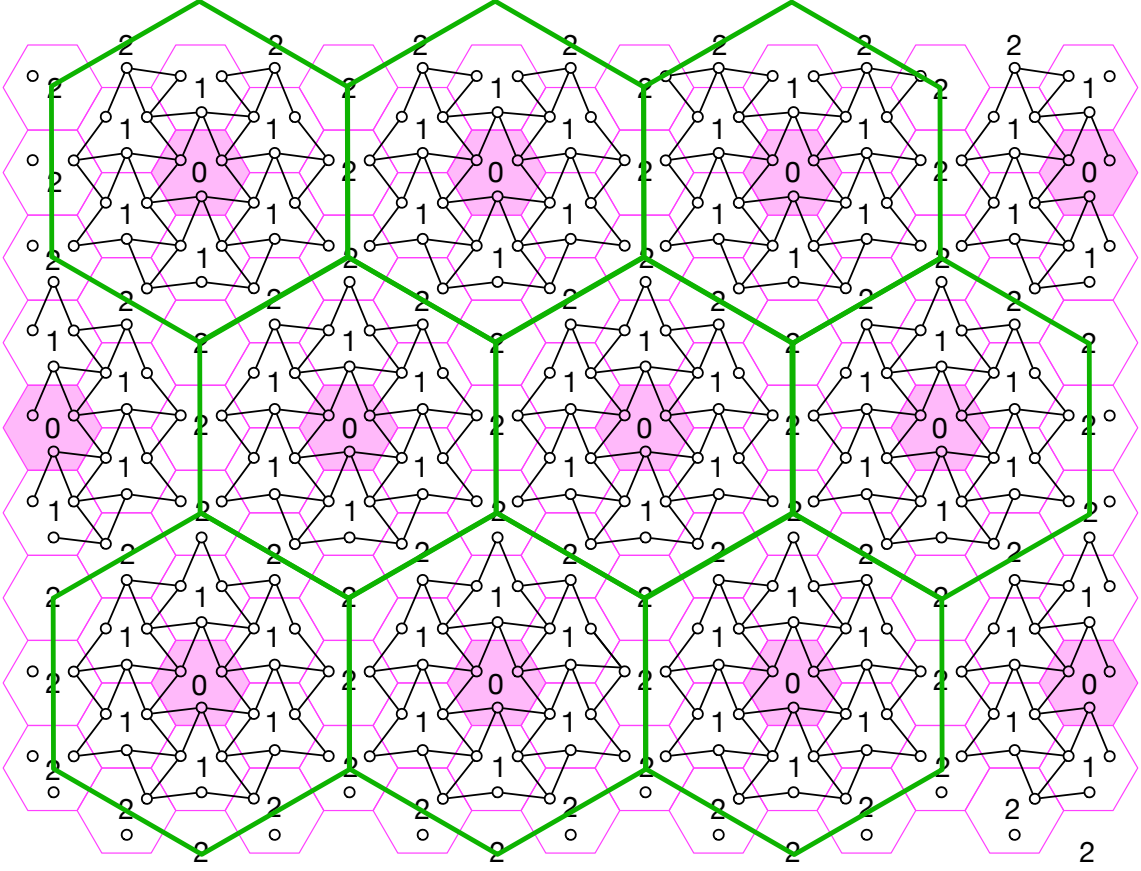


Figure 2.1: Illustration of our uplink coding scheme with BS cooperation for parameter $t = 2$. BSs in magenta cells decode all the messages sent by mobile users in the decoding regions defined by the green hexagons that we call h-clusters and then pass the decoded messages to their intended receiving BSs.

adjacent to layer-“1” cells and are not master cells as layer-“2” cells. The way we choose the master cells, every cell is either a master cell, a layer-“1” cell or a layer-“2” cell.

Encoding: The mobile users in the network that are not shown in Figure 2.1 remain silent and do not transmit anything. Each remaining mobile user u transmits its message W_u using an independent Gaussian codebook of power P^1 , that is obtained through random codebook generation².

Cooperation between BSs: Cooperation takes place over $2t = 4$ rounds as follows:

¹In order to satisfy the block power constraint in (2.2), the codebook needs to be generated with a power P' that is slightly smaller than P . This is however a technicality that we ignore.

²By random codebook generation, we mean that each time- n' signal of the transmitted codeword is a realization of the same distribution

- Round 1: Each layer-“2” BS applies an independent rate- R_q ,

$$R_q = M \cdot \frac{1}{2} \log P, \quad (2.14)$$

MIMO-Gaussian vector quantizer to the M -dimensional receive signal of each of its sectors with an active mobile user, where the codebooks are obtained through random codebook generation. Due to the random generation of codebooks for transmission and quantization, we drop the time subscript n' . Let $\hat{\mathbf{Y}}_u$ be the quantized signal of a layer-“2” BS, then the quantization noise covariance matrix for each user u , \mathbf{Q}_u , is chosen to satisfy (2.14):

$$\begin{aligned} R_q &= I(\mathbf{Y}_u; \hat{\mathbf{Y}}_u), \\ &= \frac{1}{2} \log \frac{|\sum_{v \in \mathcal{T}_u} \mathbf{H}_{u,v} \mathbf{K}_{\mathbf{X}_u} \mathbf{H}_{u,v}^T + \mathbf{Q}_u + \mathbf{I}_M|}{|\mathbf{Q}_u|} \\ &= M \cdot \frac{1}{2} \log P \end{aligned} \quad (2.15)$$

where $\mathbf{K}_{\mathbf{X}_u}$ is the covariance matrix of transmitted signal \mathbf{X}_u . Then, it sends the quantization message obtained for a given Rx u to one of the adjacent layer-“1” BSs that lie in the same green hexagonal region as the sector under consideration, see Figure 2.1.

Each layer-“1” BS applies a rate- R_q MIMO-Gaussian vector quantizer to its own 3 M -dimensional receive signals in the same manner explained above and it sends the 3 quantization messages to the adjacent master cell.

- Round 2: The layer-“1” BSs forward the Round-1 messages that they received from layer-“2” BSs during Round 1 to their adjacent master BSs.
- Rounds 3 and 4: Each master BS uses the quantization messages received in Rounds 1 and 2 to reconstruct quantized versions of the 27 M -dimensional received signals observed in the sectors lying in the same green hexagonal region as the master BS itself. Using these 27 quantized M -dimensional signals and its own 3 M -dimensional receive signals, each master BS decodes **all** the messages sent by the 30 active mobile users in the same h-cluster as the master BS itself.

In Rounds 3 and 4, messages decoded at the master BS but intended for layer-“1” or layer-“2” BSs are sent over the backhaul links to the intended BSs. Specifically, messages for layer-“1” BSs are directly passed from the master BSs to their intended BSs in Round 3. Messages for layer-“2” BSs are first passed to adjacent layer-“1” BSs in Round 3, and then to the intended layer-“2” BSs in Round 4.

Decoding: Each master BS declares the message that it has produced during the decoding steps preceding cooperation-round 3. Each layer-“1” BS declares the messages it has received during the cooperation-round 3 and that were intended for it. Each layer-“2” BS declares the messages that it has received during the cooperation-round 4.

DoF Analysis: The interest here is in the high-SNR asymptotics, i.e., on the DoF. Choosing the quantization-rate R_q as in (2.14) means that each received signal is essentially quantized at the noise level and allows to achieve the same DoF as if the master BS directly had access to all the 30 receive signals in its decoding region. That is, since the goal is to decode 30 messages, the channel matrix corresponding to the active sectors in a single green hexagonal region is of full rank with probability 1, and by the symmetry of the problem, each of these 30 transmitted messages can be decoded with arbitrarily small probability of error as if each user message is decoded in a point-to-point manner. Hence, for each active user u :

$$\begin{aligned}
\text{DoF}_u &= \lim_{P \rightarrow \infty} \frac{I(\hat{\mathbf{Y}}_u; \mathbf{X}_u)}{\frac{1}{2} \cdot \log P}, \\
&= \lim_{P \rightarrow \infty} \frac{h(\hat{\mathbf{Y}}_u) - h(\hat{\mathbf{Y}}_u | \mathbf{X}_u)}{\frac{1}{2} \log P}, \\
&= \lim_{P \rightarrow \infty} \frac{M \cdot \frac{1}{2} \log P - \frac{1}{2} \cdot \log |\mathbf{Q}_u + \mathbf{I}_M|}{\frac{1}{2} \log P}, \\
&= M
\end{aligned} \tag{2.16}$$

is achievable since when P tends to infinity quantization noise converges to a finite constant. Notice now that for large networks ($N \rightarrow \infty$) a fraction of $\frac{5}{6}$ mobile users are active, and thus the scheme achieves a DoF of

$$\text{DoF}_t = M \frac{5}{6}, \quad \text{for } t = 2. \tag{2.17}$$

Now, we analyze the backhaul load for a single green hexagonal region. In Round 1, layer-“2” BSs send in total 9 quantization messages, each of M DoF, to layer-“1” BSs, and layer-“1” BSs send in total 18 quantization messages, each of M DoF, to the adjacent master BS. In Round 2, layer-“1” BSs send in total 9 quantization messages, each of M DoF, to the adjacent master BS. In Round 3, the master BS sends 27 decoded messages, each of DoF M , to the 6 adjacent layer-“1” BSs. In Round 4, 9 quantization messages of layer-“2” BSs are forwarded to intended BSs by layer-“1” BSs. In total, 72 one cell-hop transmission of DoF M is carried out in each green hexagonal region during 4 Rounds.

The backhaul load in our scheme is unevenly distributed among backhaul links. To balance this load and to achieve fairness among the rates achieved by the various mobile users, instances of the presented scheme are time-shared, where in different instances different cells play the role of master cells. We are then interested in the **required backhaul prelog** imposed by our scheme.

To calculate this average backhaul DoF, notice that each green hexagonal region is associated with a single master cell, and that for $N \gg 1$ a cell partitioning can be obtained by associating 11 neighboring cells to each of the master cells as illustrated in Figure 2.2. (Note that the h-clusters in Figure 2.1 do not represent a valid cell partitioning because some cells are associated with multiple master cells.) Including the master cell, each subset

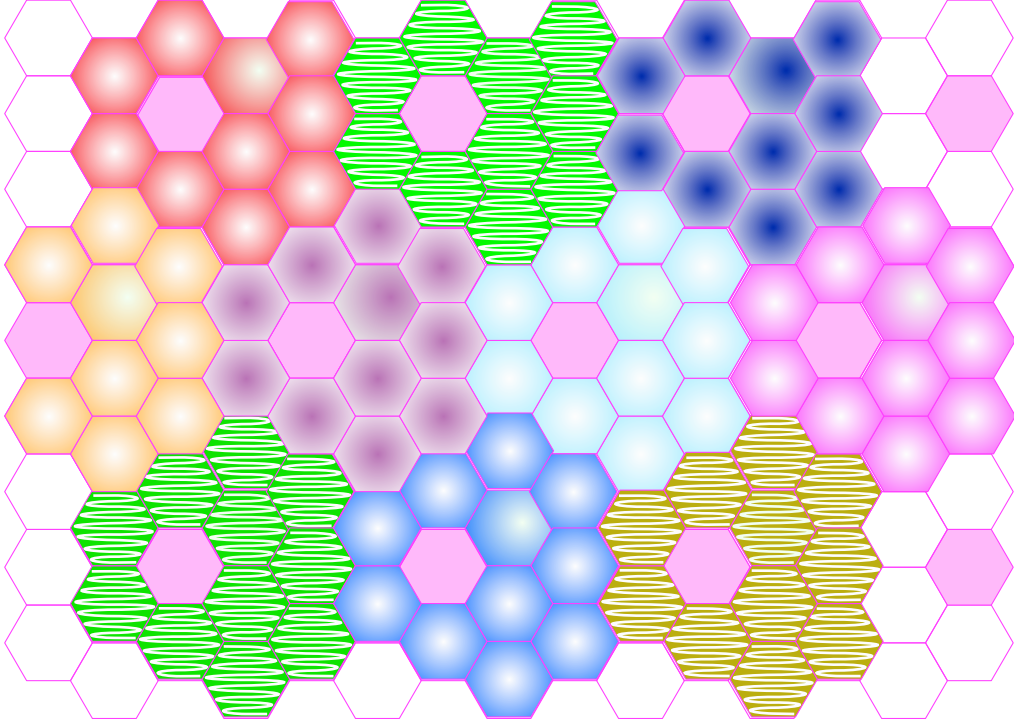


Figure 2.2: The figure illustrates the proposed cell partitioning. The subsets of 11 cells associated to different master cells are shown in different colors and different shadings. (Master cells are in pink color.)

of the cell partitioning thus consists of 12 cells. Notice further that each cell is surrounded by 6 neighbouring cells and has 6 outgoing backhaul links. The average backhaul DoF **per cooperation link** is obtained by dividing the total backhaul DoF occupied in a single hexagonal region, i.e., $72M$, by the total number of backhaul links associated to a single subset of the cell partitioning, i.e., $6 \cdot 12$:

$$\mu_{B,t} = \frac{72M}{6 \cdot 12} = M, \quad \text{for } t = 2. \quad (2.18)$$

where the factor 6 accounts for the fact that each cell has 6 outgoing cooperation links.

2.3.2 General case $t > 0$

Choose the master cells so that they form a regular pattern of equilateral triangles where the master cells building these triangles are $2t$ cell-hops apart from each other. See Figure 2.3 for a choice of magenta master cells when $t = 3$. For $\ell = 1, \dots, t$, we call **layer-“ ℓ ”** cells, the cells that are at distance ℓ from the closest master cell.

Encoding: Some of the layer-“ t ” mobile users are deactivated and do not transmit any message at all. All other mobile users are active, and send their messages using

an independent Gaussian codebook of power P . To describe the mobile users that are deactivated, we introduce the following nomenclature. We call the cells that are located t hops above the master cells the **corner** cells and the cells t hops below the master cells the **null** cells. We silence all users of the null cells and none of the corner cells. For all layer- t cells that are neither corner nor null cells, we deactivate the single mobile users that is closest to a corner cell. We conclude that among all the layer- t cells that surround a master cell, 3 of them have only active users, 3 have only deactivated users, and the remaining $6(t - 1)$ cells have exactly 2 active users. See Figure 2.3 for an example.

Cooperation between BSs: Cooperation takes place over $2t$ rounds.

- Rounds 1 to t : Each BS that is not a master BS applies a rate- R_q MIMO-Gaussian vector quantizer to any of its M -dimensional receive signals that corresponds to a sector with an active mobile user. For $\ell = 1, \dots, t - 1$, each layer-" ℓ " BS sends its 3 quantization messages to the closest master BS, by means of multi-hop communication over ℓ rounds. Each layer- t BS sends each of its produced quantization messages to the master BS that is **closest to the sector** under consideration. This transmission is again multi-hop over t rounds.
- Rounds $t + 1, \dots, 2t$: Each master BS reconstructs the M -dimensional quantized signals corresponding to the quantization messages received in Rounds $1, \dots, t$. It then decodes the messages sent by the mobile users in the sectors corresponding to these quantization messages as well as the messages sent by the mobile users in its own cell. Finally, during cooperation rounds $t + 1, \dots, 2t$, it communicates each of the decoded messages using multi-hop communication to its intended BS.

Decoding: Each master BS directly declares the messages guessed for its own cell before cooperation round $t + 1$. The other BSs declare the messages that the master BSs have guessed for their cells and when they have learned during cooperation rounds $t + 1, \dots, 2t$.

DoF Analysis: As before, the quantization rate R_q is chosen as in (2.14), and the interest is on the DoF. Choosing the quantization-rate R_q as in (2.14) allows to achieve the same DoF as if the master BSs directly had access to all the receive signals for which they receive quantization information. Since there are 6ℓ layer-" ℓ " cells around each master cell, each master BS receives the quantized version of

$$3 \cdot \sum_{\ell=1}^{t-1} 6\ell + (6t - 3) = 9t(t - 1) + 6t - 3 = 3(3t^2 - t - 1) \quad (2.19)$$

M -dimensional output signals. With these quantization messages and the 3 M -dimensional output signals observed in its own cell each master BS decodes the messages of $3(3t - 1)$ mobile users. Since each mobile user is equipped with M transmit antennas and since the master cell applies joint decoding as in a single-receiver MIMO multi-access scenario, each of the considered mobile users can reliably transmit its message with DoF M .

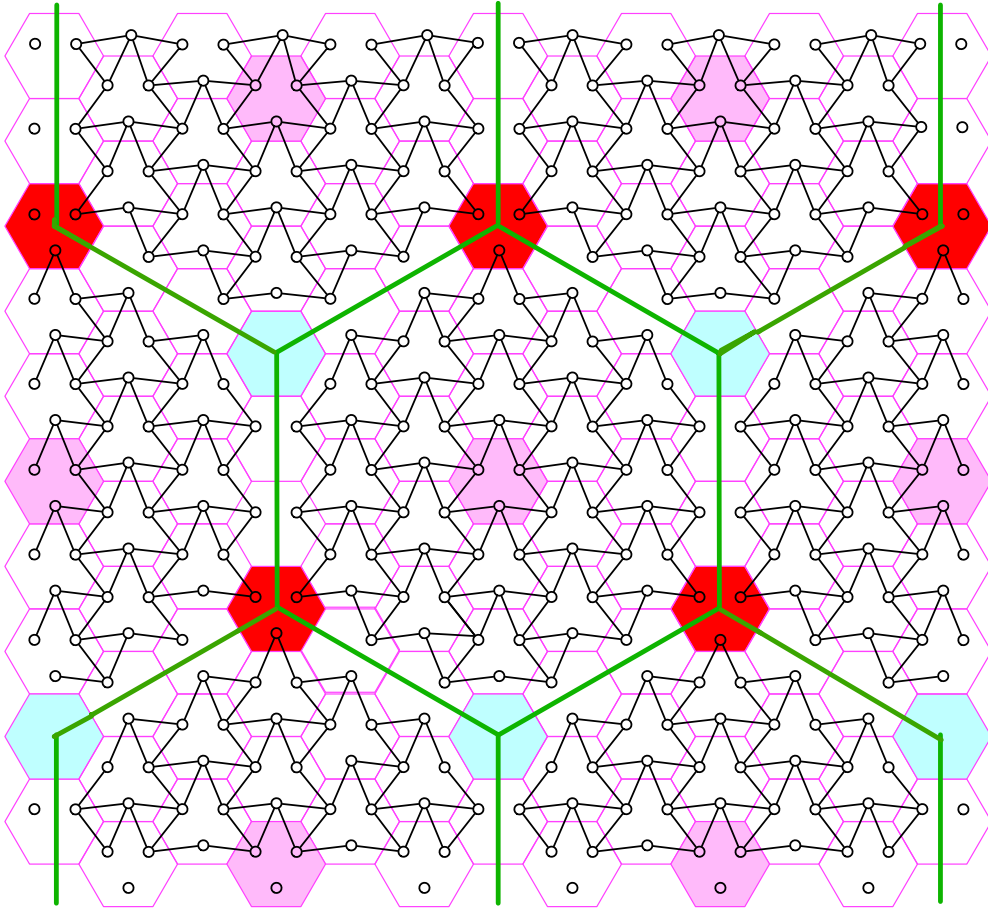


Figure 2.3: Illustration of our uplink coding scheme with BS cooperation for parameter $t = 3$. Pink cells, red cells and blue cells represent center cells, corner cells and null cells, respectively. BSs in pink cells decode all the messages sent by mobile users in the decoding regions defined by the green hexagons and then pass the decoded messages to their intended receiving BSs.

To calculate the average per-user DoF over the entire network, we describe a cell partitioning that associates each cell to a unique master cell, and that associates the same number of cells to each master cell. (Note that Figure 2.3 does not describe a valid partition, because some cells are associated with more than one master cell.) The average per-user DoF is then obtained by dividing the DoF achieved at a given master cell, i.e., $M \cdot 3t(3t - 1)$, by the total number of sectors that are contained in a single subset of the proposed cell partitioning. For $N \gg 1$ the desired cell partitioning can be obtained by associating to each master BS a set of sectors that includes **all** its layer-1, \dots , $t - 1$ cells and the layer- t cells that lie on its north-east, east, and south-east. Hereby, the corner cells in the north and the south are excluded. (See Figure 2.4.)

Each subset of the described cell partitioning thus includes a master cell, all its layer-

$1, 2, \dots, \gamma - 1$ cells, and half of its layer- γ cells but one. It's total number of cells is thus:

$$1 + \sum_{\ell=1}^{t-1} 6\ell + (3t - 1) = 3t^2, \quad (2.20)$$

and it includes $3 \cdot 3t^2$ sectors. We conclude that the proposed scheme achieves an average per-user DoF of

$$\text{DoF}_t = \frac{M \cdot 3t(3t - 1)}{3 \cdot 3t^2} = M \frac{3t - 1}{3t}, \quad t \in \left\{1, \dots, \left\lfloor \frac{\kappa}{2} \right\rfloor\right\}. \quad (2.21)$$

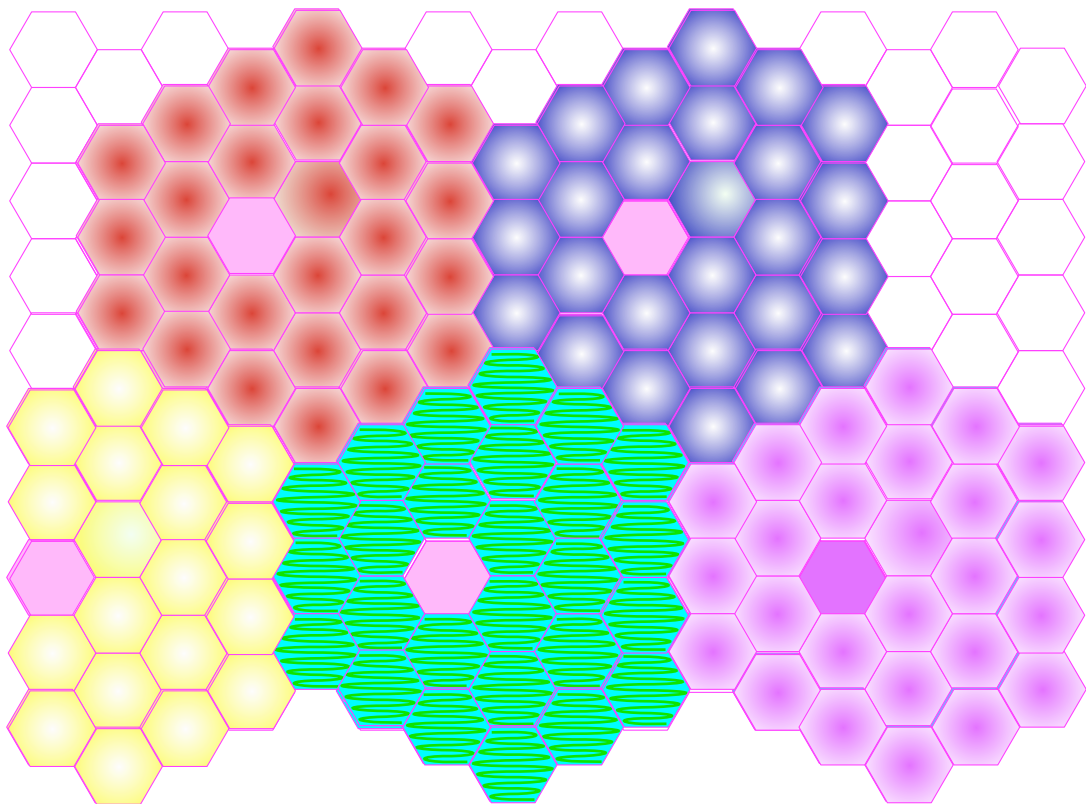


Figure 2.4: The figure illustrates the proposed cell partitioning when $t = 3$. Specifically, the pink cells indicate the master cells and different colors and shadings are used to indicate the subsets of cells associated to the different master cells.

We next analyze the backhaul load that is associated with a single master cell. During Rounds $1, \dots, t$, a master BS receives a quantization message of DoF M for each of the sectors that have an active user and that are closer to this master BS than to any other master BS. Since the quantization message for a sector in layer-“ ℓ ” is communicated over

ℓ backhaul links, the total backhaul DoF on these first t rounds is

$$\begin{aligned}
 & 3M \sum_{\ell=1}^{t-1} 6\ell \cdot \ell + M(6t-3)t \\
 &= 3M[(t-1)t(2t-1) + (2t-1)t] \\
 &= 3Mt^2(2t-1).
 \end{aligned} \tag{2.22}$$

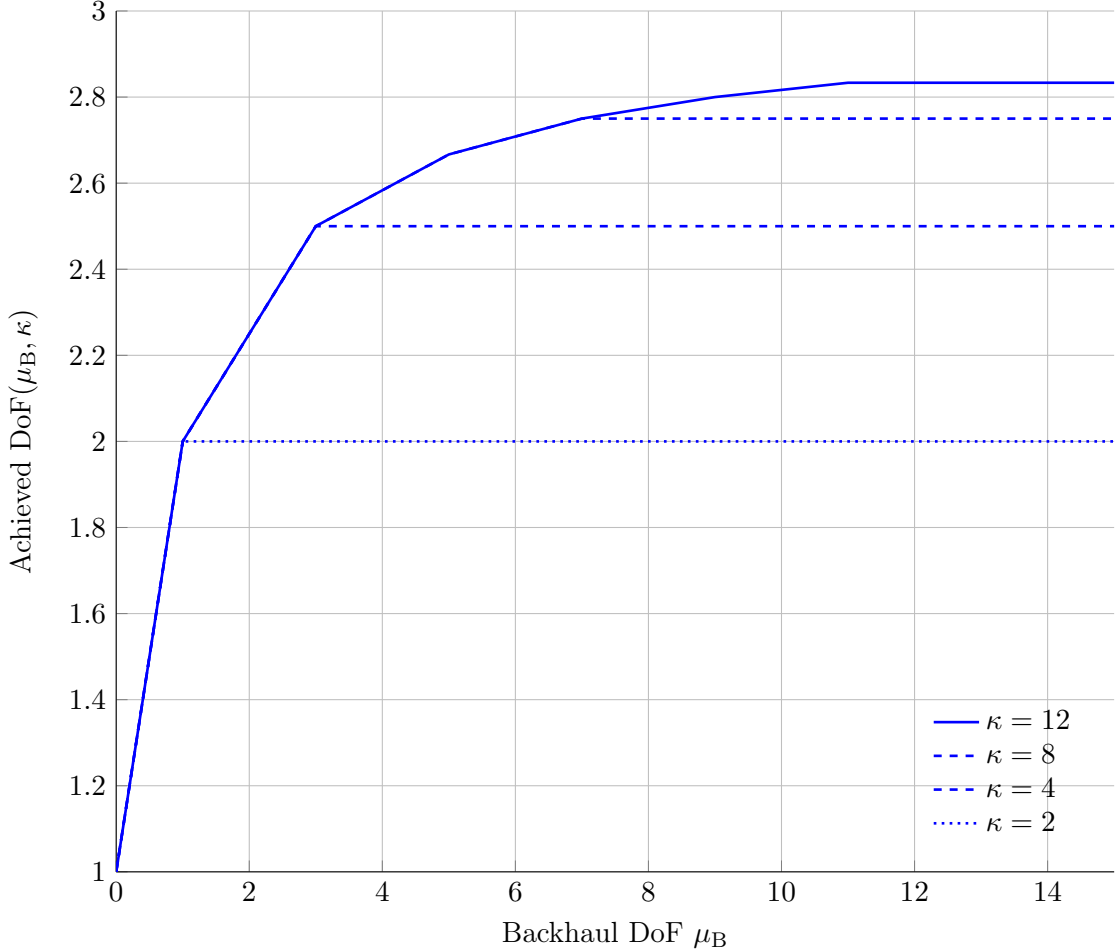


Figure 2.5: Lower bound on the DoF in Theorem 2.1 for different values of κ and in function of μ_B . We have $M = 3$.

During Rounds $t+1, \dots, 2t$ a decoded message of DoF M , is communicated from the master BS to the BSs for each quantisation message that has been sent during Rounds $1, \dots, t$. Therefore, the total backhaul load during Rounds $1, \dots, t$ coincides with the total backhaul load during Rounds $t+1, \dots, 2t$, and the total backhaul load over all rounds is thus $6Mt^2(2t-1)$.

To balance the backhaul load and to achieve fairness among the rates achieved by the various mobile users, instances of the presented scheme are time-shared, where in different instances different cells play the role of the master cells. The required backhaul prelog to

allow this process is obtained by dividing 2 times (2.22) by the number of outgoing (or incoming) backhaul links in such a cluster, which by (2.20) is $6 \cdot 3t^2$:

$$\mu_{B,t} = \frac{2 \cdot 3Mt^2(2t-1)}{6 \cdot 3t^2} = M \frac{2t-1}{3}, \quad t \in \left\{1, \dots, \left\lfloor \frac{\kappa}{2} \right\rfloor\right\}. \quad (2.23)$$

Under such a time-sharing framework, the **backhaul capacity prelog** is the limiting quantity. Time-sharing the described scheme for different parameters of t yields immediately the following theorem:

Theorem 2.1 (Achievability). *For any given $\mu_B \geq 0$ and $\kappa > 0$, the DoF is lower bounded as*

$$\text{DoF}(\mu_B, \kappa) \geq \text{upp hull} \left\{ (\mu_{B,t}, \text{DoF}_t) : t = 1, \dots, \left\lfloor \frac{\kappa}{2} \right\rfloor \right\} \quad (2.24)$$

where

$$\mu_{B,t} := M \frac{2t-1}{3} \quad \text{and} \quad \text{DoF}_t := M \left(1 - \frac{1}{3t}\right) \quad \forall t \in \left\{1, \dots, \left\lfloor \frac{\kappa}{2} \right\rfloor\right\}, \quad (2.25)$$

and

$$\mu_{B,0} = 0 \quad \text{and} \quad \text{DoF}_0 = \frac{M}{3}. \quad (2.26)$$

Figure 2.5 illustrates this lower bound for different values of κ . Notice that even with only two conferencing rounds, a DoF of $M/2$ is achievable with our scheme with a backhaul prelog of only $\mu_B = 0.5$.

2.4 Upper Bound for the Communication Model

We prove the following theorem on the achievable DoF:

Theorem 2.2 (Converse). *For any given $\mu_B \geq 0$ and $\kappa > 0$, the DoF is upper bounded as*

$$\text{DoF}(\mu_B, \kappa) \leq \min \begin{cases} \frac{M}{2} + \frac{2}{3}\mu_B & (2.27) \\ M \cdot \left(\frac{2 \cdot \kappa + 1}{2 \cdot \kappa + 2}\right) & (2.28) \end{cases}$$

We prove the Theorem 2.2 by stating the following lemma. The lemma provides MAC-type upper bound similarly to Sato's MAC-bound [59, 32] for general interference channels without cooperation and dynamic MAC-Lemma [36, Lemma 9] for interference networks with message cognition and clustered decoding. We extend [71, Lemma 1] to our sectorized hexagonal network model with receiver cooperation between adjacent BSs but without transmitter cooperation.

Let $\mathbf{W}_j = (W_{u_j,1}, W_{u_j,2}, W_{u_j,3})$, $\mathbf{X}_j^{(3n)} = (\mathbf{X}_{u_j,1}^{(n)}, \mathbf{X}_{u_j,2}^{(n)}, \mathbf{X}_{u_j,3}^{(n)})$ and $\mathbf{Z}_j^{(3n)} = (\mathbf{Z}_{u_j,1}^{(n)}, \mathbf{Z}_{u_j,2}^{(n)}, \mathbf{Z}_{u_j,3}^{(n)})$ denote messages, transmitted signals and observed noises of BS j respectively, where

$u_{j,1}, u_{j,2}, u_{j,3}$ are sector indices of BS j . For any index set of cells $\mathcal{A}_0 \subseteq \mathcal{N}$, we define

$$\mathbb{H}_{\mathcal{A}_0, \mathcal{A}_0} := \{ \mathbf{H}_{u_i, v_j} : \text{Rx } u_i \text{ is in cell } i \in \mathcal{A}_0, \text{ mobile user } v_j \text{ is in cell } j \in \mathcal{A}_0, \\ \text{sector } u_i \text{ and sector } v_j \text{ are adjacent} \},$$

$$\mathbb{W}_{\mathcal{A}_0} := \{ \mathbf{W}_j \}_{j \in \mathcal{A}_0} \quad \text{and} \quad \mathbb{X}_{\mathcal{A}_0} := \{ \mathbf{X}_j^{(3n)} \}_{j \in \mathcal{A}_0},$$

$$\mathbb{Y}_{\mathcal{A}_0} := \{ \mathbf{Y}_j^{(3n)} \}_{j \in \mathcal{A}_0} \quad \text{and} \quad \mathbb{Z}_{\mathcal{A}_0} := \{ \mathbf{Z}_j^{(3n)} \}_{j \in \mathcal{A}_0},$$

$$\mathbb{V}_{\text{to } \mathcal{A}_0}^\kappa := \{ \mathbf{V}_{\text{to } j}^\kappa \}_{j \in \mathcal{A}_0} \quad \text{and} \quad \mathbb{V}_{\mathcal{A}_0 \rightarrow \mathcal{A}_0}^\kappa := \{ \mathbf{V}_{\mathcal{A}_0 \rightarrow \mathcal{A}_0}^k \}_{k=1}^\kappa,$$

where

$$\mathbf{V}_{\mathcal{A}_0 \rightarrow \mathcal{A}_0}^k := \{ V_{i \rightarrow j}^k : i \in \mathcal{A}_0, j \in \mathcal{A}_0 \text{ and cell } i \text{ is adjacent to cell } j \},$$

and, for any index sets of cells $\mathcal{A}_0 \subseteq \mathcal{N}$ and $\mathcal{B}_0 \subseteq \mathcal{N}$, we define

$$\mathbb{H}_{\mathcal{A}_0, \mathcal{B}_0} := \{ \mathbf{H}_{u_i, v_j} : \text{Rx } u_i \text{ is in cell } i \in \mathcal{A}_0, \text{ mobile user } v_j \text{ is in cell } j \in \mathcal{B}_0, \\ \text{sector } u_i \text{ and sector } v_j \text{ are adjacent} \},$$

$$\mathbb{V}_{\mathcal{A}_0 \rightarrow \mathcal{B}_0}^\kappa := \{ \mathbf{V}_{\mathcal{A}_0 \rightarrow \mathcal{B}_0}^k \}_{k=1}^\kappa$$

where

$$\mathbf{V}_{\mathcal{A}_0 \rightarrow \mathcal{B}_0}^k := \{ V_{i \rightarrow j}^k : i \in \mathcal{A}_0, j \in \mathcal{B}_0 \text{ and cell } i \text{ is adjacent to cell } j \}.$$

Lemma 2.3 (MAC Bound for Cooperative Sectored Cellular Networks). *Consider a sectored cellular network with BS cooperation described in Section 2.2. Let \mathbb{G} be a set of genie signals that are independent of the all messages $\mathbb{W}_{\mathcal{T}}$ and partition index set of all cells into two sets \mathcal{A} and \mathcal{B} , such that the differential entropy*

$$\frac{1}{n} h(\mathbb{Z}_{\mathcal{A}} | \mathbb{G}) = o(\log P) \quad (2.29)$$

where $o(\cdot)$ denotes "little-o" Landau symbol. If for any sequence of encoding, cooperation and decoding functions $\{f_u^{(n)}\}$, $\{\psi_{j,i}^{k,(n)}\}$, and $\{h_u^{(n)}\}$, there exist deterministic function $\xi^{(n)}$ for each blocklength n , such that

$$\mathbb{Y}_{\mathcal{B}} = \xi^{(n)}(\mathbb{Y}_{\mathcal{A}}, \mathbb{V}_{\mathcal{B}_c \rightarrow \mathcal{A}_c}^\kappa, \mathbb{G}) \quad (2.30)$$

where $\mathbb{V}_{\mathcal{B}_c \rightarrow \mathcal{A}_c}^\kappa$ denotes κ -round cooperation messages from some \mathcal{B}_c cells, $\mathcal{B}_c \subseteq \mathcal{B}$, to some \mathcal{A}_c cells, $\mathcal{A}_c \subseteq \mathcal{A}$, then the sum-DoF of the network is upper bounded as

$$\mathcal{S}_{\Sigma} \leq 3 \cdot M \cdot |\mathcal{A}| + n_c \cdot \mu_{\mathcal{B}}, \quad (2.31)$$

where \mathcal{S}_{Σ} denote sum-DoF and n_c denotes the number of backhaul links from the set of \mathcal{B}_c cells to the set of \mathcal{A}_c cells.

Proof: To prove the upper bound, we introduce a super-receiver whose capacity region includes the capacity region of the original network,

$$\mathcal{C}(P, \mu_B, \kappa) \subseteq \mathcal{C}_{\text{sup}}(P, \mu_B, \kappa), \quad (2.32)$$

and whose sum-DoF, is

$$\mathcal{S}_{\Sigma}^{\text{sup}} \leq 3 \cdot M \cdot |\mathcal{A}| + n_c \cdot \mu_B. \quad (2.33)$$

The super-receiver is obtained from the original network by revealing genie signals \mathbb{G} and some κ -round cooperation messages $\mathbb{V}_{\mathcal{B}_c \rightarrow \mathcal{A}_c}^{\kappa}$ to the BSs of set \mathcal{A} , such that the BSs of this set perform decoding of all messages $\mathbb{W}_{\mathcal{T}}$ without requiring any receive signal from BSs of set \mathcal{B} .

Now, we prove the inclusion (2.32). To this end, we show that every coding scheme of the original network can be transformed to the super-receiver whenever all messages in the original network decoded successfully, hence the super-receiver can decode all messages successfully. Fix a sequence of encoding, cooperation, and decoding functions $\{f_u^{(n)}\}$, $\{\psi_{j,i}^{k,(n)}\}$, and $\{h_u^{(n)}\}$ for the original network and assume that as a result of κ -rounds cooperation phase each BS $j \in \mathcal{N}$ performs decoding successfully for its messages \mathbf{W}_j . The mobile users of the super-receiver apply the same encoding functions and it has received signals of only set \mathcal{A} BSs, i.e., $\mathbb{Y}_{\mathcal{A}}$, and κ -round cooperation messages $\mathbb{V}_{\mathcal{B}_c \rightarrow \mathcal{A}_c}^{\kappa}$. It also adopts the same cooperation functions of the original network, however, it can apply them only to available receive signals, $\mathbb{Y}_{\mathcal{A}}$. Then, the super-receiver performs the following processes:

- By using $\mathbb{Y}_{\mathcal{A}}$ and $\mathbb{V}_{\mathcal{B}_c \rightarrow \mathcal{A}_c}^{\kappa}$, it reconstructs some κ -round cooperation messages $\mathbb{V}_{\text{to } \mathcal{A}_d}^{\kappa}$, $\mathcal{A}_d \subseteq \mathcal{A}$,
- Based on $\mathbb{Y}_{\mathcal{A}_r}$ and $\mathbb{V}_{\text{to } \mathcal{A}_d}^{\kappa}$, it reconstructs $\mathbb{W}_{\mathcal{A}_d}$ and encodes the corresponding transmitted signals $\mathbb{X}_{\mathcal{A}_d}$,
- Based on the transmitted signals $\mathbb{X}_{\mathcal{A}_r}$, receive signals $\mathbb{Y}_{\mathcal{A}}$ and genie information \mathbb{G} , it produces $\mathbb{Y}_{\mathcal{B}}$,
- It produces all cooperation messages in the same way that original network does and it decodes the rest of the messages, i.e., $\mathbb{W}_{\mathcal{A} \setminus \mathcal{A}_d}$ and $\mathbb{W}_{\mathcal{B}}$.

By assumption (2.30), if the original network decodes all messages successfully, the decoding implemented at the super-receiver does not cause any additional error events compared to original decoding procedure. This proves Inclusion (2.32).

Now, we prove sum-DoF bound (2.33). Since set \mathcal{A} BSs are required to decode all

messages $\mathbb{W}_{\mathcal{T}}$, by Fano's inequality the reliable communication is possible as long as

$$\begin{aligned}
\sum_{u \in \mathcal{T}} R_u &\leq \frac{1}{n} I(\mathbb{Y}_{\mathcal{A}}, \mathbb{V}_{\mathcal{B}_c \rightarrow \mathcal{A}_c}^{\kappa}, \mathbb{G}; \mathbb{W}_{\mathcal{T}}) + \epsilon_n \\
&= \frac{1}{n} I(\mathbb{Y}_{\mathcal{A}}; \mathbb{W}_{\mathcal{T}} | \mathbb{G}) + \frac{1}{n} I(\mathbb{V}_{\mathcal{B}_c \rightarrow \mathcal{A}_c}^{\kappa}; \mathbb{W}_{\mathcal{T}} | \mathbb{Y}_{\mathcal{A}}, \mathbb{G}) + \epsilon_n \\
&= \frac{1}{n} h(\mathbb{Y}_{\mathcal{A}} | \mathbb{G}) - \frac{1}{n} h(\mathbb{Y}_{\mathcal{A}} | \mathbb{W}_{\mathcal{T}}, \mathbb{G}) + \frac{1}{n} H(\mathbb{V}_{\mathcal{B}_c \rightarrow \mathcal{A}_c}^{\kappa} | \mathbb{Y}_{\mathcal{A}}, \mathbb{G}) + \epsilon_n \\
&\leq \frac{1}{n} h(\mathbb{Y}_{\mathcal{A}}) - \frac{1}{n} h(\mathbb{Z}_{\mathcal{A}} | \mathbb{G}) + \frac{1}{n} H(\mathbb{V}_{\mathcal{B}_c \rightarrow \mathcal{A}_c}^{\kappa}) + \epsilon_n
\end{aligned} \tag{2.34}$$

where $\epsilon_n \rightarrow 0$ as $n \rightarrow \infty$. The DoF of $\frac{1}{n} h(\mathbb{Y}_{\mathcal{A}})$ and $\frac{1}{n} H(\mathbb{V}_{\mathcal{B}_c \rightarrow \mathcal{A}_c}^{\kappa})$ are bounded by $3 \cdot M \cdot |\mathcal{A}|$ and $n_c \cdot \mu_B$ respectively, and by assumption

$$\lim_{P \rightarrow \infty} \frac{\frac{1}{n} h(\mathbb{Z}_{\mathcal{A}} | \mathbb{G})}{\frac{1}{2} \log P} = 0. \tag{2.35}$$

We therefore obtain from (2.34) that

$$\lim_{P \rightarrow \infty} \frac{\sum_{u \in \mathcal{T}} R_u}{\frac{1}{2} \log P} \leq 3 \cdot M \cdot |\mathcal{A}| + n_c \cdot \mu_B. \tag{2.36}$$

This ends the proof.

2.4.1 Proof of (2.27)

Follows by specializing Lemma 2.3 to the cell partition given in Figure 2.6 such that we choose the sets \mathcal{A} , \mathcal{A}_c , \mathcal{B} and \mathcal{B}_c as

$$\begin{aligned}
\mathcal{A} &= \{j : \text{Cell } j \text{ is red}\} \quad \text{and} \quad \mathcal{A}_c = \mathcal{A}, \\
\mathcal{B} &= \{j : \text{Cell } j \text{ is white}\} \quad \text{and} \quad \mathcal{B}_c = \mathcal{B},
\end{aligned}$$

and we choose the genie information \mathbb{G} as

$$\mathbb{G} = \mathbb{Z}_{\mathcal{B}} - \mathbb{H}_{\mathcal{B}, \mathcal{B}} \mathbb{H}_{\mathcal{A}, \mathcal{B}}^{-1} \mathbb{Z}_{\mathcal{A}}.$$

To prove the bound (2.27), fix a sequence of encoding, cooperation, and decoding functions $\{f_u^{(n)}\}$, $\{\psi_{j,i}^{k,(n)}\}$, and $\{h_u^{(n)}\}$ so that for sufficiently large blocklengths n the probability of error does not exceed $\epsilon > 0$. Notice that if the super-receiver performs the following six decoding steps, then it decodes all messages $\mathbb{W}_{\mathcal{T}}$ correctly whenever the N BSs decode them correctly in the original setup. The super-receiver's probability of error can thus not be larger than the original probability of error, which was upper bounded by ϵ .

The six decoding steps at the super-receiver are:

1. For each round $k = 1, \dots, \kappa$, it applies the appropriate cooperation functions $\{\psi_{j,i}^{k,(n)}\}$ to the receive signals $\mathbb{Y}_{\mathcal{A}}$ and the previous rounds' conferencing messages $\{\mathbb{V}_{\mathcal{B} \rightarrow \mathcal{A}}^{k'}\}_{k'=1}^{k-1}$

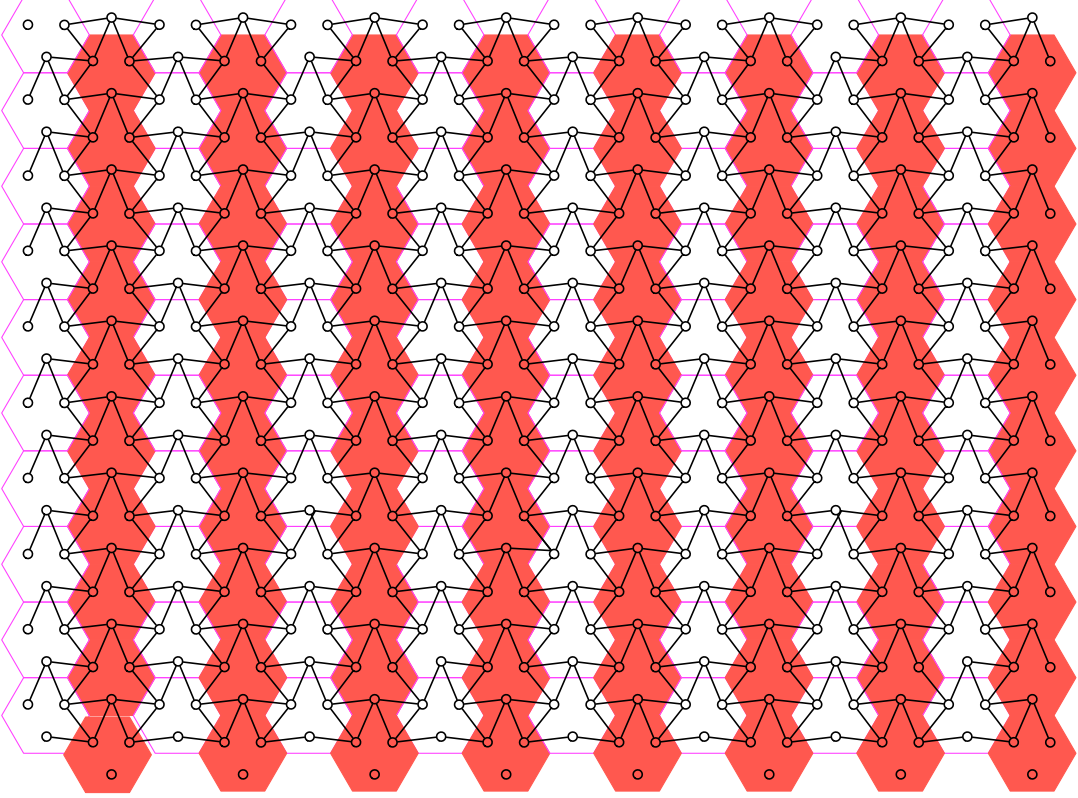


Figure 2.6: Cell partitioning used for the first converse bound.

and $\{\mathbb{V}_{\mathcal{A} \rightarrow \mathcal{A}}^{k'}\}_{k'=1}^{k-1}$. This allows the super-receiver to compute the cooperation messages of the current round $\mathbb{V}_{\mathcal{A} \rightarrow \mathcal{B}}^k$ and $\mathbb{V}_{\mathcal{A} \rightarrow \mathcal{A}}^k$. At the end, it obtains $\mathbb{V}_{\text{to } \mathcal{A}}^\kappa$. (Notice that knowledge of receive signals in cells of set \mathcal{B} or cooperation messages exchanged between cells of set \mathcal{B} are not required for this computation.)

2. It applies the appropriate decoding functions $\{h_u^{(n)}\}$ to the output signals $\mathbb{Y}_{\mathcal{A}}$ and the cooperation messages $\mathbb{V}_{\text{to } \mathcal{A}}^\kappa$ to decode messages $\mathbb{W}_{\mathcal{A}}$.
3. It applies the encoding functions $\{f_u^{(n)}\}$ to the previously decoded messages $\mathbb{W}_{\mathcal{A}}$ to construct input signals $\mathbb{X}_{\mathcal{A}}$.
4. With the transmit and receive signals, $\mathbb{X}_{\mathcal{A}}$ and $\mathbb{Y}_{\mathcal{A}}$, and chosen genie-information \mathbb{G} , it reconstructs $\mathbb{Y}_{\mathcal{B}}$. To see that this is possible, notice that since there are as many set \mathcal{A} cells as set \mathcal{B} cells, since the interference structure is regular, and since the channel coefficients are drawn independently from a continuous distribution, the matrices, $\mathbb{H}_{\mathcal{A},\mathcal{A}}$, $\mathbb{H}_{\mathcal{A},\mathcal{B}}$, $\mathbb{H}_{\mathcal{B},\mathcal{A}}$ and $\mathbb{H}_{\mathcal{B},\mathcal{B}}$ are squared and full rank. Then, the receive signals in the set \mathcal{B} cells can be constructed as:

$$\mathbb{Y}_{\mathcal{B}} = \mathbb{H}_{\mathcal{B},\mathcal{B}}\mathbb{H}_{\mathcal{A},\mathcal{B}}^{-1}(\mathbb{Y}_{\mathcal{A}} - \mathbb{H}_{\mathcal{A},\mathcal{A}}\mathbb{X}_{\mathcal{A}}) + \mathbb{H}_{\mathcal{B},\mathcal{A}}\mathbb{X}_{\mathcal{A}} + \mathbb{G}. \quad (2.37)$$

5. For each round $k = 1, \dots, \kappa$, it applies the appropriate cooperation functions $\{\psi_{j,i}^{k,(n)}\}$ to the receive signals $\mathbb{Y}_{\mathcal{A}}$ and $\mathbb{Y}_{\mathcal{B}}$, to the previously calculated cooperation messages and $\{\mathbb{V}_{\mathcal{B} \rightarrow \mathcal{B}}^{k'}\}_{k'=1}^{k-1}$, to compute the cooperation messages of the current round $\mathbb{V}_{\mathcal{B} \rightarrow \mathcal{B}}^k$. Then, it obtains $\mathbb{V}_{\text{to } \mathcal{B}}^\kappa$
6. It applies the appropriate decoding functions $\{h_u^{(n)}\}$ to the output signals $\mathbb{Y}_{\mathcal{B}}$ and the cooperation messages $\mathbb{V}_{\text{to } \mathcal{B}}^\kappa$ so as to decode messages $\mathbb{W}_{\mathcal{B}}$.

Notice that, in Figure 2.6, there are 4 red cells adjacent to each white cell, therefore

$$n_c = 4(N - |\mathcal{B}|). \quad (2.38)$$

Dividing by $|\mathcal{T}| = 3 \cdot N$ and letting $N \rightarrow \infty$ establishes the desired bound after noticing that

$$\overline{\lim}_{N \rightarrow \infty} \frac{|\mathcal{A}|}{N} = \overline{\lim}_{N \rightarrow \infty} \frac{|\mathcal{B}|}{N} = 1/2. \quad (2.39)$$

2.4.2 Proof of (2.28)

Follows by specializing Lemma 2.3 to partitioning the cells regarding the parameter κ as seen in Figures 2.7 and 2.8 such that we choose the sets \mathcal{A} , \mathcal{A}_c , \mathcal{B} and \mathcal{B}_c as

$$\begin{aligned} \mathcal{A} &= \{j : \text{Cell } j \text{ is red or blue}\} \quad \text{and} \quad \mathcal{A}_c = \emptyset, \\ \mathcal{B} &= \{j : \text{Cell } j \text{ is white}\} \quad \text{and} \quad \mathcal{B}_c = \emptyset. \end{aligned}$$

Define the sets

$$\begin{aligned} \mathcal{A}_r &= \{j : \text{Cell } j \text{ is red}\}, \\ \mathcal{A}_b &= \{j : \text{Cell } j \text{ is blue}\}. \end{aligned}$$

In Figures 2.7 and 2.8, notice that any closest \mathcal{A}_r and \mathcal{B} cells are chosen as $\kappa + 1$ cell-hops apart from each other so that the cooperation messages that is function of $\mathbb{Y}_{\mathcal{B}}$ is not required for decoding $\mathbb{W}_{\mathcal{A}_r}$. For this partition, we define

$$\bar{\mathbb{V}}_{\mathcal{A}_b \rightarrow \mathcal{A}_b}^k := \left\{ V_{i \rightarrow j}^{k,(n)} : i \in \mathcal{A}_b, j \in \mathcal{A}_b, i \text{ is at most } \kappa - k \text{ cell-hops apart from a cell of } \mathcal{A}_r \right\},$$

also, notice that

$$\begin{aligned} \mathbb{H}_{\mathcal{A}, \mathcal{A}} &= \{\mathbb{H}_{\mathcal{A}_r, \mathcal{A}_r}, \mathbb{H}_{\mathcal{A}_r, \mathcal{A}_b}, \mathbb{H}_{\mathcal{A}_b, \mathcal{A}_r}, \mathbb{H}_{\mathcal{A}_b, \mathcal{A}_b}\} \\ \mathbb{H}_{\mathcal{A}, \mathcal{A}}^{-1} &= \{\hat{\mathbb{H}}_{\mathcal{A}_r, \mathcal{A}_r}, \hat{\mathbb{H}}_{\mathcal{A}_r, \mathcal{A}_b}, \hat{\mathbb{H}}_{\mathcal{A}_b, \mathcal{A}_r}, \hat{\mathbb{H}}_{\mathcal{A}_b, \mathcal{A}_b}\}, \end{aligned}$$

for some matrices $\hat{\mathbb{H}}_{\mathcal{A}_r, \mathcal{A}_r}$, $\hat{\mathbb{H}}_{\mathcal{A}_r, \mathcal{A}_b}$, $\hat{\mathbb{H}}_{\mathcal{A}_b, \mathcal{A}_r}$ and $\hat{\mathbb{H}}_{\mathcal{A}_b, \mathcal{A}_b}$ satisfying $\mathbb{H}_{\mathcal{A}, \mathcal{A}} \mathbb{H}_{\mathcal{A}, \mathcal{A}}^{-1} = \mathbb{I}$. Then, we choose the genie information \mathbb{G} as

$$\begin{aligned} \mathbb{G} = \mathbb{Z}_{\mathcal{B}} &+ [\mathbb{H}_{\mathcal{B}, \mathcal{A}_b} \hat{\mathbb{H}}_{\mathcal{A}_b, \mathcal{A}_b} \mathbb{H}_{\mathcal{A}_b, \mathcal{B}} (\hat{\mathbb{H}}_{\mathcal{A}_r, \mathcal{A}_b} \mathbb{H}_{\mathcal{A}_b, \mathcal{B}})^{-1} \mathbb{H}_{\mathcal{A}_r, \mathcal{A}_r} - \\ &\quad \mathbb{H}_{\mathcal{B}, \mathcal{B}} (\hat{\mathbb{H}}_{\mathcal{A}_r, \mathcal{A}_b} \mathbb{H}_{\mathcal{A}_b, \mathcal{B}})^{-1} \mathbb{H}_{\mathcal{A}_r, \mathcal{A}_r} - \mathbb{H}_{\mathcal{B}, \mathcal{A}_b} \hat{\mathbb{H}}_{\mathcal{A}_b, \mathcal{A}_r}] \mathbb{Z}_{\mathcal{A}_r} \\ &+ [\mathbb{H}_{\mathcal{B}, \mathcal{A}_b} \hat{\mathbb{H}}_{\mathcal{A}_b, \mathcal{A}_b} \mathbb{H}_{\mathcal{A}_b, \mathcal{B}} (\hat{\mathbb{H}}_{\mathcal{A}_r, \mathcal{A}_b} \mathbb{H}_{\mathcal{A}_b, \mathcal{B}})^{-1} \mathbb{H}_{\mathcal{A}_r, \mathcal{A}_b} - \\ &\quad \mathbb{H}_{\mathcal{B}, \mathcal{B}} (\hat{\mathbb{H}}_{\mathcal{A}_r, \mathcal{A}_b} \mathbb{H}_{\mathcal{A}_b, \mathcal{B}})^{-1} \mathbb{H}_{\mathcal{A}_r, \mathcal{A}_b} - \mathbb{H}_{\mathcal{B}, \mathcal{A}_b} \hat{\mathbb{H}}_{\mathcal{A}_b, \mathcal{A}_b}] \mathbb{Z}_{\mathcal{A}_b} \end{aligned} \quad (2.40)$$

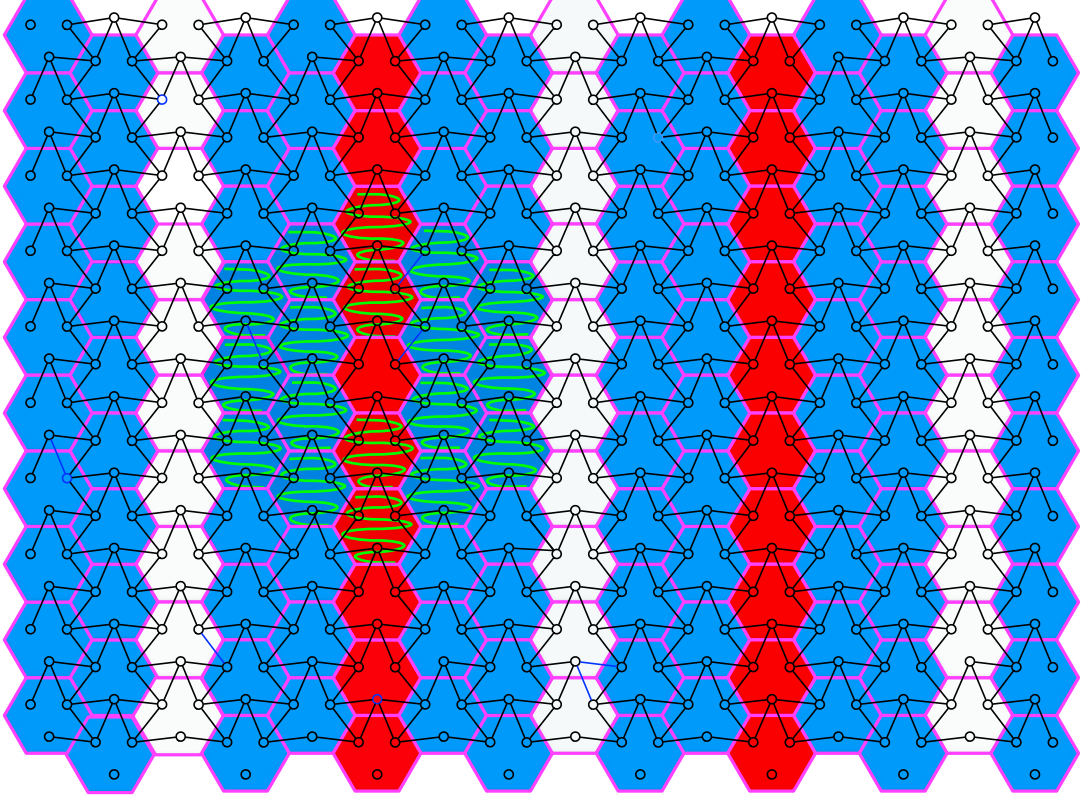


Figure 2.7: Proposed cell-partitioning for $\kappa = 2$. Observe that, for each red cell j , cooperation messages that is function of receive signals inside a 2-layer hexagonal region (e.g., cells squiggled with green) are required to decode the transmitted message \mathbf{W}_j .

To prove (2.28), fix a sequence of encoding, cooperation, and decoding functions $\{f_u^{(n)}\}$, $\{\psi_{j,i}^{k,(n)}\}$, and $\{h_u^{(n)}\}$ so that for sufficiently large blocklengths n the probability of error does not exceed $\epsilon > 0$. Notice that if the super-receiver performs the following six decoding steps, then it decodes all messages $\mathbb{W}_{\mathcal{T}}$ correctly whenever the N BSs decode them correctly in the original setup. Therefore, the super-receiver's probability of error can thus not be larger than the probability of error of the original setup.

The six decoding steps at the super-receiver are:

1. For each round $k = 1, \dots, \kappa$, it applies the appropriate cooperation functions $\{\psi_{j,i}^{k,(n)}\}$ to the output signals $\mathbb{Y}_{\mathcal{A}}$ to the previously computed cooperation messages $\{\mathbb{V}_{\mathcal{A}_r \rightarrow \mathcal{A}_b}^{k'}\}_{k'=1}^{k-1}$, $\{\mathbb{V}_{\mathcal{A}_b \rightarrow \mathcal{A}_r}^{k'}\}_{k'=1}^{k-1}$, $\{\mathbb{V}_{\mathcal{A}_r \rightarrow \mathcal{A}_r}^{k'}\}_{k'=1}^{k-1}$ and $\{\bar{\mathbb{V}}_{\mathcal{A}_b \rightarrow \mathcal{A}_b}^{k'}\}_{k'=1}^{k-1}$, so as to obtain the cooperation messages of the current round $\mathbb{V}_{\mathcal{A}_b \rightarrow \mathcal{A}_r}^k$, $\mathbb{V}_{\mathcal{A}_r \rightarrow \mathcal{A}_b}^k$, $\mathbb{V}_{\mathcal{A}_r \rightarrow \mathcal{A}_r}^k$ and $\bar{\mathbb{V}}_{\mathcal{A}_b \rightarrow \mathcal{A}_b}^k$. Then, it obtains $\mathbb{V}_{\text{to } \mathcal{A}_r}^k$. (Notice that knowledge of receive signals of \mathcal{B} cells or cooperation messages exchanged with \mathcal{B} cells are not required for this computation.)
2. It applies the appropriate decoding functions $\{h_j^{(n)}\}$ to the output signals $\mathbb{Y}_{\mathcal{A}_r}$ and the cooperation messages $\mathbb{V}_{\text{to } \mathcal{A}_r}^k$ so as to decode messages $\mathbb{W}_{\mathcal{A}_r}$.

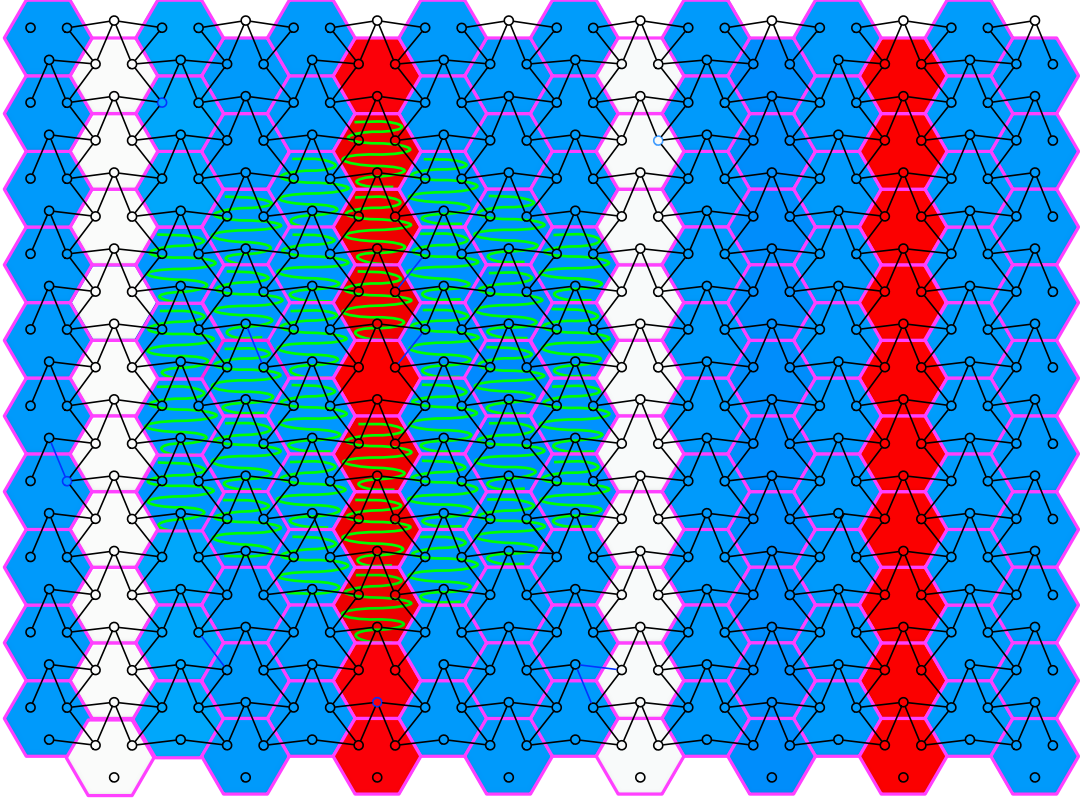


Figure 2.8: Proposed cell-partitioning for $\kappa = 3$. Observe that, for each red cell j , cooperation messages that is function of receive signals inside a 3-layer hexagonal region (e.g., cells squiggled with green) are required to decode the required message \mathbf{W}_j .

3. It applies the encoding functions $\{f_u^{(n)}\}$ to the previously decoded messages $\mathbb{W}_{\mathcal{A}_r}$ to construct input signals $\mathbb{X}_{\mathcal{A}_r}$.
4. With the transmit signals $\mathbb{X}_{\mathcal{A}_d}$, receive signals $\mathbb{Y}_{\mathcal{A}}$ and with the chosen genie-information \mathbb{G} , it reconstructs the output signals received at the BS of \mathcal{B} cells $\mathbb{Y}_{\mathcal{B}}$. To see this notice the following:

$$\begin{aligned} \mathbb{H}_{\mathcal{A}_r, \mathcal{A}}^{-1} \mathbb{Y}_{\mathcal{A}} &= \{ \mathbb{X}_{\mathcal{A}_r} + \hat{\mathbb{H}}_{\mathcal{A}_r, \mathcal{A}_b} \mathbb{H}_{\mathcal{A}_b, \mathcal{B}} \mathbb{X}_{\mathcal{B}} + \hat{\mathbb{H}}_{\mathcal{A}_r, \mathcal{A}_r} \mathbb{Z}_{\mathcal{A}_r} + \hat{\mathbb{H}}_{\mathcal{A}_r, \mathcal{A}_b} \mathbb{Z}_{\mathcal{A}_b}, \\ &\quad \mathbb{X}_{\mathcal{A}_b} + \hat{\mathbb{H}}_{\mathcal{A}_b, \mathcal{A}_b} \mathbb{H}_{\mathcal{A}_b, \mathcal{B}} \mathbb{X}_{\mathcal{B}} + \hat{\mathbb{H}}_{\mathcal{A}_b, \mathcal{A}_r} \mathbb{Z}_{\mathcal{A}_r} + \hat{\mathbb{H}}_{\mathcal{A}_b, \mathcal{A}_b} \mathbb{Z}_{\mathcal{A}_b} \}. \end{aligned}$$

Since, the number of \mathcal{A}_r cells are equal the number of \mathcal{B} cells $\hat{\mathbb{H}}_{\mathcal{A}_r, \mathcal{A}_b} \mathbb{H}_{\mathcal{A}_b, \mathcal{B}}$ is square and hence it is invertible. Therefore, we can write

$$\begin{aligned} \mathbb{X}_{\mathcal{B}} + (\hat{\mathbb{H}}_{\mathcal{A}_r, \mathcal{A}_b} \mathbb{H}_{\mathcal{A}_b, \mathcal{B}})^{-1} \hat{\mathbb{H}}_{\mathcal{A}_r, \mathcal{A}_r} \mathbb{Z}_{\mathcal{A}_r} - \hat{\mathbb{H}}_{\mathcal{A}_r, \mathcal{A}_b} \mathbb{Z}_{\mathcal{A}_b} &= (\hat{\mathbb{H}}_{\mathcal{A}_r, \mathcal{A}_b} \mathbb{H}_{\mathcal{A}_b, \mathcal{B}})^{-1} (\hat{\mathbb{H}}_{\mathcal{A}_r, \mathcal{A}_r} \mathbb{Y}_{\mathcal{A}_r} + \\ &\quad \hat{\mathbb{H}}_{\mathcal{A}_r, \mathcal{A}_b} \mathbb{Y}_{\mathcal{A}_b} - \mathbb{X}_{\mathcal{A}_r}) \end{aligned} \quad (2.41)$$

and

$$\begin{aligned} \mathbb{X}_{\mathcal{A}_b} + \hat{\mathbb{H}}_{\mathcal{A}_b, \mathcal{A}_r} \mathbb{Z}_r + \hat{\mathbb{H}}_{\mathcal{A}_b, \mathcal{A}_b} \mathbb{Z}_b &= \hat{\mathbb{H}}_{\mathcal{A}_b, \mathcal{A}_r} \mathbb{Y}_{\mathcal{A}_r} + \hat{\mathbb{H}}_{\mathcal{A}_b, \mathcal{A}_b} \mathbb{Y}_{\mathcal{A}_b} - \\ &\hat{\mathbb{H}}_{\mathcal{A}_b, \mathcal{A}_b} \mathbb{H}_{\mathcal{A}_b, \mathcal{B}} \mathbb{X}_{\mathcal{B}}. \end{aligned} \quad (2.42)$$

and, with the help of \mathbb{G} function, the received signal $\mathbb{Y}_{\mathcal{B}}$ can be reconstructed as follows:

$$\begin{aligned} \mathbb{Y}_{\mathcal{B}} &= \mathbb{H}_{\mathcal{B}, \mathcal{B}} (\hat{\mathbb{H}}_{\mathcal{A}_r, \mathcal{A}_b} \mathbb{H}_{\mathcal{A}_b, \mathcal{B}})^{-1} (\hat{\mathbb{H}}_{\mathcal{A}_r, \mathcal{A}_r} \mathbb{Y}_{\mathcal{A}_r} + \hat{\mathbb{H}}_{\mathcal{A}_r, \mathcal{A}_b} \mathbb{Y}_{\mathcal{A}_b} - \mathbb{X}_{\mathcal{A}_r}) + \\ &\mathbb{H}_{\mathcal{B}, \mathcal{A}_b} (\hat{\mathbb{H}}_{\mathcal{A}_b, \mathcal{A}_r} \mathbb{Y}_{\mathcal{A}_r} + \hat{\mathbb{H}}_{\mathcal{A}_b, \mathcal{A}_b} \mathbb{Y}_{\mathcal{A}_b} - \hat{\mathbb{H}}_{\mathcal{A}_b, \mathcal{A}_b} \mathbb{H}_{\mathcal{A}_b, \mathcal{B}} (\hat{\mathbb{H}}_{\mathcal{A}_r, \mathcal{A}_b} \mathbb{H}_{\mathcal{A}_b, \mathcal{B}})^{-1} \\ &(\hat{\mathbb{H}}_{\mathcal{A}_r, \mathcal{A}_r} \mathbb{Y}_{\mathcal{A}_r} + \hat{\mathbb{H}}_{\mathcal{A}_r, \mathcal{A}_b} \mathbb{Y}_{\mathcal{A}_b} - \hat{\mathbb{H}}_{\mathcal{A}_r, \mathcal{A}_r} \mathbb{Z}_r - \hat{\mathbb{H}}_{\mathcal{A}_r, \mathcal{A}_b} \mathbb{Z}_b - \mathbb{X}_{\mathcal{A}_r})) + \mathbb{G} \end{aligned} \quad (2.43)$$

5. It applies the appropriate decoding functions $\{h_u^{(n)}\}$ to the output signals $\mathbb{Y}_{\mathcal{A}}$ and $\mathbb{Y}_{\mathcal{B}}$ and to the κ -round cooperation messages $\mathbb{V}_{\text{to } \mathcal{A}_b}^{\kappa}$ and $\mathbb{V}_{\text{to } \mathcal{B}}^{\kappa}$ so as to decode messages $\mathbb{W}_{\mathcal{A}_b}$ and $\mathbb{W}_{\mathcal{B}}$.

Note that $\mathcal{B}_c = \emptyset$, therefore $n_c = 0$. Dividing by $|\mathcal{T}| = 3 \cdot N$ and letting $N \rightarrow \infty$ establish the desired bound (2.28) after noticing that

$$\overline{\lim}_{N \rightarrow \infty} \frac{|\mathcal{A}|}{N} = \frac{2 \cdot \kappa + 1}{2 \cdot \kappa + 2}. \quad (2.44)$$

2.5 DoF without Sectorization

A naive alternative to our scheme would be to ignore the interference pattern caused by the sectorization of the cells and to simply deactivate all mobile users in layer- t cells, and hence, it reduces the number of required cooperation rounds from $2t$ to $2(t-1)$ since the first and the last cooperation rounds of our protocol become useless when all layer- t users are deactivated. That is, to compare both scheme at $\kappa = 4$, we choose the master cells 5 cell-hops apart from each other and we deactivate all layer-"3" mobile users to create a naive scheme with $t = 2$ layers. Compared to our scheme this naive approach reduces the DoF from $M(1 - \frac{1}{3t})$ to $M(1 - \frac{3t+2}{3(t+1)^2})$ and increases the backhaul load prelog to $M \frac{t(2t+1)}{3(t+1)}$.

Therefore, the DoF of this naive approach is then given by

$$\text{DoF}_{\text{naive}} \geq \text{upp conv hull} \left\{ (\mu_{\text{naive}, t}, \text{DoF}_{\text{naive}, t}) : t = 0, \dots, \left\lfloor \frac{\kappa}{2} \right\rfloor \right\}. \quad (2.45)$$

where

$$\mu_{\text{naive}, t} = M \frac{t(2t+1)}{3(t+1)} \quad \text{for} \quad \text{DoF}_{\text{naive}, t} = M \left(1 - \frac{3t+2}{3(t+1)^2}\right) \quad (2.46)$$

for $t \in \left\{1, \dots, \left\lfloor \frac{\kappa}{2} \right\rfloor\right\}$, and

$$\mu_{\text{naive}, 0} = 0 \quad \text{and} \quad \text{DoF}_{\text{naive}, 0} = \frac{M}{3}. \quad (2.47)$$

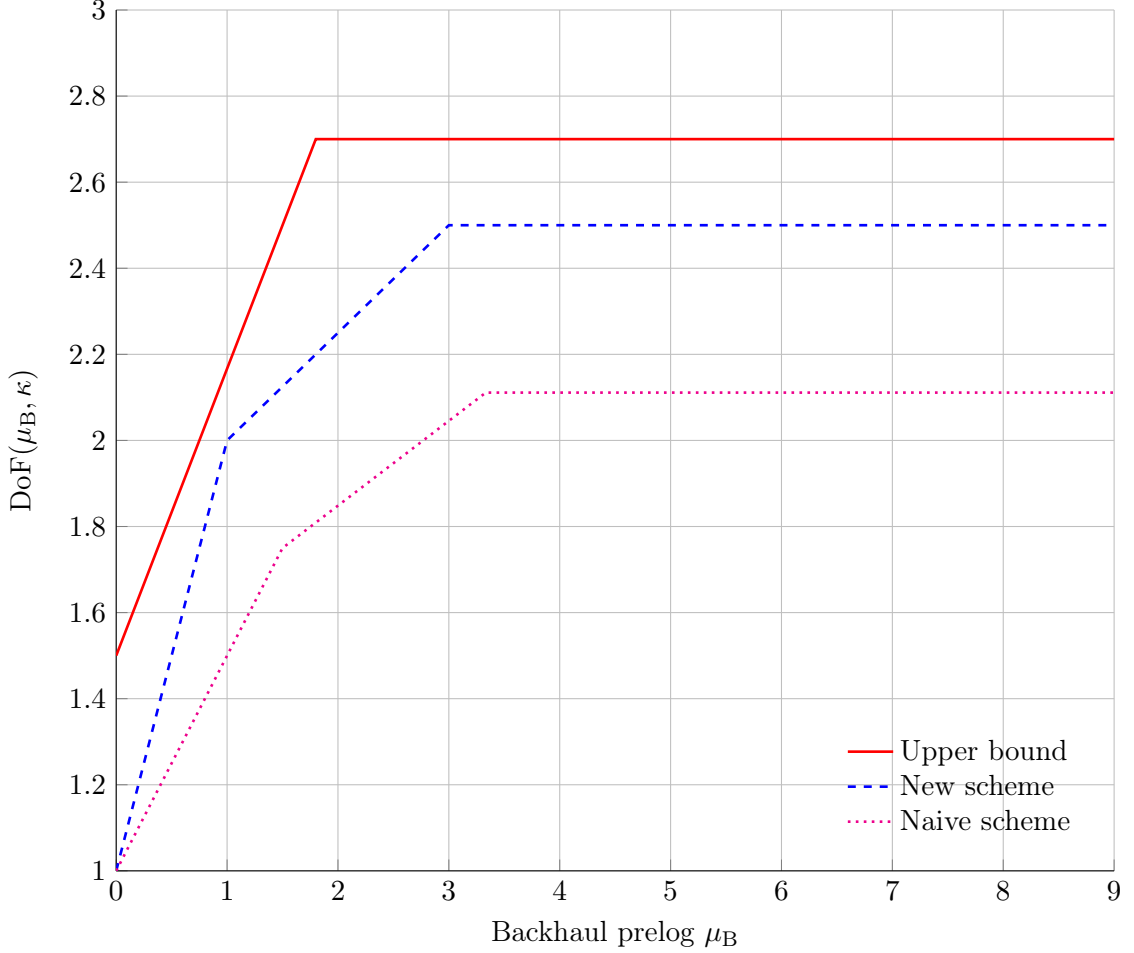


Figure 2.9: Lower and upper bounds on the DoF in function of μ_B for $M = 3$ and $\kappa = 4$.

Here, $\text{DoF}_{\text{naive},0} = \frac{M}{3}$ is obtained by silencing all layer-"1" cells after choosing active cells as if choosing master cells for $t = 1$ scheme.

The Figures 2.9 and 2.10 compare the proposed lower bound in Theorem 2.1 with the lower bound achieved by the naive approach. The figure also shows an information theoretic upper bound. Notice that the lower bounds on the DoF are based on practically implementable coding schemes. In particular, classical interference alignment is not used, even though it is known to achieve a DoF of $M/2$ over a generic network in the absence of BS cooperation. In contrast, the information-theoretic upper bound holds for any possible coding scheme, obviously including interference alignment. It is thus natural that the presented upper and lower bounds match only approximately.

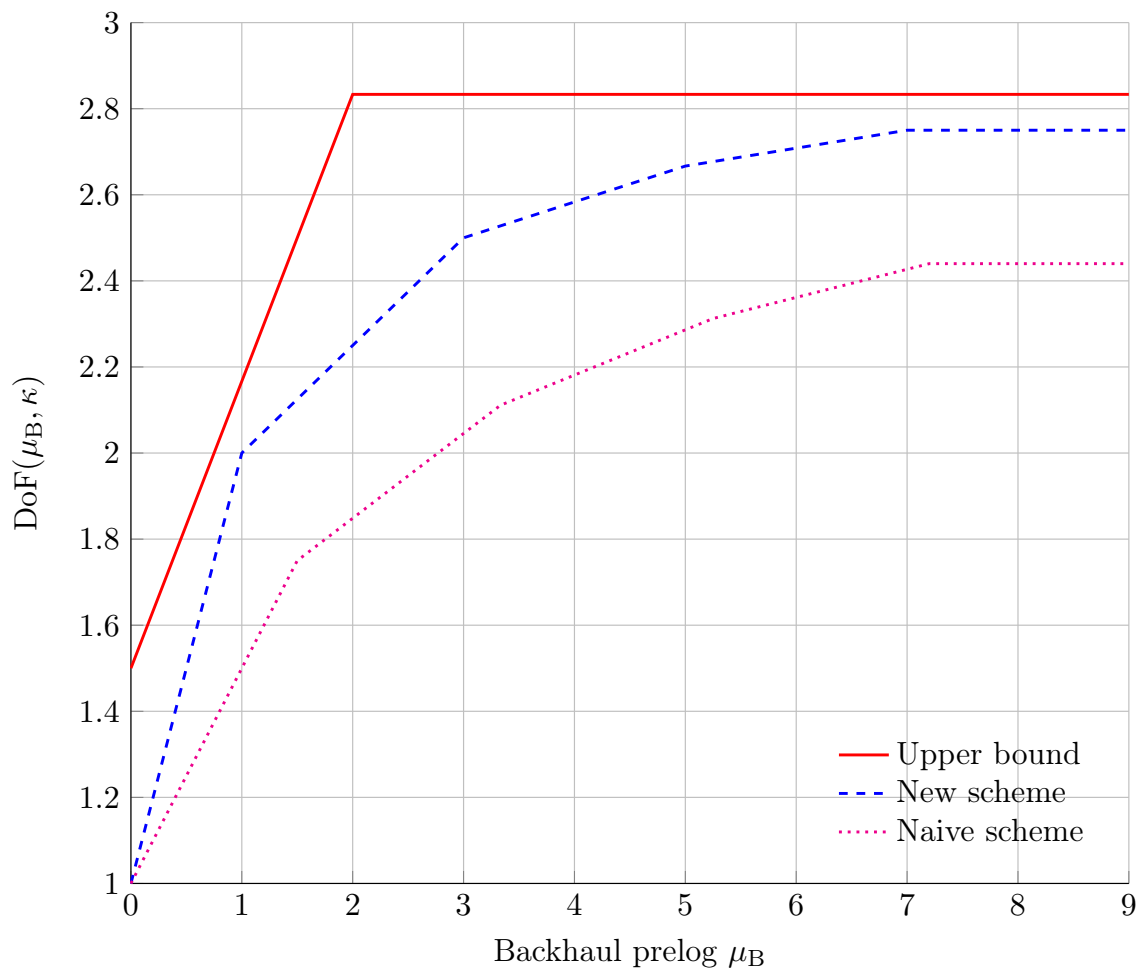


Figure 2.10: Lower and upper bounds on the DoF in function of μ_B for $M = 3$ and $\kappa = 8$.

2.6 Finite SNR Analysis

In this section, we proceed the finite SNR analysis of the proposed h-clustering scheme and compare it with the schemes where there is no deactivated users and a practical scheme, which will be explained in the following, and the naive scheme explained in Section 2.5. In the analysis, since the finite SNR DoF is measured by (1.3), we assume that the backhaul capacity between any two adjacent BSs proportionates with $\frac{1}{2} \log(1 + MP)$, i.e.,

$$C_B = \mu_B \cdot \frac{1}{2} \log(1 + MP), \quad (2.48)$$

where M is the number of antennas at Rx side. However, for simplicity, we assume that all users and sectors have single antenna throughout the section and impose that received signal of each sector antenna is quantized with independent poin-to-point Gaussian quantizer at the same rate. For any hexagon cluster of size- t , due to time-sharing, the quantization rate R_q for each user is chosen as

$$R_q = \frac{3\mu_B}{(2t-1)} \cdot \frac{1}{2} \log(1 + P) \quad (2.49)$$

for the given backhaul capacity prelog μ_B by (2.23).

In view of the clustering symmetry, we focus on only one cluster and only one instant of time-sharing. We proceed the analysis over time- n' signals and, for simplicity, we drop the time subscripts. For any hexagon of size- t , let $\mathcal{N}_t = \{1, \dots, 9t^2 - 3t\}$ denote the index set of sectors, and as defined before, let \mathcal{T}_u denote the index set of users whose transmitted signals are observed by Rx u (i.e., \mathcal{T}_u includes index u). The received signal at Rx $u \in \mathcal{N}_t$ is

$$Y_u = \mathbf{h}_u \mathbf{X}_t + Z_u \quad (2.50)$$

where $\mathbf{h}_u = [h_{u,1}, \dots, h_{u,9t^2-3t}]$ with $h_{u,v} = 0$ for $v \notin \mathcal{T}_u$ is channel vector and $\mathbf{X}_t = [X_1, \dots, X_{9t^2-3t}]^T$ is transmitted signal vector of the users in the cluster. After quantization process, except sectors of master cell, each sector $u \in \mathcal{N}_t$ obtains the quantization signal

$$\hat{Y}_u = Y_u + Z_{q,u} \quad (2.51)$$

where $Z_{q,u} \sim \mathcal{N}(0, \sigma_{q,u}^2)$. The requirement of having equal quantization rate imposes that the quantization variance for each sector is chosen differently, which is determined as follows:

$$R_q = I(\hat{Y}_u; Y_u) \quad (2.52)$$

$$= h(\hat{Y}_u) - h(\hat{Y}_u | Y_u) \quad (2.53)$$

and, since the transmitted signals and quantization noise is Gaussian, \hat{Y}_u is also Gaussian, which leads to

$$h(\hat{Y}_u) = \frac{1}{2} \log(2\pi e \sigma_{\hat{Y}_u}^2) = \frac{1}{2} \log(2\pi e (P \|\mathbf{h}_u\|^2 + \sigma_{q,u}^2 + 1)). \quad (2.54)$$

Then, the quantization variance is obtained as

$$\sigma_{q,u}^2 = \frac{P \|\mathbf{h}_u\|^2 + 1}{2^{2R_q} - 1}. \quad (2.55)$$

After reconstruction at master cell, the received signal vector is given by

$$\hat{\mathbf{Y}}_t = \mathbf{H}_t \mathbf{X}_t + \mathbf{Z}_{q,t} + \mathbf{Z}_t \quad (2.56)$$

where

- $\hat{\mathbf{Y}}_t = [\hat{Y}_1, \dots, \hat{Y}_{9t^2-3t}]^T$ is the reconstructed signal vector;
- $\mathbf{H}_t = [\mathbf{h}_1^T, \dots, \mathbf{h}_{9t^2-3t}^T]^T$ is the channel matrix of the cluster;
- $\mathbf{Z}_{q,t} = [Z_{q,1}, \dots, Z_{q,9t^2-3t}]^T$ is the quantization noise vector obtained at sectors of the cluster where the quantization noises of master cell sectors are zero;
- $\mathbf{Z}_t = [Z_1, \dots, Z_{9t^2-3t}]^T$ is the noise vector observed at sector receivers of cluster.

The average rate per-user for any time sharing instant is then obtained by equally partitioning the deactivated users to hexagon clusters

$$R_{\text{avg},t} = \frac{1}{9t^2} I(\hat{\mathbf{Y}}_t; \mathbf{X}_t) \quad (2.57)$$

$$= \frac{1}{9t^2} \frac{1}{2} \log \frac{|P \mathbf{H}_t \mathbf{H}_t^T + \mathbf{K}_{q,t} + \mathbf{I}_{|\mathcal{N}_t|}|}{|\mathbf{K}_{q,t} + \mathbf{I}_{|\mathcal{N}_t|}|} \quad (2.58)$$

where $\mathbf{K}_{q,t}$ is the covariance matrix of the quantization noise vector and has only diagonal elements due to independent quantization codebooks. Note that the average rate per-user is obtained by averaging over all time sharing instants.

To evaluate the performance of the proposed scheme at finite SNR, we numerically compare this rate to the rates of the naive scheme introduced in Section 2.5 and the following two schemes:

- First scheme is a variation of our proposed scheme, in which the network is decomposed into non-overlapping but interfering clusters regarding the parameter t . Note that there are $6t$ deactivated users around a cluster of size- t . For a specific cluster, we associate the deactivated users on the borders of any three adjacent clusters, e.g. east, south-east and south-west, to the cluster under consideration. Then, we replicate this process for each cluster with the same relative directions of adjacent clusters.

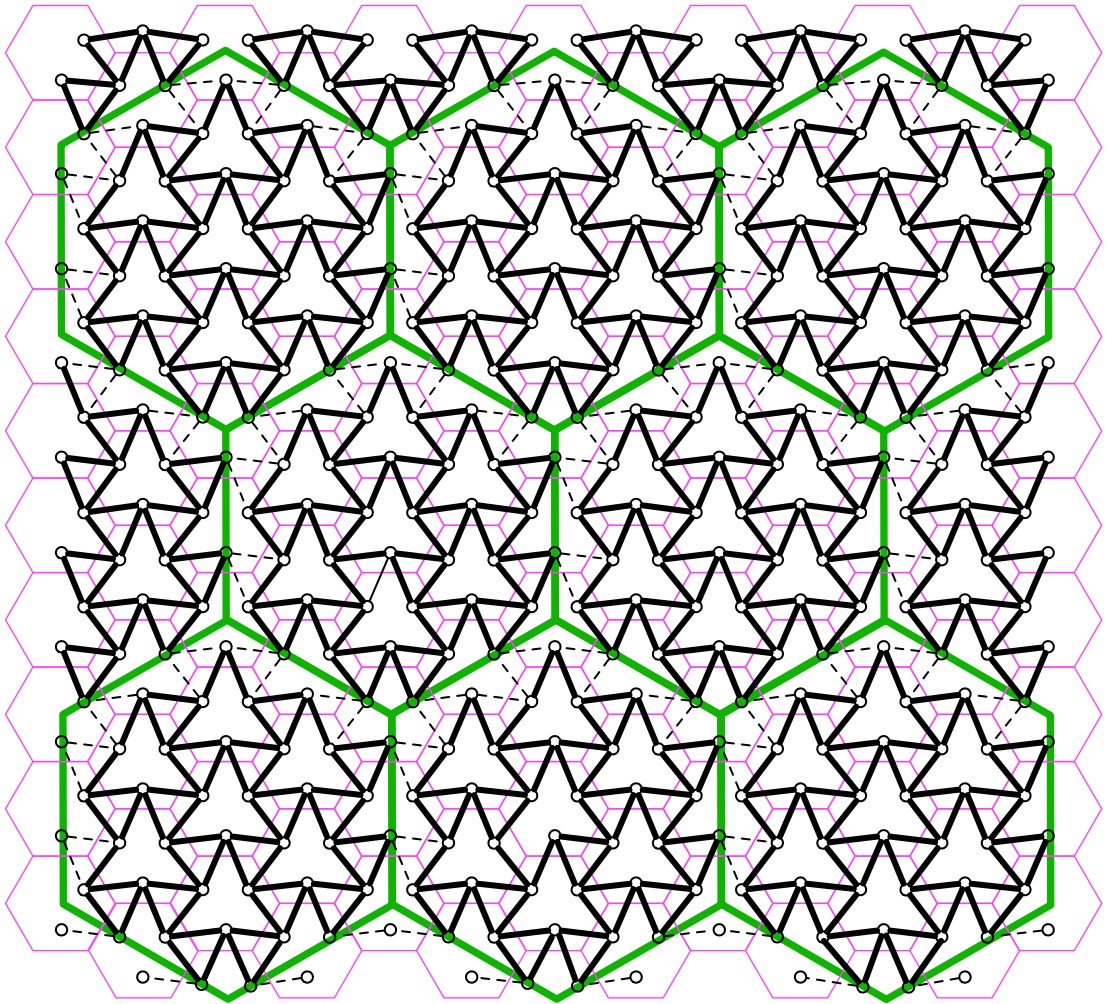


Figure 2.11: Decomposition of network into non overlapping but interfering clusters for $t = 2$.

Subsequently, we activate all deactivated users and, for joint decoding, and each master BS collects also the quantized messages of received signals of reactivated users in t -rounds. This process partitions the network into interfering but non-overlapping clusters, which we call I_h -cluster throughout the chapter. An example of such a partition for $t = 2$ is shown in Figure 2.11, where the circles connected with solid lines represents I_h -cluster users and sectors, the dashed lines separate different I_h -clusters.

- Second scheme is inspired by current practical systems. The decoding depends on the realization of the channel coefficients. With the help of its neighbors, each BS identifies for each user in its cell the 3 adjacent sectors that give the best **joint** decoding performance for the corresponding message. It then collects the (quantized versions of) these $3M$ output signals, and based on them decodes the desired messages. (Notice that this scheme only involves one collaboration step and hence can be implemented for any positive cooperation complexity $\kappa \geq 1$.)

By following the similar arguments for the backhaul load analysis of the proposed

scheme in Section 2.3.2, one can easily obtain the quantization rate R_{q_i} for each sector as

$$R_{q_i} = \frac{3\mu_B}{2t} \cdot \frac{1}{2} \log(1 + P). \quad (2.59)$$

The average per-user rate is obtained by following the similar arguments applied for the proposed scheme by treating out-of-cluster interference as noise.

In our numerical comparison, we average the rate over 10000 realizations of the channel matrices, where for each realization all channel gains are drawn independently of each other according to the standard Gaussian distribution. The cross channel gains of inter-sector links however are multiplied with α , where α models the path attenuation. Figures 2.12 and 2.13 show the average rates of the different schemes as a function of the SNR in dB for different choices of the path loss factor $\alpha \in \{0.25, 0.8\}$, the backhaul capacity prelog $\mu_B \in \{1, 5\}$, and the maximum allowed cooperation complexity $\kappa = 4$. When $\kappa = 4$, two different choices for the parameter t are possible. For all the clustering schemes, the choices $t = 1$ or $t = 2$ are allowed. Notice that for a given quantization rate, it is always beneficial to choose t as large as possible because it increases the benefit of cooperation. However, the larger t , the more backhaul capacity is required. For a fixed backhaul capacity it can thus be beneficial to choose a smaller t which allows to increase the quantization rate and thus the quality of the master BS's observations. Our numerical results reveal that, for $\mu_{\text{DoF}} = 1$ and $\alpha = 0.25$, it is optimal to choose parameter $t = 1$ for SNRs below 12 dB in the h-clustering, for SNRs below 18 dB in the I_h -clustering and for SNRs below 24 dB in the naive scheme. For a larger backhaul DoF, e.g., $\mu_{\text{DoF}} = 5$, the choice $t = 2$ is optimal for all SNRs. For $\alpha = 0.25$ and $\mu_{\text{DoF}} = 5$, large quantization rates are available for all choices of t , and as a consequence this parameter should be chosen as large as possible in all schemes and at all power levels. Similar observations hold also under a strong interference assumption that we model as $\alpha = 0.8$.

Comparing Figures 2.12 and 2.13, we observe that the practical scheme outperforms the others until moderate SNR levels when $\alpha = 0.25$ and $\mu_B = 1$. At higher SNRs however the performance of the practical scheme significantly degrades compared to the other schemes. We also observe that the h-clustering scheme performs always better than the practical scheme under strong interference, i.e., $\alpha = 0.8$. For large backhaul capacity, the I_h -clustering outperforms the others at high and moderate SNRs for $\alpha = 0.25$ and $\alpha = 0.8$, respectively. The h-clustering scheme outperforms all other schemes for sufficiently large powers, irrespectively of the available backhaul capacity.

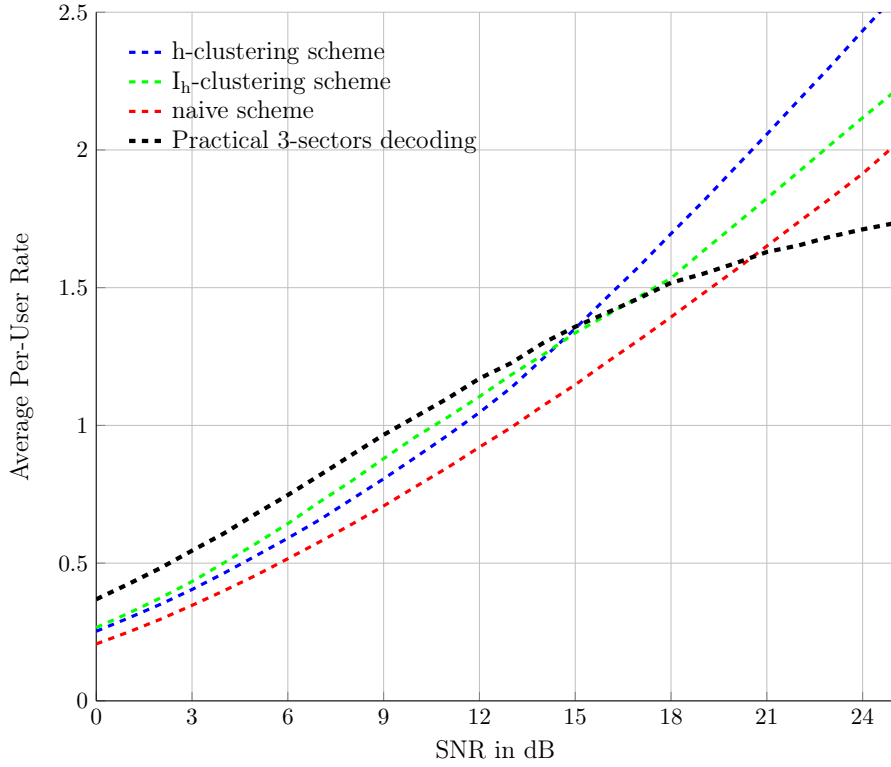
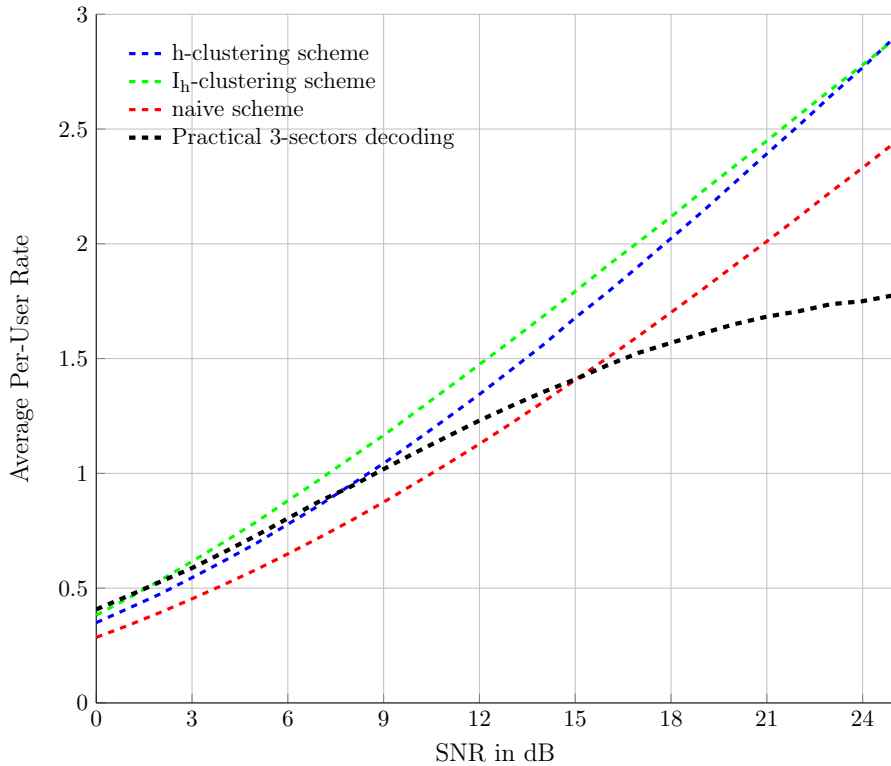
(a) For $\mu_B = 1$.(b) For $\mu_B = 5$.

Figure 2.12: Performance comparison of hexagonal like schemes and practical scheme for $\kappa = 4$ and $\alpha = 0.25$.

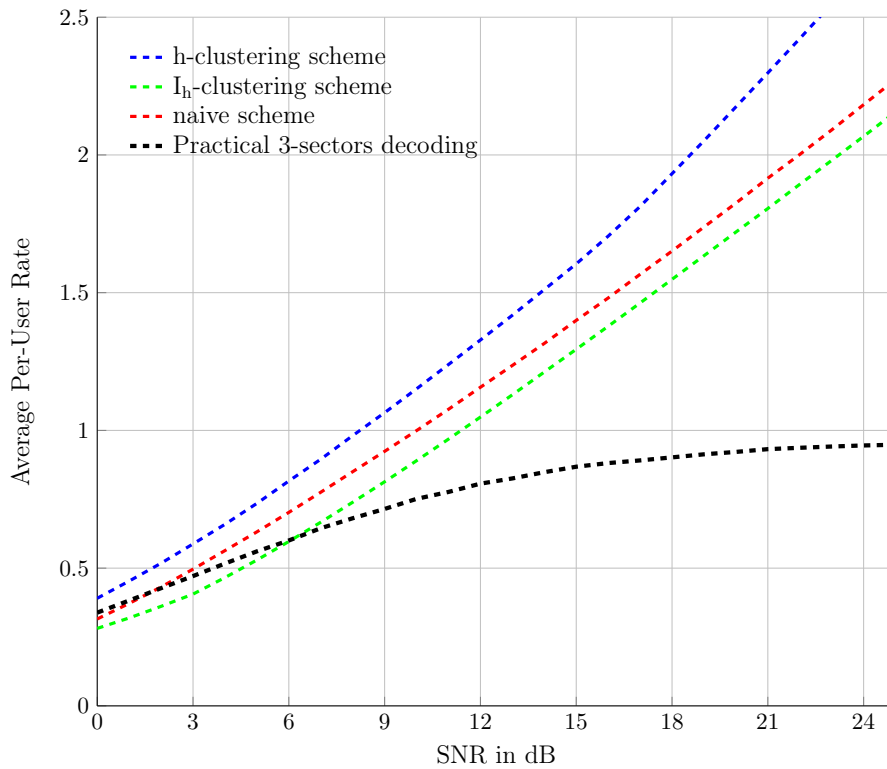
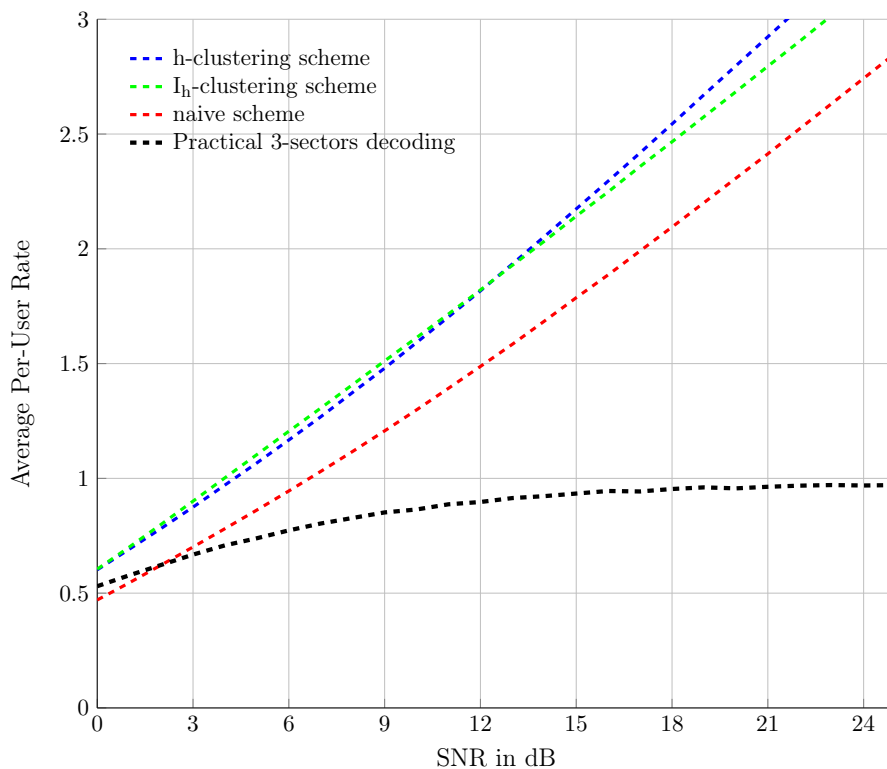
(a) For $\mu_B = 1$.(b) For $\mu_B = 5$.

Figure 2.13: Performance comparison of hexagonal like schemes and practical scheme for $\kappa = 4$ and $\alpha = 0.8$.

2.7 Summary

The chapter presents upper and lower bounds on the DoF of the uplink of a sectored cellular network with backhaul cooperation between BSs. Main feature of the proposed results is that DoF is characterized as function of the **backhaul rate** and the **maximum** number of allowed **cooperation rounds**. The presented results show that limiting the number of cooperation rounds also limits the achievable DoF over the network. In particular, by Theorem 2.1, to get a DoF of M an infinite number of cooperation rounds is required as the number of cells in the network grows. When the number of cooperation rounds does not grow with the number of cells but is bounded, then also the DoF is bounded away from M , even in the idealized case of an unlimited backhaul cooperation rate. The upper bound is information-theoretic and applies to any coding scheme. It is generally close to the obtained lower bounds on the DoF.

The obtained lower bound on the DoF is based on a simple practically implementable scheme: the transmitting mobiles use Gaussian point-to-point codes; receiving BSs apply point-to-point vector quantizer to their M -dimensional receive signals and send the quantization messages over the backhaul links to the so called master BSs. Each master BS decodes messages in the corresponding h-cluster based on its own receive signals and the quantization signals that it receives over the backhaul links. Thus, no advanced tools such as interference alignment are required. The main novelty of the scheme is the proposed choice of which mobiles remain silent and which transmit their messages. In fact, this choice exploits the sectorization of the network and is done in a way that only few users remain silent but the network still decomposes into non-interfering clusters. The decomposition ensures that interference is not propagated across clusters and therefore facilitates decoding at the BSs.

The finite SNR analysis shows that the idea of partitioning the network into non-interfering clusters regarding delay parameter κ provides higher performance than the interfering clustering case except low SNR regime when the backhaul prelog is high enough to have small quantization error. For practical considerations, it is also deduced that the small delay parameters achieves higher sum-rate than larger ones if the backhaul capacity is not high enough to handle the data traffic of larger clusters.

It is straightforward to obtain the dual results also for the downlink. To this end, BSs should first send messages to their closest master cells, which then **jointly encodes all its available messages**, i.e., it pre-calculates the transmit signals at the closeby BSs. These transmit signals are quantized and distributed over the backhaul links to their respective BSs, which in their turn send these quantized signals over the network. Mobile users apply simple point-to-point reception techniques. This however does not limit their achievable DoF if the master cell has well encoded the messages, i.e., has chosen a good precoding matrix.

Chapter 3

Benefits of Local MCP in Multi-Cloud Based Sectorized Cellular Networks

3.1 Introduction

The main interest of this chapter is to understand highest achievable **DoF per-user**, referred to as DoF in short throughout this chapter, and achievable **sum-rate** in a multi cloud based sectorized cellular networks (M-CRAN), when the local MCP is constrained by limited fronthaul capacity, BBUP processing capacity, and BBUP-BS ratio. We propose two coding schemes in each of which some mobile users are deactivated to decompose the network into isolated parallelogram and hexagonal clusters, respectively. For both clustering types, the minimum number of mobile users/sectors are determined regarding BBUP-BS ratio due to one-to-one association between BBUPs and clusters. Then, each BBUP collects quantized versions of the received signals of the associated cluster through fronthaul links and jointly decodes all received signals. The considered decoding scheme is thus reminiscent of clustered decoding as performed in [31, 29].

The upper bound in this paper is obtained through a cut-set argument. In several cases, we show the optimality of our coding schemes. For small and moderate fronthaul capacities, the achievability gap is given as a function of fronthaul capacity and BBUP-BS ratio irrespective of processing capacity.

Finite SNR analysis shows that the proposed coding schemes outperform the case in which the network is decomposed into non-overlapping but interfering clusters at all SNR values. The only exception of the superiority of the proposed scheme is at low SNR when the fronthaul or BBUP processing capacity is scarce so that quantization rate is low.

Overall, the information theoretic analysis in this chapter provides intuition about how to group the sectors and users to have higher gains for the given system parameters in a M-CRAN network.

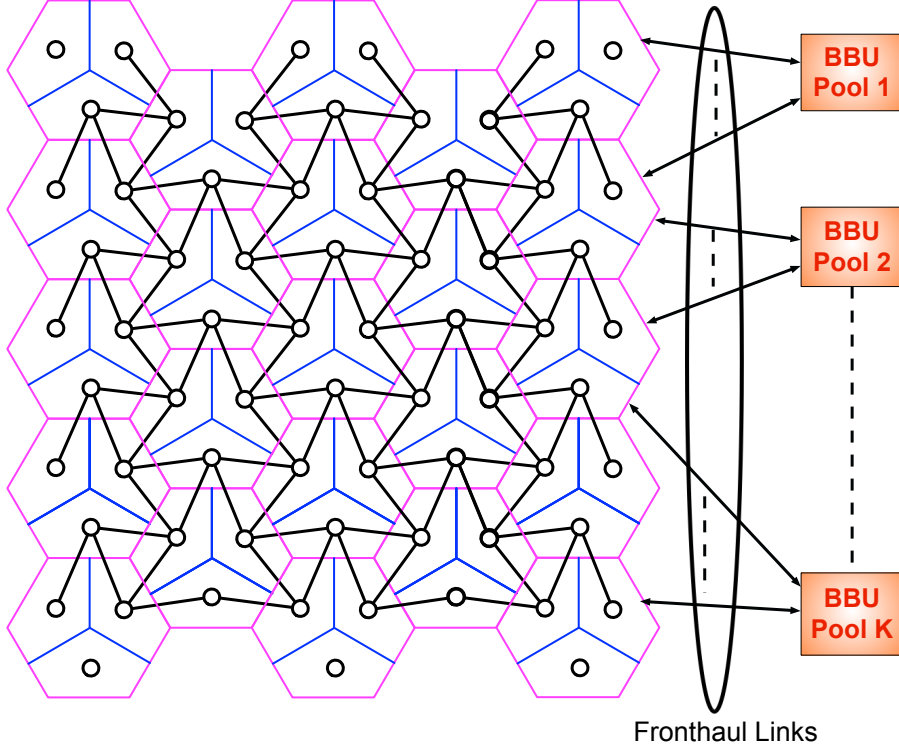


Figure 3.1: Multi-cloud based Sectored Cellular Network.

The rest of the chapter is organized as follows. In Section 3.2, the network and communication model are presented. The obtained results are given in Section 3.3. The proposed coding schemes are presented in Sections 3.4 and 3.5. The DoF analysis without sectorization is carried out in Section 3.6. In Section 3.7, numerical evaluation of the analytical results is presented and discussed. In Section 3.8, the finite SNR analysis is performed and the corresponding results are presented, and the article is concluded with Section 3.9.

3.2 Problem Definition

3.2.1 Network Model

Consider the uplink communication in a cellular network consisting of $N \gg 1$ hexagonal cells as depicted in Figure 3.1. Each single cell contains a base station (BS) equipped with $3M$ directional receive antennas and is divided into three sectors, where each sector is covered by M antennas. Usage of directional antennas, where side lobe radiation patterns are negligible, implies that communications in the three sectors of a cell do not interfere with each other. It is assumed that different mobile users in the same sector perform orthogonal multiple-access as is typical for current 4G networks [54]. Thus, the model is restricted to a single mobile user per sector. For simplicity and symmetry, it is supposed that each mobile user is equipped with M transmit antennas.

Due to the shadowing effects and distance dependent loss [41], it is assumed that the signal from a mobile user attenuates rapidly enough so that it cannot cause interference to sector antennas (Rx) in non-adjacent sectors. These assumptions lead to the interference graph in Figure. 3.1, where each small circle depicts a mobile user and Rx pair. Solid black lines between any two circles represent symmetric interference between mobile users and Rxs of adjacent sectors. Let $\mathcal{N} = \{1, \dots, N\}$ be index set of all cells and associated BS in the network, and let $\mathcal{T} = \{1, \dots, 3N\}$ be index set of all sectors and their corresponding users and Rxs. Then, the observed signal at the Rx $u \in \mathcal{T}$ is given by the following discrete-time input-output relation:

$$\mathbf{y}_{u,n'} = \sum_{v \in \mathcal{T}_u} \mathbf{H}_{u,v} \mathbf{x}_{v,n'} + \mathbf{z}_{u,n'}, \quad n' \in \{1, \dots, n\}, \quad (3.1)$$

where

- n denotes the number of channel use;
- \mathcal{T}_u denotes the index set of mobile users whose transmitted signal is observed by Rx u (including mobile user u);
- $\mathbf{x}_{v,n'}$ denotes the M -dimensional time- n' signal sent by mobile user v ;
- $\mathbf{z}_{u,n'}$ denotes the M -dimensional i.i.d. standard Gaussian noise vector corrupting the time- n' signal at Rx u ; it is independent of all other noise vectors;
- and $\mathbf{H}_{u,v}$ denotes an M -by- M dimensional random matrix with entries that are independently drawn according to a standard Gaussian distribution that models the channel from mobile user v to Rx u .

Channel matrices are randomly drawn but assumed constant over the n channel uses employed for the transmission of a message. In other words, the block length of a transmission is assumed shorter than the coherence time of the channel. Realizations of the channel matrices are assumed to be known at Rx side, but not the mobile users (Txs).

3.2.2 Uplink Communication Model with M-CRAN Architecture

Consider the network model defined in Section 3.2.1. Assume that the mobile user in sector $u \in \mathcal{T}$ wishes to send its message W_u , which is selected at random from the set $\{1, \dots, 2^{nR_u}\}$, to the BS in which its sector is located. To this end, mobile user u encodes its message with the function

$$f_u^{(n)} : \mathcal{W}_u \rightarrow \mathbb{R}^{M \times n}, \quad W_u \mapsto \mathbf{X}_u^{(n)} \quad (3.2)$$

where $\mathbf{X}_u^{(n)} = (\mathbf{X}_{u,1}, \dots, \mathbf{X}_{u,n})$, and $\mathbf{X}_{u,i} \in \mathbb{R}^M$ is a column vector for $n' = 1, \dots, n$. We impose the power constraint

$$\frac{1}{n} \sum_{n'=1}^n \|\mathbf{X}_{u,n'}\|^2 \leq P \quad \text{with probability 1.} \quad (3.3)$$

For decoding, assume that the decoding processes of receive signals during the uplink communication is implemented by K BBUPs, where $K \leq N$, and that any BS $j \in \mathcal{N}$ can have access to any BBUP $k \in \{1, \dots, K\}$ through one-hop fronthaul link which can be modelled as noise-free but capacity limited.

Definition 3.1 (Observation Function). *Let \mathcal{U}_k be the index set of BSs communicating to BBUP k . Each BS $j \in \mathcal{U}_k$ sends an **observation function**, $\phi_{j,k}^{(n)}(\mathbf{Y}_{B_j}^{(3n)})$, to BBUP k , where*

$$\phi_{j,k}^{(n)} : \mathbb{R}^{M \times 3n} \rightarrow \mathbb{R}, \quad (3.4)$$

and

$$\mathbf{Y}_{B_j}^{(3n)} := \left(\mathbf{Y}_{u_{j,1}}^{(n)}, \mathbf{Y}_{u_{j,2}}^{(n)}, \mathbf{Y}_{u_{j,3}}^{(n)} \right), \quad (3.5)$$

with $u_{j,1}$, $u_{j,2}$, and $u_{j,3}$ denoting the three sectors of BS j .

To account for capacity limits of the fronthaul links, we require

$$\frac{1}{n} \sum_{k=1}^K H \left(\phi_{j,k}^{(n)} \left(\mathbf{Y}_{B_j}^{(3n)} \right) \right) \leq C_F, \quad \forall j, \quad (3.6)$$

where

$$C_F = \mu_F \cdot \frac{1}{2} \log P, \quad (3.7)$$

and μ_F is **fronthaul capacity prelog**, which is a positive constant.

Let \mathcal{D}_k be the index set of sectors whose messages are to be decoded at BBUP k . After receiving observation functions, for each BBUP k and each $u \in \mathcal{D}_k$, BBUP k applies a deterministic and invertible function $g_{k,u}^{(n)}$ on the relevant observation functions to decode the message W_u :

$$\hat{W}_u = g_{k,u}^{(n)} \left(\left\{ \phi_{l,k}^{(n)} \left(\mathbf{Y}_{B_l}^{(3n)} \right) \right\}_{l \in \mathcal{U}_k} \right). \quad (3.8)$$

Decoding is successful if, for all $u \in \mathcal{T}$:

$$\hat{W}_u = W_u. \quad (3.9)$$

Increasing computational power of a processor leads to increase in complexity. Hence, to take the computational limitation into consideration, we impose a complexity constraint on the BBUPs in terms of **bit processing capacity** per channel use. We assume that any BBUP k can implement the decoding process if and only if the sum rate of all observation functions that is sent to BBUP k satisfies

$$\frac{1}{n} \sum_{j \in \mathcal{U}_k} H \left(\phi_{j,k}^{(n)} \left(\mathbf{Y}_{B_j}^{(3n)} \right) \right) \leq C_{\text{BBU}}, \quad \forall k, \quad (3.10)$$

where

$$C_{\text{BBU}} = \mu_{\text{BBU}} \cdot \frac{1}{2} \log P, \quad (3.11)$$

and μ_{BBU} is **processing capacity prelog**, which is a positive constant.

3.2.3 Capacity and Degrees of Freedom

A rate-tuple $\{R_u\}_{u \in \mathcal{T}}$ is said to be achievable if for every $\epsilon > 0$ and sufficiently large n there exists encoding, observation, and decoding functions $\{f_u^{(n)}\}$, $\{\phi_{j,k}^{(n)}\}$, and $\{g_{k,j}^{(n)}\}$ satisfying (3.3), (3.6) and (3.10), such that

$$\Pr \left[\bigcup_{u \in \mathcal{T}} \{\hat{W}_u \neq W_u\} \right] \leq \epsilon. \quad (3.12)$$

The **capacity region** $\mathcal{C}(P, \mu_F, \mu_{\text{BBU}}, K)$ is the closure of all achievable rate-tuples $\{R_u\}_{u \in \mathcal{T}}$, and the **maximum sum-rate** is defined as

$$\mathcal{C}_\Sigma(P, \mu_F, \mu_{\text{BBU}}, K) = \sup \sum_{u \in \mathcal{T}} R_u \quad (3.13)$$

where the supremum is over all achievable rates $\{R_u\}_{u \in \mathcal{T}} \in \mathcal{C}(P, \mu_F, \mu_{\text{BBU}}, K)$.

Definition 3.2 (Per-user DoF). *For any BBUP-BS ratio $r \in (0, 1]$, fronthaul capacity prelog $\mu_F > 0$ and processing capacity prelog $\mu_{\text{BBU}} > 0$, the per user DoF is given as*

$$\text{DoF}(\mu_F, \mu_{\text{BBU}}, r) := \lim_{N \rightarrow \infty} \lim_{P \rightarrow \infty} \frac{\mathcal{C}_\Sigma(P, \mu_F, \mu_{\text{BBU}}, r \cdot N)}{|\mathcal{T}| \cdot \frac{1}{2} \log P}. \quad (3.14)$$

3.3 Main Results

We present two lower bounds and an upper bound on the DoF. As we will show, they match in some cases. The first and second lower bounds are achieved by the schemes described in Section 3.4 and 3.5, respectively. Both of the schemes are based on deactivating some set of mobile users. In each scheme, the mobile users are deactivated in a way that, in the first scheme, the remaining active users form **parallelogram-like** clusters, and in the second, the remaining active users form **hexagon-like** clusters. In the rest we name them as **parallelogram bound** and **hexagon bound**, respectively. In Section A.1, it is shown that, for $\mu_F \leq 2M$, parallelogram bound achieves at least the same performance as hexagon bound.

Theorem 3.1 (Lower Bound). *For any $\mu_{\text{BBU}} > 0$, $\mu_F > 0$, and $0 < r \leq 1$, the achievable DoF is given by*

$$\text{DoF}(\mu_{\text{BBU}}, \mu_F, r) \geq \text{conv hull} \{ \text{DoF}_P(\mu_{\text{BBU}}, \mu_F, r), \text{DoF}_H(\mu_{\text{BBU}}, \mu_F, r) \} \quad (3.15)$$

where

$$\text{DoF}_P(\mu_{\text{BBU}}, \mu_F, r) = \begin{cases} \max_{t_1, t_2} \min \left\{ \frac{\mu_F}{3}, \frac{\mu_{\text{BBU}}}{3t_1 t_2} \right\}, & \text{if } \mu_F \leq M \\ \max_{t_1, t_2} \min \left\{ \frac{M + \mu_F(t_1 t_2 - 1)}{3t_1 t_2}, \frac{\mu_{\text{BBU}}}{3t_1 t_2} \right\}, & \text{if } M \leq \mu_F \leq 2M \\ \max_{t_1, t_2} \min \left\{ \frac{M(2t_1 + 2t_2 - 3) + \mu_F(t_1 t_2 - t_1 - t_2 + 1)}{3t_1 t_2}, \frac{\mu_{\text{BBU}}}{3t_1 t_2} \right\}, & \text{if } 2M \leq \mu_F \leq 3M \\ \max_{t_1, t_2} \min \left\{ M \left(1 - \frac{(t_1 + t_2)}{3t_1 t_2} \right), \frac{\mu_{\text{BBU}}}{3t_1 t_2} \right\}, & \text{if } 3M \leq \mu_F \end{cases} \quad (3.16)$$

where above maximizations are over all positive integers t_1, t_2 satisfying $t_1 t_2 \geq \lceil \frac{1}{r} \rceil$, and

$$\text{DoF}_H(\mu_{\text{BBU}}, \mu_F, r) = \begin{cases} \max_t \min \left\{ \mu_F \frac{3t^2 - 1}{9t^2}, \frac{\mu_{\text{BBU}}}{9t^2} \right\}, & \text{if } \mu_F \leq 2M \\ \max_t \min \left\{ \frac{M(6t - 6) + \mu_F(3t^2 - 3t + 2)}{9t^2}, \frac{\mu_{\text{BBU}}}{9t^2} \right\}, & \text{if } 2M \leq \mu_F \leq 3M \\ \max_t \min \left\{ M \frac{3t - 1}{3t}, \frac{\mu_{\text{BBU}}}{9t^2} \right\}, & \text{if } 3M \leq \mu_F \end{cases} \quad (3.17)$$

where above maximizations are over all positive integers t satisfying $t \geq \lceil \sqrt{\frac{1}{3r}} \rceil$.

Proof: The proof is given Sections 3.4 and 3.5.

Remark 3.1. For $\mu_{\text{BBU}} \geq 0$ and $0 < r \leq 1$

$$\text{DoF}_P(\mu_{\text{BBU}}, \mu_F, r) \supseteq \text{DoF}_H(\mu_{\text{BBU}}, \mu_F, r), \quad \text{for } \mu_F \leq 2M.$$

Proof: The proof is given in Appendix A.1.

Theorem 3.2 (Cut-Set Bound). For any $\mu_{\text{BBU}} > 0$, $\mu_F > 0$, and $0 < r \leq 1$, the achievable DoF is upper bounded by

$$\text{DoF}(\mu_F, \mu_{\text{BBU}}, r) \leq \min \left\{ \frac{\mu_{\text{BBU}}}{3} \cdot r, \frac{\mu_F}{3}, M \right\} \quad (3.18)$$

Proof: The proof is given in Appendix A.2.

Corollary 3.1 (Optimality in some special cases).

- If $\mu_F \leq M$ and $\mu_F \leq \frac{\mu_{\text{BBU}}}{\lceil \frac{1}{r} \rceil}$, then

$$\text{DoF}(\mu_F, \mu_{\text{BBU}}, r) = \frac{\mu_F}{3}. \quad (3.19)$$

- If $\mu_F \leq M$, $\frac{1}{r} \in \mathbb{Z}^+$ and $\mu_{\text{BBU}} \leq \frac{\mu_F}{r}$, then

$$\text{DoF}(\mu_F, \mu_{\text{BBU}}, r) = \frac{\mu_{\text{BBU}}}{3} \cdot r. \quad (3.20)$$

- For $M \leq \mu_F \leq 2M$

$$\text{DoF}(\mu_F, \mu_{\text{BBU}}, r) = \frac{\mu_{\text{BBU}}}{3} \cdot r, \quad (3.21)$$

if $\mu_{\text{BBU}} \leq \min\{M + \mu_F(t_1 t_2 - 1), \frac{\mu_F}{r}\}$ and $\frac{1}{r} \in \mathbb{Z}^+$, where (t_1, t_2) is a positive integer solution to $t_1 t_2 = \frac{1}{r}$.

- For $2M \leq \mu_F \leq 3M$

$$\text{DoF}(\mu_F, \mu_{\text{BBU}}, r) = \frac{\mu_{\text{BBU}}}{3} \cdot r, \quad (3.22)$$

– if $\mu_{\text{BBU}} \leq \min\{M(2t_1 + 2t_2 - 3) + \mu_F(t_1 t_2 - t_1 - t_2 + 1), \frac{\mu_F}{r}\}$, $\frac{1}{r} \in \mathbb{Z}^+$ and $\sqrt{\frac{1}{3r}} \notin \mathbb{Z}^+$, where (t_1, t_2) is the integer solution to $t_1 t_2 = \frac{1}{r}$ that minimizes $t_1 + t_2$ among all positive integer solutions, or

– if $\mu_{\text{BBU}} \leq \min\{M(2t_1 + 2t_2 - 3) + \mu_F(t_1 t_2 - t_1 - t_2 + 1), M(6t - 6) + \mu_F(3t^2 - 3t + 2), \frac{\mu_F}{r}\}$ and $\sqrt{\frac{1}{3r}} \in \mathbb{Z}^+$, where (t_1, t_2) is the integer solution to $t_1 t_2 = \frac{1}{r}$ that minimizes $t_1 + t_2$ among all positive integer solutions and $t = \sqrt{\frac{1}{3r}}$.

- For $3M \leq \mu_F$

$$\text{DoF}(\mu_F, \mu_{\text{BBU}}, r) = \frac{\mu_{\text{BBU}}}{3} \cdot r, \quad (3.23)$$

– if $\mu_{\text{BBU}} \leq \min\{M(3t_1 t_2 - t_1 - t_2), \frac{\mu_F}{r}\}$ and $\frac{1}{r} \in \mathbb{Z}^+$, where (t_1, t_2) is the integer solution to $t_1 t_2 = \frac{1}{r}$ that minimizes $t_1 + t_2$ among all positive integer solutions, or

– if $\mu_{\text{BBU}} \leq \min\{M(9t^2 - 3t), \frac{\mu_F}{r}\}$ and $\sqrt{\frac{1}{3r}} \in \mathbb{Z}^+$ where $t = \sqrt{\frac{1}{3r}}$.

Proof: The proofs are given in Appendix A.3.

Theorem 3.3. The achievability gap $\Delta(\mu_F, \mu_{\text{BBU}}, r)$ is upper bounded by

$$\Delta(\mu_{\text{BBU}}, \mu_F, r) < \frac{\mu_F}{3 \lceil \frac{1}{r} \rceil}, \quad \text{if } \mu_F \leq 2M. \quad (3.24)$$

Proof: The proof is given in Appendix A.4.

3.4 Uplink Scheme with Parallelogram Clustering

In the proposed uplink scheme, we deactivate a subset of mobile users so as to partition the network into non-interfering clusters of active users and their sectors. These clusters have parallelogram shapes and are parametrized by positive integer pair (t_1, t_2) .

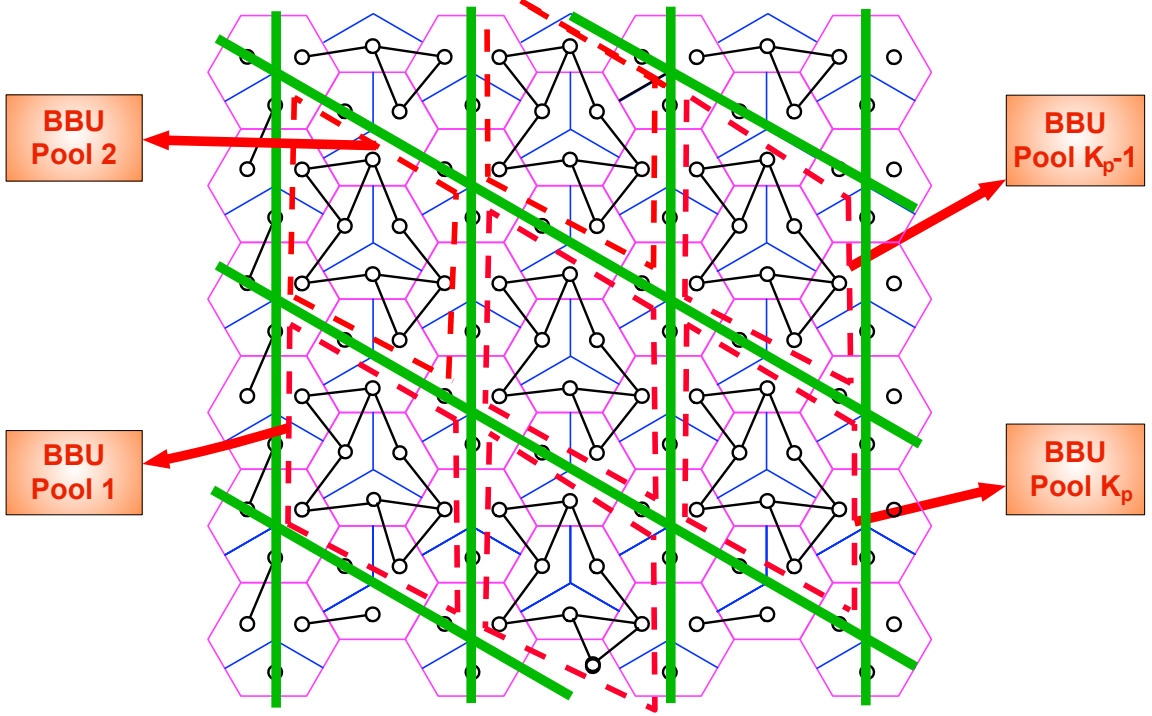


Figure 3.2: Parallelogram clustering for $(t_1, t_2) = (2, 2)$.

3.4.1 Construction of Parallelogram Clusters

For a given (t_1, t_2) pair, we define a regular parallelogram grid such that the length of sides in the diagonal direction (-30 degree with horizontal axis) is t_1 cell-hop length, and the length of sides in the vertical direction is t_2 cell-hop length. Then, we fit this parallelogram grid into our figurative network in a way that the intersections of the parallelogram grid coincides with BSs, which are assumed to be at the centers of cells. Subsequently, we deactivate all mobile users coinciding with the sides of the grid. This process divides the network into parallelogram-like **non-interfering** clusters of active users and their sectors, and we refer to them shortly as p -clusters. See Figure 3.2 for $(t_1, t_2) = (2, 2)$, on which users coinciding with green lines are deactivated. Throughout this section, we refer to **active** users as only **users** later on. Users of a p -cluster are located in:

- $(t_1 - 1)(t_2 - 1)$ BSs with three users,
- $2(t_1 - 1) + 2(t_2 - 1)$ BSs with two users,
- Single BS with one user.

Therefore, the number of users n_p in a p -cluster is:

$$n_p = 3t_1t_2 - t_1 - t_2. \quad (3.25)$$

Let $\mathcal{K} = \{1, \dots, K_p\}$, with $K_p \leq K$, be index set of p -clusters. We associate each p -cluster with single BBUP and denote the associated BBUP with the same index $k \in \mathcal{K}$

as the p-cluster. Let \mathcal{I}_k be the index set of BSs whose users are elements of k^{th} p-cluster. Each BS $j \in \mathcal{I}_k$ sends an observation function to k^{th} BBUP, i.e., $\mathcal{U}_k = \mathcal{I}_k$.

To be able to find BBUP-BS ratio, we need to equally partition all BSs to BBUPs. Note that any BS $j \in \mathcal{N}$ with one user or three users is element of single index set \mathcal{I}_k , $k \in \mathcal{K}$, and any BS $j \in \mathcal{N}$ with two users is element of two different index sets, i.e., \mathcal{I}_k and $\mathcal{I}_{k'}$, $k, k' \in \mathcal{K}$. Therefore, of the \mathcal{I}_k BSs of p-cluster k , we associate all of them with one user or three users, and half of them with two users to the BBUP k . This leads to the BBUP-BS ratio r_p :

$$r_p = \frac{1}{t_1 t_2}. \quad (3.26)$$

We can choose any $(t_1, t_2) \in \mathbb{Z}^+$ pair to construct p-clusters that satisfies with $r_p \leq r$:

$$t_1 t_2 \geq \left\lceil \frac{1}{r} \right\rceil. \quad (3.27)$$

3.4.2 Coding Scheme

Each mobile user u encodes its message W_u , which is uniformly distributed over the set $\mathcal{W}_u = \{1, \dots, 2^{nR_u}\}$, with a multi-antenna Gaussian codebook of power P . Since Rxs of silenced user sectors observe only interference, each BS j generates its observation function for (active) Rxs through independent quantization codebooks. To generate quantization codebooks, each BS j applies a point-to-point Gaussian vector quantizer to receive signal of each Rx as explained in Section 2.3.1 so that the quantization rates imposed in the following are satisfied. Let \mathcal{J}_k denote the sector index set of p-cluster k . We choose $\mathcal{D}_k = \mathcal{J}_k$. Each BS $j \in \mathcal{I}_k$ with three users transmits a message consisting of three quantization messages of its Rxs to BBUP k and each BS $j \in \mathcal{I}_k$ with two users transmits only quantization message of Rx u to BBUP k if $u \in \mathcal{J}_k$. The BS $j \in \mathcal{I}_k$ with single user transmits the only quantization message of its cell to the BBUP k . Depending on the prelogs μ_{BBU} and μ_{F} , there maybe three different quantization rates: all BSs with three users quantize each received signal at the rate $R_{q1} = \mu_{q1} \frac{1}{2} \log P$ and all BSs with two users quantize each received signal at the rate $R_{q2} = \mu_{q2} \frac{1}{2} \log P$, and all BSs with one active user quantize their received signals at the rate $R_{q3} = \mu_{q3} \frac{1}{2} \log P$. After receiving quantization messages, each BBUP k reconstructs all observations with quantization noise term, i.e., $\{\hat{\mathbf{Y}}_u^{(n)}\}_{u \in \mathcal{D}_k}$. The input-output relationship experienced by each BBUP k is a multi-user MIMO-MAC channel, where the effective noise consists of channel and quantization noises. Since the channel matrix from mobile users of \mathcal{D}_k to Rxs of \mathcal{D}_k is known by BBUP k and is square and full rank with probability 1, each BBUP k can perform joint decoding with vanishingly small average probability of error, which leads to achieve DoFs μ_{q1} , μ_{q2} and μ_{q3} as explained in Section 2.3.1, for respective mobile users.

To be able to find DoF for asymptotic case¹, i.e., while $N \rightarrow \infty$, we need to equally partition deactivated users of the network to p-clusters. Note that deactivated users around

¹The limit $N \rightarrow \infty$ is only needed to eliminate edge effects.

a p-cluster are located on green lines of four different sides and each side is on the border of two p-clusters. Therefore, when half of the deactivated users around a p-cluster, i.e., $(t_1 + t_2)$, are associated with the p-cluster itself, the equal partition of the deactivated users is performed. Then, the DoF of the scheme can be obtained as:

$$\text{DoF}_P(\mu_F, \mu_{\text{BBU}}, r) = \frac{\mu_{q1}(3t_1t_2 - 3t_1 - 3t_2 + 3) + \mu_{q2}(2t_1 + 2t_2 - 4) + \mu_{q3}}{3t_1t_2} \quad (3.28)$$

where the expression in the numerator refers to the sum-DoF in a given p-cluster and the expression in the denominator refers to the total number of active and deactivated users for a given p-cluster. In the following, we will give a policy to choose quantization rates for any (t_1, t_2) satisfying (3.27).

3.4.2.1 Case 1: $\mu_{\text{BBU}} \geq n_p M$

The DoF of $M \times M$ MIMO system with independently fading channels, which is the same as our case, is M by [67]: the quantization rate $\frac{M}{2} \log P$ is enough to describe message set \mathcal{W}_u of any user u in the asymptotic case. Thus, here we are not restricted by the processing capacity prelog μ_{BBU} , i.e., the only restricting factor is fronthaul capacity prelog μ_F . The main policy in this case is to distribute transmission resources between (active) user sectors of any given BS unless the per sector transmission capacity is more than the rate providing maximum DoF M for asymptotic case, i.e., $\frac{M}{2} \log P$. To this end, we determine the quantization rates regarding μ_F :

- If $\mu_F \leq M$, transmission resource of a fronthaul link is allocated equally among Rxs of a BS:

$$R_{q1} = \frac{\mu_F}{3} \cdot \frac{1}{2} \log P, \quad R_{q2} = \frac{\mu_F}{2} \cdot \frac{1}{2} \log P, \quad R_{q3} = \mu_F \frac{1}{2} \log P,$$

and the achievable DoF is given as

$$\text{DoF}_P(\mu_F, \mu_{\text{BBU}}, r) = \frac{\mu_F}{3}. \quad (3.29)$$

- If $M \leq \mu_F \leq 2M$, transmission resource of a fronthaul link is equally allocated among Rxs of a BS with two or three users, however, any BS with one user quantizes its received signal at the maximum rate since each fronthaul link has enough capacity to support that communication rate ($M \leq \mu_F$):

$$R_{q1} = \frac{\mu_F}{3} \cdot \frac{1}{2} \log P, \quad R_{q2} = \frac{\mu_F}{2} \cdot \frac{1}{2} \log P, \quad R_{q3} = M \frac{1}{2} \log P.$$

and the achievable DoF is given by

$$\text{DoF}_P(\mu_F, \mu_{\text{BBU}}, r) = \frac{\mu_F(t_1t_2 - 1) + M}{3t_1t_2}, \quad (3.30)$$

- If $2M \leq \mu_F \leq 3M$, transmission resource of a fronthaul link is equally allocated among Rxs of a BS with three users, however, any BS with one or two users quantizes their receive signals at the maximum rate for each Rx since each fronthaul link has enough capacity to support that communication rate ($2M \leq \mu_F$):

$$R_{q1} = \frac{\mu_F}{3} \cdot \frac{1}{2} \log P, \quad R_{q2} = M \frac{1}{2} \log P, \quad R_{q3} = M \frac{1}{2} \log P,$$

and the achievable DoF is given by

$$\text{DoF}_P(\mu_F, \mu_{\text{BBU}}, r) = \frac{\mu_F(t_1 t_2 - t_1 - t_2 + 1) + M(2t_1 + 2t_2 - 3)}{3t_1 t_2}. \quad (3.31)$$

- If $3M \leq \mu_F$, all BSs quantize their received signal at the maximum rate at each sector:

$$R_{q1} = R_{q2} = R_{q3} = M \cdot \frac{1}{2} \log P,$$

and achievable DoF is given as:

$$\text{DoF}_P(\mu_F, \mu_{\text{BBU}}, r) = M \left(1 - \frac{(t_1 + t_2)}{3t_1 t_2} \right). \quad (3.32)$$

3.4.2.2 Case 2: $\mu_{\text{BBU}} \leq n_p M$

Under this condition, depending on μ_F , the achievable sum-DoF of a p-cluster, which is given in the numerator of (3.28), can be restricted the processing capacity prelog μ_{BBU} . If the μ_{BBU} is not smaller than the achievable sum-DoF of a p-cluster for the given interval of μ_F :

- If $\mu_F t_1 t_2 \leq \mu_{\text{BBU}} \leq n_p M$ for $\mu_F \leq M$,
- If $\mu_F(t_1 t_2 - 1) + M \leq \mu_{\text{BBU}} \leq n_p M$ for $M \leq \mu_F \leq 2M$,
- If $\mu_F(t_1 t_2 - t_1 - t_2 + 1) + M(2t_1 + 2t_2 - 3) \leq \mu_{\text{BBU}} \leq n_p M$ for $2M \leq \mu_F \leq 3M$,
- If $\mu_{\text{BBU}} = n_p M$ for $\mu_F \geq 3M$,

the process that has been implemented in Section 3.4.2.1 is applied and, therefore, the DoF expressions are given as in (3.29), (3.30), (3.31) and (3.32), respectively. However, if the processing capacity prelog μ_{BBU} is smaller than the sum-DoF for the given μ_F :

- If $\mu_{\text{BBU}} \leq \mu_F t_1 t_2$ for $\mu_F \leq M$,
- If $\mu_{\text{BBU}} \leq \mu_F(t_1 t_2 - 1) + M$ for $M \leq \mu_F \leq 2M$,
- If $\mu_{\text{BBU}} \leq \mu_F(t_1 t_2 - t_1 - t_2 + 1) + M(2t_1 + 2t_2 - 3)$ for $2M \leq \mu_F \leq 3M$,
- If $\mu_{\text{BBU}} \leq n_p M$ for $\mu_F \geq 3M$,

we distribute the processing resource of a BBUP equally among sectors of a cluster and the quantization rate at each sector is chosen as

$$R_{q1} = R_{q2} = R_{q3} = \frac{\mu_{\text{BBU}}}{n_p} \cdot \frac{1}{2} \log P,$$

which leads to:

$$\text{DoF}_P(\mu_F, \mu_{\text{BBU}}, r) = \frac{\mu_{\text{BBU}}}{3t_1 t_2}. \quad (3.33)$$

To provide fairness among the achievable DoFs of users, instances of the proposed scheme are time-shared so that each mobile user takes all relative positions in a p-cluster, which requires

$$\frac{1}{r_p} = t_1 t_2 \quad (3.34)$$

different instances.

3.5 Uplink Scheme with Hexagon Clustering

In the proposed uplink scheme, we deactivate a subset of mobile users so as to partition the network into non-interfering clusters of active users and their sectors. As we will see, these clusters have shapes that resemble hexagon and size of hexagons are parametrized by positive integer t .

3.5.1 Construction of Hexagon Clusters

For a given design parameter t , we determine some portion of the BSs as **center** BSs and choose them to construct a regular grid of equilateral triangles where every three closest center BSs are $2t$ cell-hops apart from each other. Therefore, the maximum distance to the closest center BS is t cell-hops and we name the BSs whose distance is ℓ cell-hops to the closest center BS as layer-“ ℓ ” BSs, for $\ell = 1, \dots, t$. We determine all BSs located at t cell-hops above and below of any center BS as **corner** and **null** BSs, respectively. Then, we create solid green lines between any closest null and corner BSs (t cell-hop apart from each other), which creates hexagon grids along entire network. Subsequently, we deactivate mobile users coinciding with solid green lines. This process divides the network hexagon-like **non-interfering** clusters and we shortly name as **h-clusters**. Figure 3.3 shows an example of partition for $t = 3$. Later on, we refer to **active** users as only **users**. In a h-cluster,

- There are 3 users in center BS,
- There are 6ℓ layer-“ ℓ ”, $\ell = 1, \dots, t - 1$, BSs with 3 users around center BS, i.e. in total $3 \cdot \sum_{\ell=1}^{t-1} 6\ell = 9t^2 - 9t$,
- There are $6t - 3$ users in layer-“ t ” BSs.

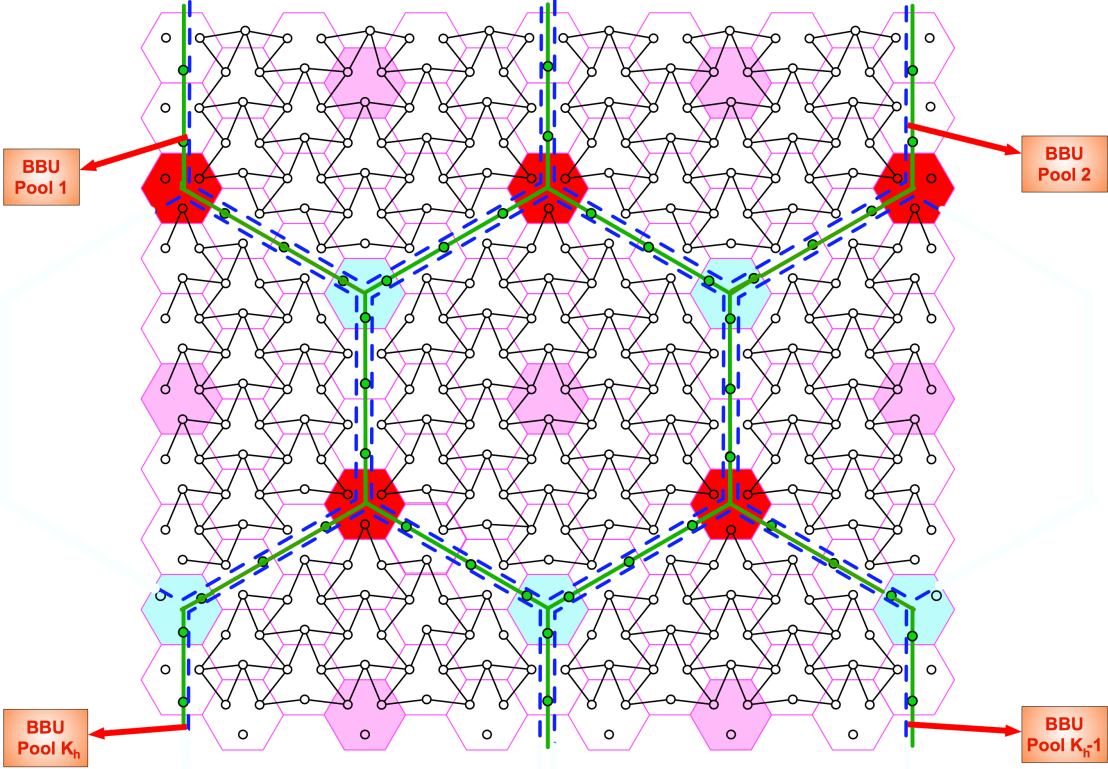


Figure 3.3: Illustration of h-clusters for $t = 3$. Pink, red and blue cells represent center, corner and null cells, respectively. Green-filled circles refer to deactivated users. All users and their sectors inside a blue dashed hexagon are associated to the same BBUP .

Therefore, the number of users in a h-cluster, n_h , is:

$$n_h = 9t^2 - 3t. \quad (3.35)$$

Let $\mathcal{K} = \{1, \dots, K_h\}$, with $K_h \leq K$, be index set of h-clusters. We associate each h-cluster with single BBUP and denote the associated BBUP with the same index $k \in \mathcal{K}$ of the h-cluster. Let \mathcal{I}_k be the index set of BSs whose users are elements of k^{th} h-cluster. Each \mathcal{I}_k BS sends an observation function to k^{th} BBUP, i.e., $\mathcal{U}_k = \mathcal{I}_k$.

To be able to find a BBUP-BS ratio, r_h , we need to equally partition all BSs to BBUPs. Note that, each layer- t BS except corner one is element of 2 different index sets, i.e., \mathcal{I}_k and $\mathcal{I}_{k'}$, $k, k' \in \mathcal{K}$. Each corner BS is element of 3 different index sets, i.e., \mathcal{I}_k , $\mathcal{I}_{k'}$ and $\mathcal{I}_{k''}$, $k, k', k'' \in \mathcal{K}$. Also, note that each null BS around a h-cluster k is on the border of 3 different h-clusters. To this end, of the \mathcal{I}_k BSs and null BSs around h-cluster k , we partition all layer- ℓ , $\ell = 1, \dots, t - 1$, BSs including center BS, half of the layer- t BSs except corner and null BSs, and one third of corner and null BSs to the BBUP k , which leads to :

$$r_h = \frac{1}{3t^2}. \quad (3.36)$$

Since we have a given ratio r , we can choose any $t \in \mathbb{Z}^+$ such that $r_h \leq r$, i.e.,

$$t \geq \left\lceil \sqrt{\frac{1}{3r}} \right\rceil. \quad (3.37)$$

3.5.2 Coding Scheme

Each mobile user u encodes its message W_u , which is uniformly distributed over the set $\mathcal{W}_u = \{1, \dots, 2^{nR_u}\}$, with a multi-antenna Gaussian codebook of power P . As in Section 3.4, after observation at sector antennas, each BS j generates observation function for (active) Rxs through independent quantization codebooks. To generate quantization codebooks, each BS j applies a point-to-point Gaussian vector quantizer to received signal of each Rx as explained in Section 2.3.1 such that the following rate constraints are met. Let \mathcal{J}_k denote the sector index set of h-cluster k . We choose $\mathcal{D}_k = \mathcal{J}_k$. Each BS $j \in \mathcal{I}_k$ of layer-" ℓ ", $\ell = 1, \dots, t-1$, transmits a message consisting of 3 independent quantization messages of Rxs to BBUP k and each BS $j \in \mathcal{I}_k$ of layer-" t " transmits only quantization message of sector u to BBUP k if $u \in \mathcal{J}_k$. Depending on the prelogs μ_{BBU} and μ_{F} , there maybe two different quantization rates: Each BS with three users quantize each received signal at the rate $R_{q1} = \mu_{q1} \frac{1}{2} \log P$ and each BS with two users quantize each received signal at the rate $R_{q2} = \mu_{q2} \frac{1}{2} \log P$. That is, in h-cluster k , the received signals of all layer-" ℓ " BSs, $\ell = 1, \dots, t-1$, and the received signals of every corner BS is quantized at rate R_{q1} , i.e., $9t^2 - 9t + 6$, and received signals of layer-" t " BSs other than corner BSs are quantized at R_{q2} , i.e. $6t - 6$. After obtaining quantization messages, BBUP k reconstructs all $\{\hat{\mathbf{Y}}_u^{(n)}\}_{u \in \mathcal{D}_k}$ with quantization error. The input-output relationship experienced at the BBUP k is multi-user Gaussian MIMO-MAC. Then, each BBUP k performs joint decoding with vanishingly small probability of error since the channel matrix from users of \mathcal{D}_k to Rxs of \mathcal{D}_k is known by BBUP k , and is square and full rank with probability 1. This leads to achieve DoFs μ_{q1} and μ_{q2} as explained in Section 2.3.1, for respective mobile users.

To be able to find DoF for asymptotic case, i.e., $N \rightarrow \infty$, we need to equally partition deactivated users of the network to h-clusters. The number of deactivated users around h-cluster k is $6t$. Since each deactivated user is on the border of two h-clusters, to be able to find DoF of the scheme, we partition half of them, i.e., $3t$, to users of h-cluster k , which gives the DoF expression:

$$\text{DoF}(\mu_{\text{F}}, \mu_{\text{BBU}}, r) = \frac{\mu_{q1} (9t^2 - 9t + 6) + \mu_{q2} (6t - 6)}{9t^2}. \quad (3.38)$$

In the following, we will give the policy for choosing quantization rates.

3.5.2.1 Case 1: $\mu_{\text{BBU}} \geq n_h M$

As for in Section 3.4.2.1, the fronthaul capacity prelog μ_{F} is the only limiting factor since the quantization rate $M \cdot \frac{1}{2} \log P$ is enough to describe message \mathcal{W}_u of any user u in the asymptotic case. The policy is again to distribute transmission resources equally among (active) Rxs of any given BS. To this end, we choose the quantization rates regarding μ_{F} :

- If $\mu_F \leq 2M$, transmission resources of fronthaul links is equally allocated between Rxs

$$R_{q1} = \frac{\mu_F}{3} \cdot \frac{1}{2} \log P, \quad R_{q2} = \frac{\mu_F}{2} \cdot \frac{1}{2} \log P, \quad (3.39)$$

and the achievable DoF is given as

$$\text{DoF}(\mu_F, \mu_{\text{BBU}}, r) = \frac{\mu_F(3t^2 - 1)}{9t^2}. \quad (3.40)$$

- If $2M \leq \mu_F \leq 3M$, transmission resource of a fronthaul link is equally allocated among Rxs of a BS with three users, however any BS with two users quantizes its received sector signals at the maximum rate at each Rx since each fronthaul link has enough capacity to support that communication rate ($M \leq \frac{\mu_F}{2}$):

$$R_{q1} = \frac{\mu_F}{3} \cdot \frac{1}{2} \log P, \quad R_{q2} = M \cdot \frac{1}{2} \log P, \quad (3.41)$$

and the achievable DoF is given as

$$\text{DoF}(\mu_F, \mu_{\text{BBU}}, r) = \frac{\mu_F(3t^2 - 3t + 2) + M(6t - 6)}{9t^2}. \quad (3.42)$$

- If $\mu_F \geq 3M$, all BSs quantize their receive signals at the maximum quantization rate ($M \leq \frac{\mu_F}{3}$):

$$R_{q1} = R_{q2} = M \cdot \frac{1}{2} \log P, \quad (3.43)$$

and the achievable DoF is given as

$$\text{DoF}(\mu_{\text{BBU}}, \mu_F, r) = M \frac{3t - 1}{3t}. \quad (3.44)$$

3.5.2.2 Case 2: $\mu_{\text{BBU}} \leq n_h M$

Under this condition, depending on μ_F , the achievable sum-DoF of a h-cluster can be restricted by the processing capacity prelog μ_{BBU} . Achievable sum-DoF is given in the numerator of (3.38). Therefore, if the processing capacity prelog μ_{BBU} is not smaller than the achievable sum-DoF of a h-cluster for the given interval of μ_F :

- If $\mu_F(3t^2 - 1) \leq \mu_{\text{BBU}} \leq n_h M$ for $\mu_F \leq 2M$,
- If $\mu_F(3t^2 - 3t + 2) + M(6t - 6) \leq \mu_{\text{BBU}} \leq n_h M$ for $2M \leq \mu_F \leq 3M$,
- If $\mu_{\text{BBU}} = n_h M$ for $3M \leq \mu_F$,

the process that has been implemented in Section 3.5.2.1 is applied and, therefore, the DoF expressions are given as in (3.40), (3.42) and (3.44), respectively. However, if the processing capacity prelog μ_{BBU} is smaller than the sum-DoF for the given μ_F :

- If $\mu_{\text{BBU}} \leq \mu_F(3t^2 - 1)$ for $\mu_F \leq 2M$,

- If $\mu_{\text{BBU}} \leq \mu_{\text{F}} (3t^2 - 3t + 2) + M(6t - 6)$ for $2M \leq \mu_{\text{F}} \leq 3M$,
- If $\mu_{\text{BBU}} \leq n_{\text{h}}M$ for $\mu_{\text{F}} \geq 3M$,

we distribute the processing resource of a BBUP equally among sectors of a cluster and the quantization rate at each sector is chosen as

$$R_{\text{q1}} = R_{\text{q2}} = \frac{\mu_{\text{BBU}}}{n_{\text{h}}} \cdot \frac{1}{2} \log P,$$

which leads to:

$$\text{DoF}(\mu_{\text{F}}, \mu_{\text{BBU}}, r) = \frac{\mu_{\text{BBU}}}{9t^2}. \quad (3.45)$$

To provide fairness among the achievable DoFs of users, instances of the proposed scheme are time-shared so that each mobile user takes all relative positions in a h-cluster, which requires

$$\frac{1}{r_{\text{h}}} = 3t^2 \quad (3.46)$$

different instances.

3.6 DoF Without Sectorization

A naive alternative for both of the proposed achievability schemes would be to ignore the interference pattern caused by the sectorization of cells. That is, for p-clustering, it requires deactivation of all users in the cells with one or two active mobile users and, for h-clustering, it requires deactivation of all users in the corner cells and the cells with two active users. This means that the network consists of only cells with three active user and cells with no active users for both schemes. This would again partition the network into non-interfering parallelogram-like and hexagonal-like clusters without changing the r_{p} and r_{h} for any given (t_1, t_2) pair or t , and we call them **p-naive** and **h-naive** clustering, respectively.

By following the similar procedure introduced in Sections 3.4 and 3.5, one can easily state the following result by simply distributing the available transmission resources equally among three Rxs of a given cell as long as the BBUP capacity is enough or, otherwise, distributing BBUP processing resources equally among the Rxs of a cluster. This leads to the following lemma:

Lemma 3.4 (DoF for naive scheme). *For any $\mu_{\text{BBU}} > 0$, $\mu_{\text{F}} > 0$, and $0 < r \leq 1$, the achievable DoF in a multi cloud based non-sectored cellular network is lower bounded by*

$$\text{DoF}_{\text{naive}}(\mu_{\text{BBU}}, \mu_{\text{F}}, r) \geq \text{conv hull} \{ \text{DoF}_{\text{P,naive}}(\mu_{\text{BBU}}, \mu_{\text{F}}, r), \text{DoF}_{\text{H,naive}}(\mu_{\text{BBU}}, \mu_{\text{F}}, r) \}, \quad (3.47)$$

where

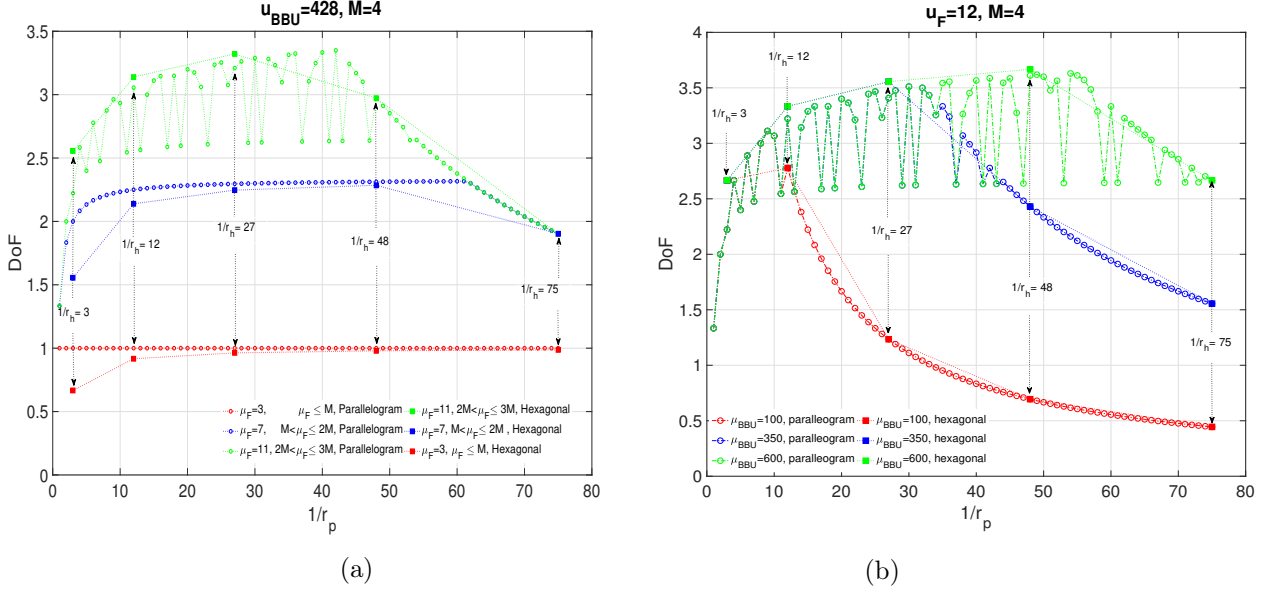


Figure 3.4: The impact of r_p : a-) For various values of μ_{F} . b-) For various values of μ_{BBU} .

$$\text{DoF}_{\text{P,naive}}(\mu_{\text{BBU}}, \mu_{\text{F}}, r) = \begin{cases} \max_{t_1, t_2} \min \left\{ \frac{\mu_{\text{F}}(t_1 t_2 - t_1 - t_2 + 1)}{3t_1 t_2}, \frac{\mu_{\text{BBU}}}{3t_1 t_2} \right\}, & \text{if } \mu_{\text{F}} \leq 3M, \\ \max_{t_1, t_2} \min \left\{ M \left(1 - \frac{(t_1 + t_2 - 1)}{t_1 t_2} \right), \frac{\mu_{\text{BBU}}}{3t_1 t_2} \right\}, & \text{if } \mu_{\text{F}} \geq 3M, \end{cases} \quad (3.48)$$

and above maximizations are over all positive integers t_1, t_2 satisfying $t_1 t_2 \geq \lceil \frac{1}{r} \rceil$, and

$$\text{DoF}_{\text{H}}(\mu_{\text{BBU}}, \mu_{\text{F}}, r) = \begin{cases} \max_t \min \left\{ \frac{\mu_{\text{F}}(3t^2 - 3t + 2)}{9t^2}, \frac{\mu_{\text{BBU}}}{9t^2} \right\}, & \text{if } \mu_{\text{F}} \leq 3M, \\ \max_t \min \left\{ M \frac{(3t^2 - 3t + 2)}{3t^2}, \frac{\mu_{\text{BBU}}}{9t^2} \right\}, & \text{if } \mu_{\text{F}} \geq 3M, \end{cases} \quad (3.49)$$

where above maximizations are over all positive integers t satisfying $t \geq \lceil \sqrt{\frac{1}{3r}} \rceil$.

Notice that the same cut-set bound, Theorem 3.2, applies also for the naive scheme since the observation functions in Definition 3.1 are defined not on the sector basis but on the BS basis.

3.7 Numerical Results and Discussion

In this section we present simulation results demonstrating the efficiency of our coding scheme. In Figure 3.4a, we investigate effect of clustering size on the achievable DoF for the following fronthaul capacities $\mu_{\text{F}} = [3, 7, 11]$, and BBUP processing capacity $\mu_{\text{BBU}} = 428$.

We define size of p-cluster as inverse of r_p , i.e., $\frac{1}{r_p} = t_1 t_2$, and we denote it also with side length pair (t_1, t_2) . We define size of h-cluster as inverse r_h , i.e., $\frac{1}{r_h} = 3t^2$, and we denote it also with the parameter t . It is observed that for p-clustering, when the fronthaul capacity is small, i.e., $\mu_F \leq M$, clustering size has no effect on DoF since μ_F becomes a bottleneck. In general, we see that, for both p-clustering and h-clustering, the clustering size giving highest DoF decreases with μ_F . The figure verifies the Remark 3.1 since, for all $r_p = r_h$, p-clustering outperforms h-clustering for $\mu_F = [3, 7]$. It is also interesting to note that for p-clustering, the achievable DoF is not monotonically increasing (decreasing) until (after) reaching the maximum for $\mu_F = 11$ (i.e. $2M < \mu_F \leq 3M$), since not only the clustering size but also the **side length** of the p-cluster is important for exploiting interference. The idea behind this observation is that: For any r_p , choosing (t_1, t_2) pair that is minimum in the sum gives the maximum DoF since it provides higher joint processing gain for a p-cluster for the given size (i.e. $\frac{1}{r_p}$), i.e., the more t_1 and t_2 becomes closer to each other the more mutual information clusters have. Therefore larger p-cluster sizes may not result in higher DoF owing to the side length effect. However, for $\mu_F \leq 2M$, the side lengths of p-cluster has no effect on achievable DoF for a given cluster size.

Figure 3.4b shows effect of clustering size on DoF for various values of $\mu_{\text{BBU}} = [100, 300, 500]$ and $\mu_F = 12$. It is seen that for each μ_{BBU} achievable DoF increases with cluster size until it becomes a bottleneck, i.e., until μ_{BBU} becomes active in the achievability expression. Accordingly, the results clearly indicate that having more processing power makes possible larger cluster sizes and, hence larger DoF.

In Figure 3.5, we plot the achievable DoF per user and cut-set bound vs μ_F for $M = 4$, $r = 0.025$, and $\mu_{\text{BBU}} = 428$, which illustrates the case that BBUP processing capacity is equal to the required processing capacity for which each received signal in a p-cluster of size $(t_1, t_2) = (5, 8)$ is quantized at the **maximum** quantization rate $R_q = \frac{M}{2} \log P$. From the figure, it is deduced that the p-clustering scheme achieves very close to the upper bound for $\mu_F \leq 2M$, which means that $\frac{2M}{3}$ DoF is almost achievable at $\mu_F = 2M$ given that processing capacity is high enough. In Figure 3.5, the operating points of clustering sizes is also depicted. For $\mu_F \leq 8$, equivalently $2M$, any p-clustering with $\frac{1}{r_p} = 40$ gives the highest achievable DoF for the given system parameters. However, for $\mu_F > 8$, there are several different operating points. For example, for $8 < \mu_F \leq 9.4$, the h-clustering of size $t = 4$ is the optimal clustering size, which means, for $\mu_F > 2M$, dividing the network into h-clusters provides higher joint processing gain than p-clustering for the same $r_h = r_p$ if the BBUP processing capacity is enough. For the rest, the clustering size r_p is decreasing with μ_F due to the given BBUP capacity is not enough to handle the quantized data for larger cluster sizes. At the operating point $\mu_F = 12$, which allows maximum quantization rate for each receive signal, the p-clustering of size $(t_1, t_2) = (5, 8)$ achieves capacity. This means the proposed scheme utilizes the system resources optimally at this operating point and approximately $\frac{9M}{10}$ DoF is achievable, which is impossible to achieve with conventional interference alignment techniques. The figure also shows the lower bound achieved by

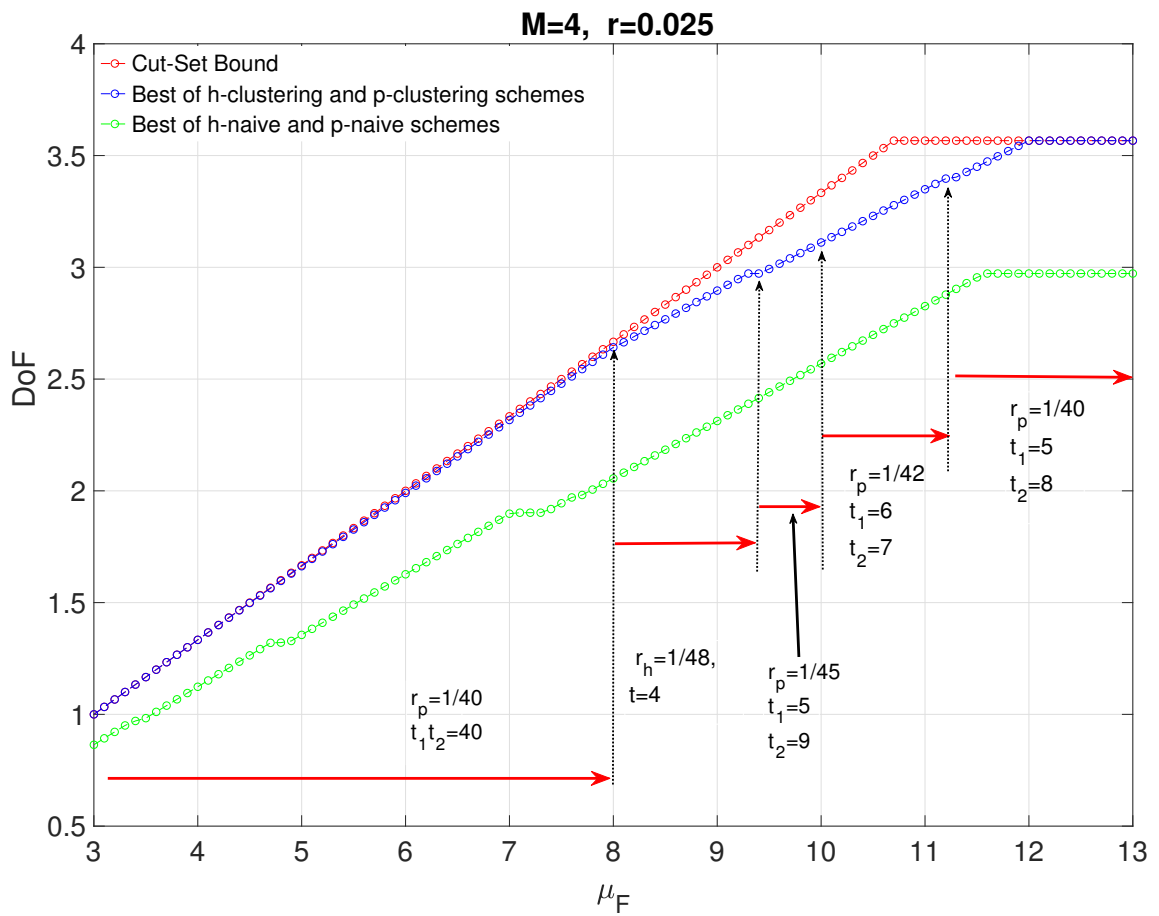
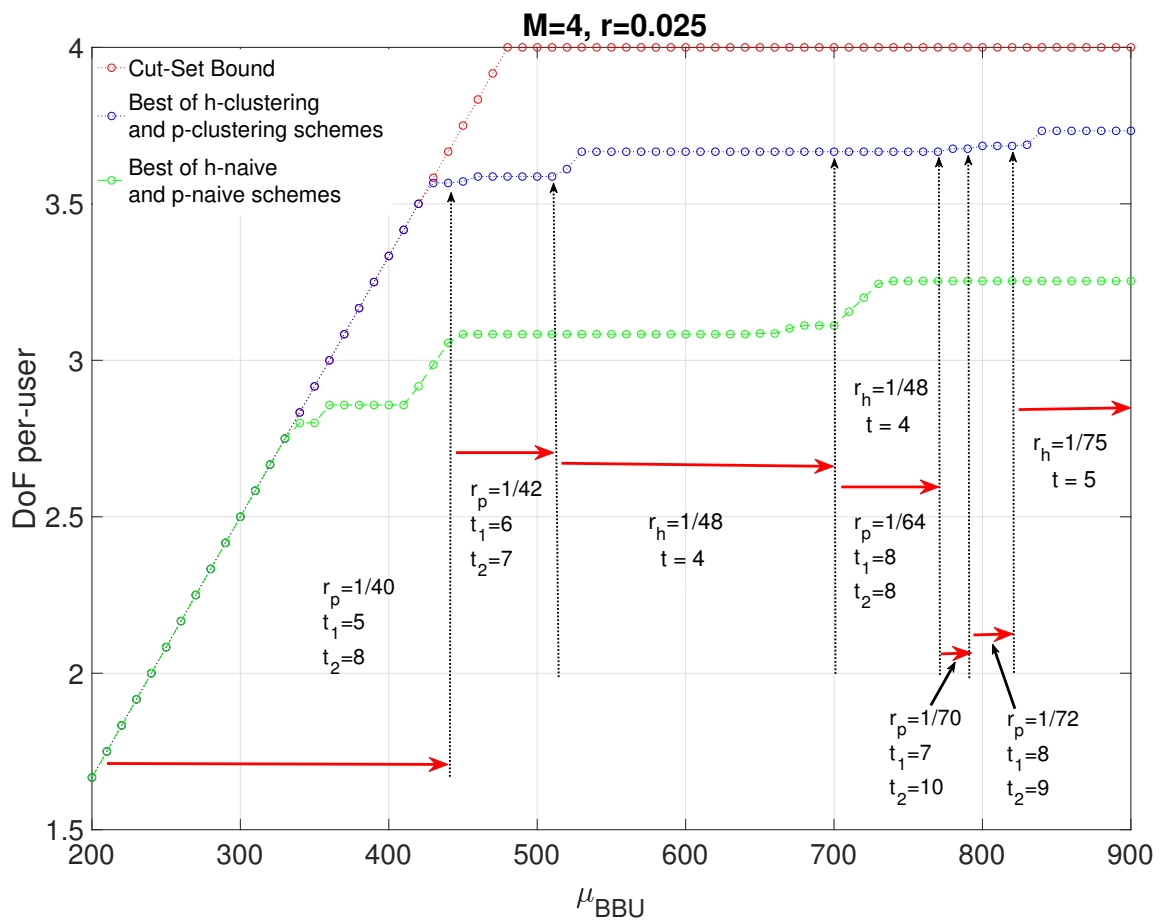
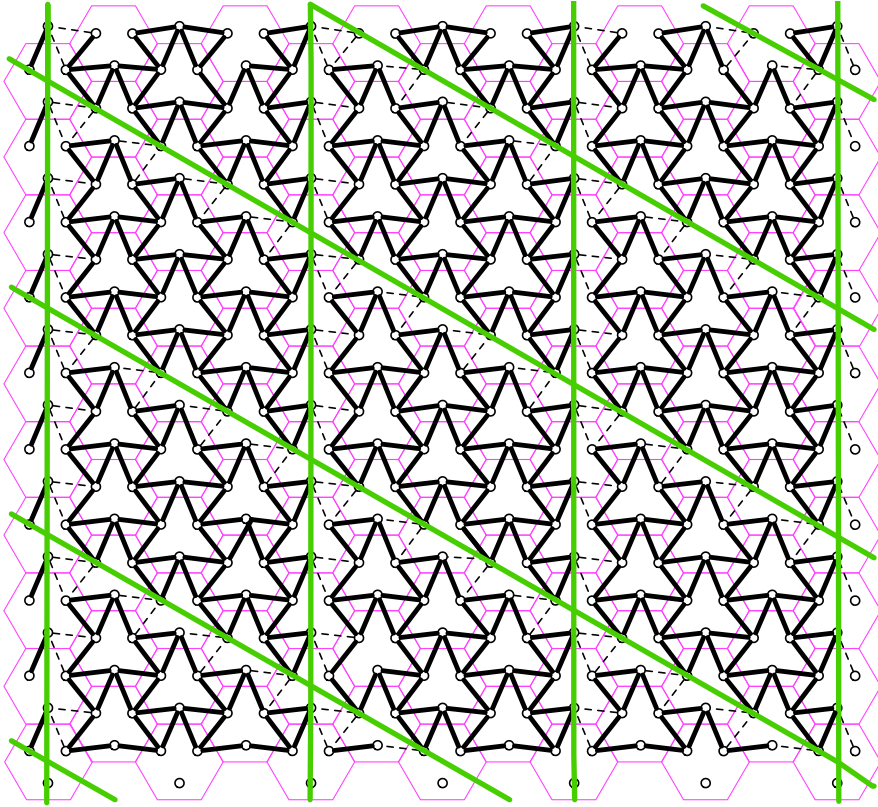
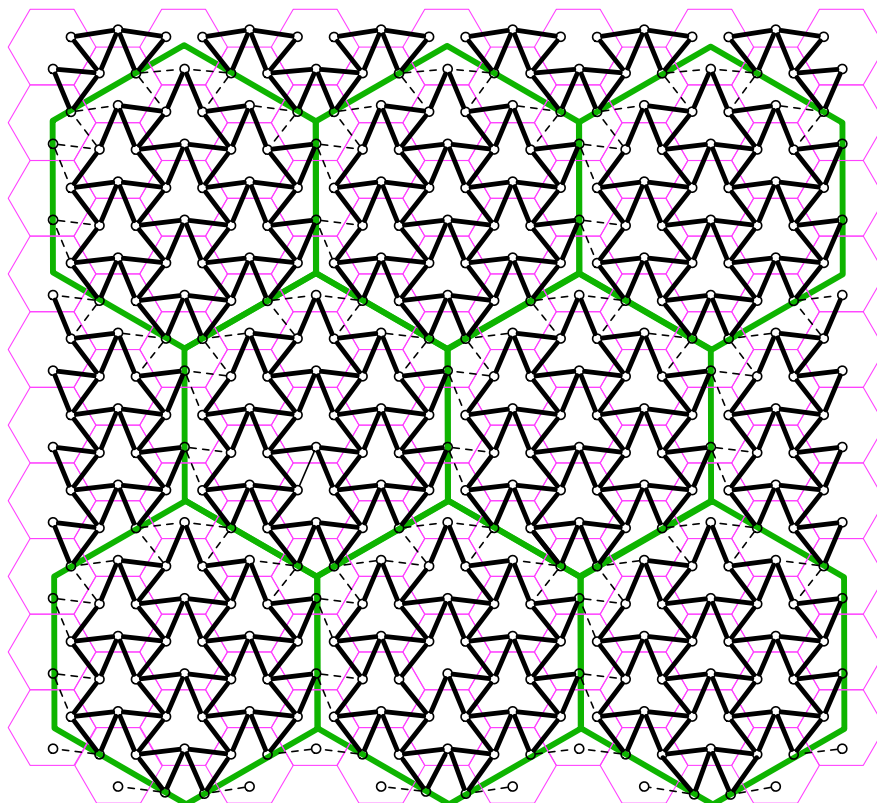


Figure 3.5: The impact of μ_F at $\mu_{BBU} = 428$.

Figure 3.6: The impact of μ_{BBU} at $\mu_{\text{F}} = 12$.

Figure 3.7: I_p -clustering for $(t_1, t_2) = (4, 3)$.

the naive approach vs μ_F for the same parameters. It is seen that the performance of the sectorized network scheme is considerably higher than naive scheme such that while the proposed scheme achieves almost optimal values in many cases, there is a huge gap for naive implementation. This is, in fact, the gain that sectorization brings by negating intra-cell interference. In Figure 3.6, we plot the achievable DoF and cut-set bound as a function of processing capacity prelog μ_{BBU} , for $r = 0.025$ and $\mu_F = 12$, which means that the fronthaul capacity has no restrictive effect on the achievable DoF. The operating points of clustering sizes regarding to μ_{BBU} is also shown in the figure. The plot clearly indicates that the cut set bound is achieved until $\mu_{\text{BBU}} = 428$, i.e., the processing resources is used efficiently even while achieving $\frac{9M}{10}$ DoF. At the rest of μ_{BBU} range, it is seen that the optimal clustering sizes ($\frac{1}{r_p}$ or $\frac{1}{r_h}$) increase with μ_{BBU} , and for most of $\mu_{\text{BBU}} > 428$, h-clustering provides highest DoF that indicates the advantage of employing h-clustering when the processing capacity high enough. For some range of μ_{BBU} , both h-clustering of size $t = 4$ and p-clustering of size $(t_1, t_2) = (8, 8)$ provide highest DoF, which shows that h-clustering with lower clustering size provides higher joint processing gain than p-clustering with larger clustering sizes due to clustering geometry. The figure also depicts the lower bound achieved by the naive approach vs μ_{BBU} for the same parameters and the gain of sectorization is clearly seen for higher values of processing capacity.

Figure 3.8: I_h -clustering for $t = 2$.

3.8 Finite SNR Analysis

In this section, we proceed finite SNR analysis of the proposed schemes and compare each of them with the schemes where there are no deactivated users, which will be introduced at the end of section. The finite SNR analysis procedure of the proposed schemes are quite similar to the analysis introduced in Section 2.6, and therefore, we will highlight the difference between two analysis. As before, by following the definition of [43] for finite SNR DoF, we assume the fronthaul and BBU processing capacities proportionate with $\frac{1}{2} \log(1 + MP)$, i.e.,

$$C_F = \mu_F \cdot \frac{1}{2} \log(1 + MP) \quad \text{and} \quad C_{\text{BBUP}} = \mu_{\text{BBU}} \cdot \frac{1}{2} \log(1 + MP), \quad (3.50)$$

for given μ_F , μ_{BBU} , where M is the number of receive antennas. The quantization rates are chosen as stated in Sections 3.4.2 and 3.5.2, but the conditions regarding high SNR regime are not applied, i.e., the prelog of any quantization rate is not reduced to the number of antennas M . Then each BBUP implements joint decoding for the users for the associated cluster after reconstructing all sector received signals of the cluster. Throughout the section, we perform the analysis for $M = 1$ for simplicity.

To evaluate the performance of the proposed p-clustering scheme at finite SNR values, we numerically compare average sum-rate of the scheme with the following two schemes

and the p-naive scheme introduced in Section 3.6:

- First scheme is a variation of our p-clustering scheme in which the network is decomposed into non-overlapping but interfering clusters respect to the parameters (t_1, t_2) pair. In p-clustering, each p-cluster is surrounded by deactivated users located on the sides of (t_1, t_2) -hop parallelogram, where each side has t_1 and t_2 deactivated users respectively. For each p-cluster, we associate all deactivated users on the lower side and right side of a (t_1, t_2) -hop parallelogram to the p-cluster under consideration. Subsequently, we activate all deactivated users and allow each BBUP to collect quantization messages of reactivated user sectors associated to its own p-cluster. This process partitions the network into non-overlapping but **interfering** parallelogram-like clusters, which we call **I_p-clusters** later on, see Figure 3.7 for $(t_1, t_2) = (4, 3)$. Note that I_p-clustering requires same BBUP-BS ratio r_p as for p-clustering case. With reactivation of all deactivated mobile users, there are $3t_1t_2$ active users in each I_p-cluster and all cells consists of 3 active users. Therefore, each BS equally partitions its fronthaul transmission resources to Rxs if BBU processing resources is enough to implement the joint decoding, otherwise, the processing resources is evenly distributed among all Rxs of the I_p-cluster, i.e., the quantization rate is chosen as

$$\max_{t_1, t_2} \min \left\{ \frac{\mu_F}{3}, \frac{\mu_{\text{BBU}}}{3t_1t_2} \right\} \cdot \frac{1}{2} \log(1 + MP) \quad (3.51)$$

over all positive integer (t_1, t_2) pairs satisfying $t_1t_2 \geq \lceil \frac{1}{r} \rceil$. To be able to guess the user messages, each BBUP implement joint decoding by treating out-of-cluster interference as noise.

- Second scheme is another variation of the practical systems that is different from explained in Section 2.6. For each user, including the sector under consideration, quantized version of all adjacent sectors are collected at a BBUP and it performs the decoding operation. In this case, we don't impose a processing capacity constraint on BBUPs, therefore the quantization rates are trivially chosen as one third of available fronthaul capacity for each BS.

To evaluate the performance of the proposed h-clustering scheme at finite SNR, we numerically compare the average per-user achieved by h-clustering scheme with h-naive scheme explained in Section 3.6, the practical scheme explained above, and the following scenario: This scenario is a variation of h-clustering scheme, where the network is decomposed to non-overlapping but interfering hexagon-like clusters respect to the parameter t is obtained as explained in Section 2.6, see Figure 3.8 for $t = 2$. By following the same convention, we call them **I_h-clusters**. Note that I_h-clustering requires same BBUP-BS ratio as for h-clustering case. With reactivation of deactivated users, there are $9t^2$ active users in each I_h-cluster. Therefore, by applying similar arguments as explained in Section 3.5, the quantization rate for I_h-clustering is chosen as

$$\max_t \min \left\{ \frac{\mu_F}{3}, \frac{\mu_{\text{BBU}}}{9t^2} \right\} \cdot \frac{1}{2} \log(1 + MP) \quad (3.52)$$

over positive integers t satisfying $t \geq \lceil \sqrt{\frac{1}{3r}} \rceil$. To be able to guess the user messages, each BBUP implements joint decoding by treating out-of-cluster interference as noise.

In simulations, we average the per-user rate over 10000 realizations of the channels matrices, where for each realization all channel coefficients are drawn independently of each other according to standard Gaussian distribution however all cross channel coefficients from adjacent sectors are multiplied by a constant α , where α models path attenuation. Figures 3.9 and 3.10 shows the average per-user rate of different schemes as a function of SNR for different choices of path loss factor $\alpha \in \{0.25, 0.8\}$, the BBUP capacity $\mu_{\text{BBU}} \in \{25, 150\}$, the fronthaul capacity $\mu_F = 15$, and the BBUP-BS ratio $r = \frac{1}{12}$ for $(t_1, t_2) = (4, 3)$ and $t = 2$, respectively. Note that when $\mu_{\text{BBU}} = 150$, the quantization rates are determined respect to μ_F , however, when $\mu_{\text{BBU}} = 25$, the BBUP processing capacity becomes bottleneck and, hence the quantization rates are determined respect to it.

In Figure 3.9, when $\mu_{\text{BBU}} = 150$, it is seen that for both $\alpha = 0.25$ and $\alpha = 0.8$, the p-clustering scheme outperforms p-naive scheme in all SNR regime and I_p -clustering scheme except low SNR regime. However, the practical scheme outperforms the proposed one until 10 dB SNR for $\alpha = 0.25$. For $\mu_{\text{BBU}} = 25$, Figure 3.9 shows that the proposed scheme achieves better than both I_p -clustering and p-naive schemes at all SNR range. However, note that, the I_p -clustering performs better than p-naive scheme until around 18 dB since the inter-cluster interference is not tolerable for higher SNR range.

In Figure 3.10, when $\mu_{\text{BBU}} = 150$, we see that I_h -clustering scheme outperforms the h-clustering at all practical SNR range for $\alpha = 0.25$, however, it outperforms h-clustering until around 13 dB for $\alpha = 0.8$. When $\mu_{\text{BBU}} = 25$, h-clustering achieves almost the same performance with I_h -clustering until 12 dB and 3dB for $\alpha = 0.25$ and $\alpha = 0.8$, respectively. The I_h -clustering scheme performs better than h-naive scheme until 13 dB.

In general we draw the following conclusions from the proposed simulations results: The proposed schemes are always better than the other schemes at high SNR regime, however, at low SNR regime mostly the interfering clustering schemes outperforms the proposed schemes.

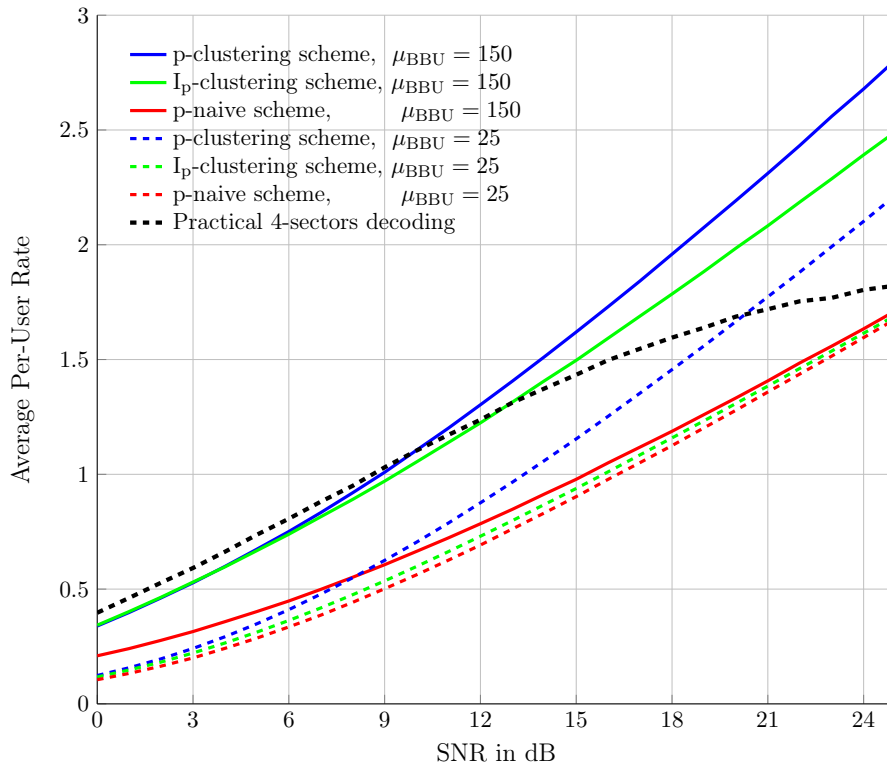
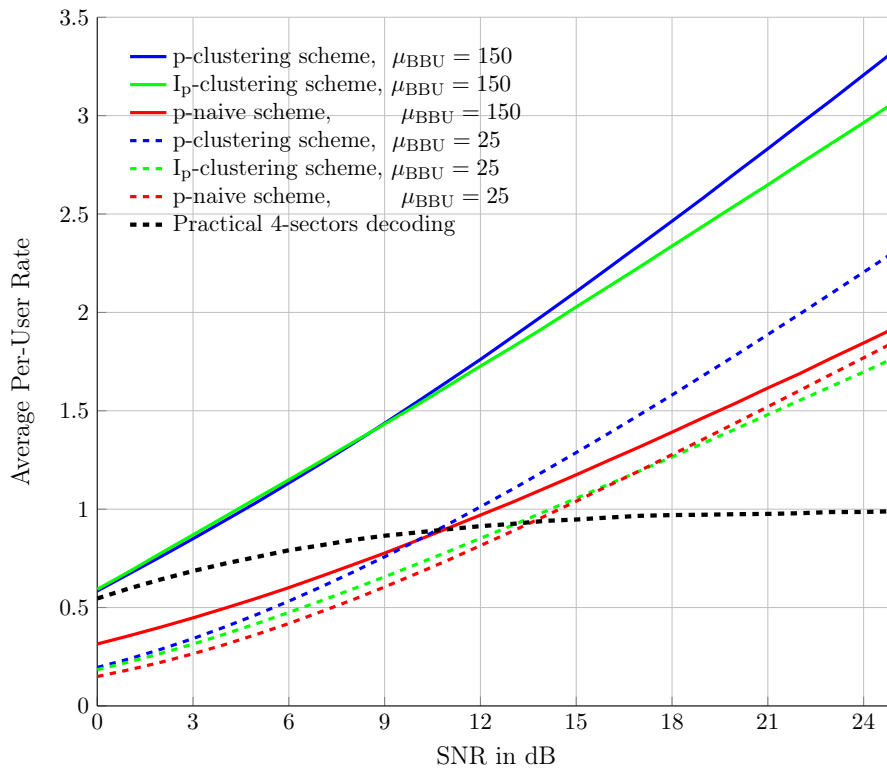
(a) For $\alpha = 0.25$.(b) For $\alpha = 0.8$.

Figure 3.9: Comparison of the rates achieved by the parallelogram-like schemes in the finite SNR regime for $(t_1, t_2) = (4, 3)$ and $\mu_F = 15$.

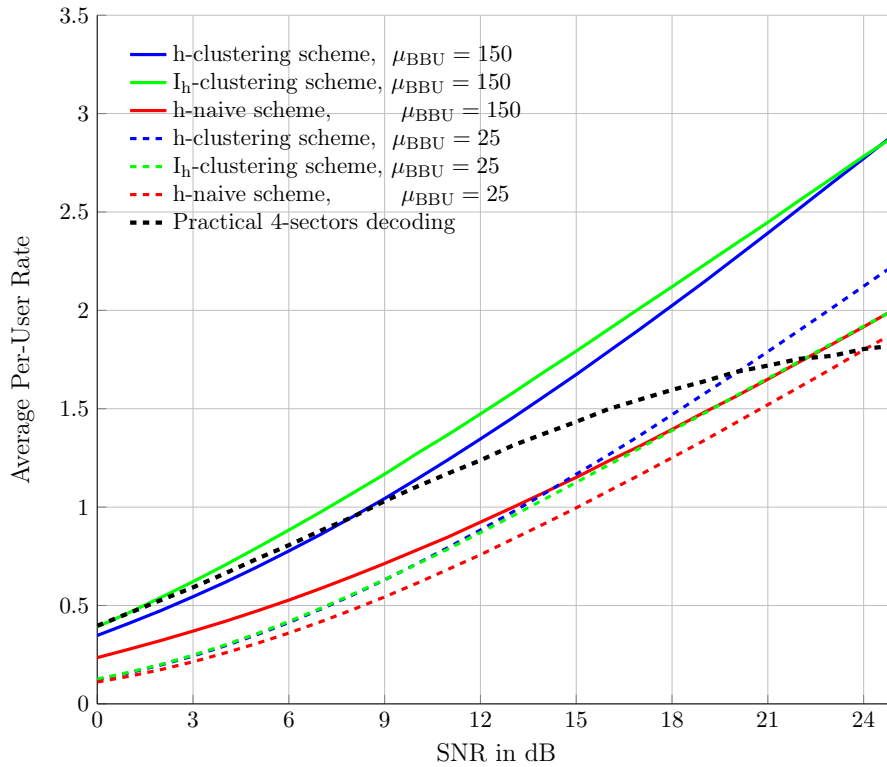
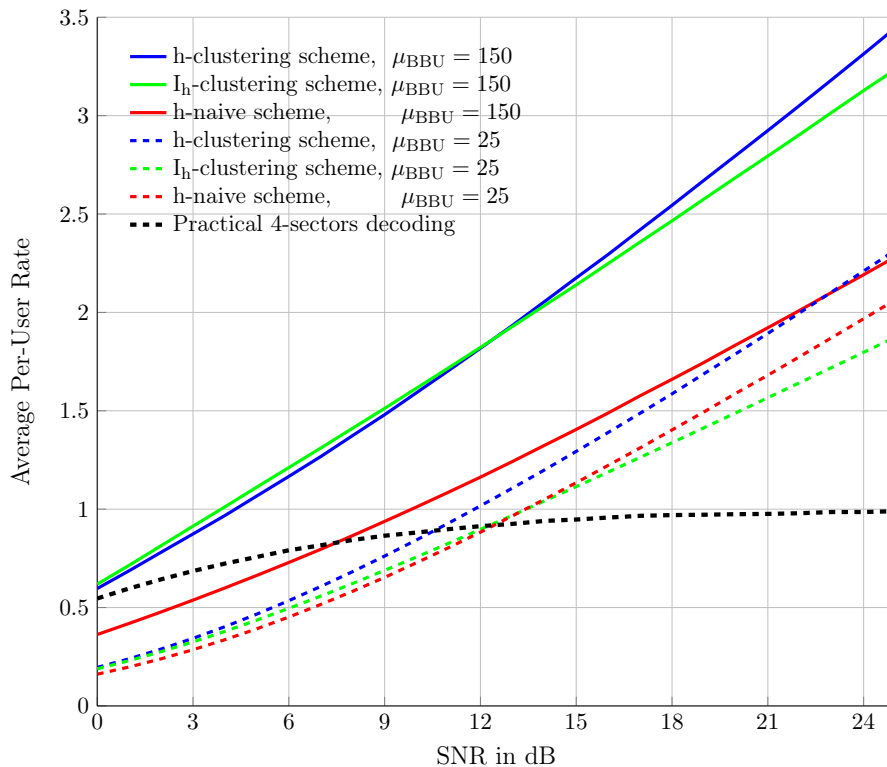
(a) For $\alpha = 0.25$.(b) For $\alpha = 0.8$.

Figure 3.10: Comparison of the rates achieved by the hexagonal-like schemes in the finite SNR regime for $t = 2$ and $\mu_{\text{F}} = 15$.

3.9 Summary

In this chapter, we analyze the uplink DoF of multi cloud based sectorized cellular systems. The main contribution of this chapter is that DoF is characterized as a function of fronthaul and processing capacity prelogs, and BBUP-BS ratio. The lower bound is obtained through two coding schemes based on decomposing the network into non-interfering parallelogram and hexagonal clusters, respectively, in each of which the number of mobile users are determined respect to BBUP-BS ratio. In both schemes, BSs apply point-point Gaussian vector quantizers to receive signals and send the quantization messages to the associated BBUPs over fronthaul links for joint decoding. For small and moderate fronthaul capacities, i.e., $\mu_F \leq 2M$, the achievability gap between lower and cut-set bounds decreases with inverse of the BBUP-BS ratio. Therefore, the cut-set bound is almost achieved even for small cluster sizes. For higher fronthaul capacity prelogs, the achievability gap is not always tight but decreases with processing capacity prelog. However, the cut-set bound, e.g. at $\frac{5M}{6}$, can be achieved with a moderate clustering size of $\frac{1}{r_h} = 12$ or $\frac{1}{r_p} = 16$.

The results also show that, for low and moderate fronthaul capacities, parallelogram clustering achieves at worst what hexagonal clustering achieves. However, for large fronthaul capacities, any clustering can outperform the other regarding the design parameters and, due to the clustering geometry, smaller hexagonal clusters can provide higher joint decoding gain than relatively larger parallelogram clusters. Therefore, the results provide valuable insights into appropriate ways of clustering for mobile users/sectors, emphasizing the isolation of clusters, particularly if inter-cell interference is highly detrimental.

The finite SNR analysis shows that the proposed scheme outperforms the interfering clustering case at all SNR range except low SNR given that the quantization variance can be chosen low enough not to make out-of-cluster interference detrimental. The performance gap between these two cases increases with SNR.

The dual results are obtained for downlink straightforwardly. To this end, the BBUPs should jointly encode all message of a cluster, i.e., the transmit signals at sector antennas are generated. Then, the quantized versions of transmit signals are sent to BSs through fronthaul links and noisy recovered versions of transmitted signals are emitted through sector antennas. Each mobile user applies point-to-point decoding techniques. The same DoF is achieved if the good precoding matrix is obtained.

Chapter 4

Local MCP with Lattice Codes in Multi-Cloud Based Sectorized Cellular Networks

4.1 Introduction

In this chapter, we investigate the benefit of local MCP in a M-CRAN that employs lattice based codes, CoF and QCoF¹. We analyse this benefit by decomposing the network into **non-overlapping** but **interfering** hexagonal clusters (I_h -clustering) that we propose in both Section 2.6 and 3.8. In a general interference network, it is known by [46, Theorem 11] that, for CoF, successful decoding of messages is possible if the integer coefficient vectors are linearly independent, i.e., full rank integer coefficient matrix. In our network, which is a **local** interference model, the channel matrix of a I_h -cluster of any size is inherently sparse, which result in rank deficiency for integer coefficient matrix of CoF with high probability. Therefore, we proceed the analysis for I_h -cluster of size $t = 1$. However, it could be easily extended for larger cluster sizes.

For $t = 1$, other than I_h -clustering, there is only one type of non-overlapping but interfering hexagon-like clustering, which we call wind-spinner-clustering (WSC) due to its shape. We compare the performance of the I_h -clustering of size $t = 1$, referred to as I_h -cluster in short throughout the chapter, with WSC for CoF, QCoF and also Gaussian code to show the effectiveness of the clustering way of I_h -clustering. By simulations, we show that it outperforms WSC in all SNR range for lattice code implementations, and also analytically for Gaussian codes in Appendix C. As we stated above, CoF is a rank dependent scheme and therefore it suffers from rank deficiency of integer coefficient matrix. Therefore, we propose QCoF [5] as a suitable candidate for the clustered sectorized cellular networks since it is not a rank dependent scheme. We show that QCoF substantially improves the sum-rate performance of both I_h -clustering and WSC over CoF implementation

¹The details of CoF and QCoF can be found in Appendix B.

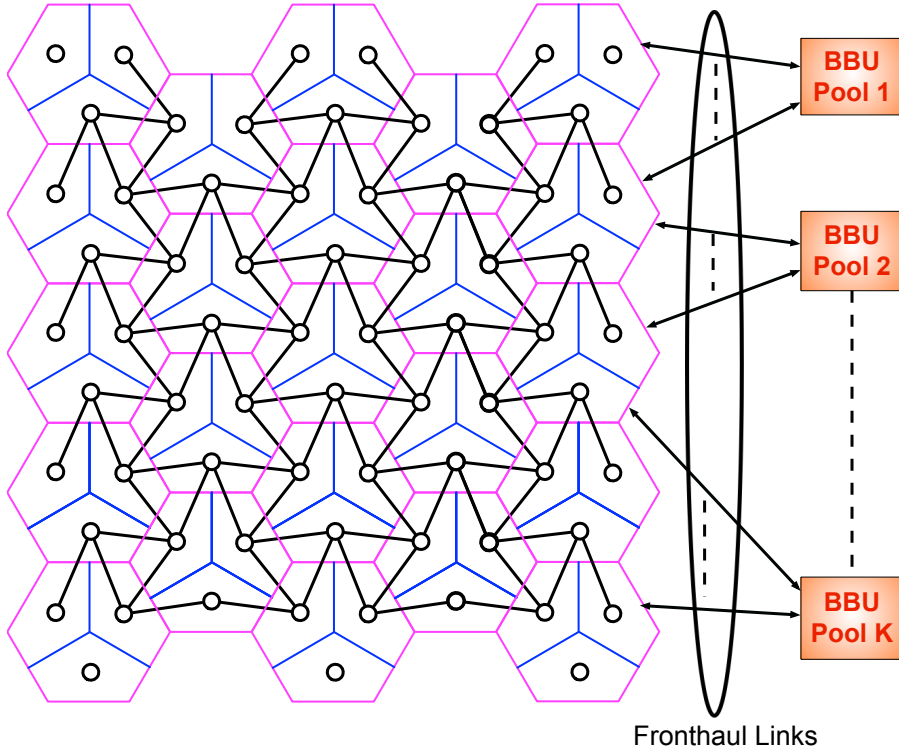


Figure 4.1: Sectored cellular model with C-RAN.

in all SNR range.

Owing to the complexity in generation of nested lattice codes, we study the effect of reducing the number of nested lattices for QCoF implementation. We reduce required number of nested lattices by assigning the same lattice codebook to more than one users during all transmission block and choosing the rate of the lattice codebook as the minimum of assigned user rates. We show by simulations that reducing number of employed nested lattices provides a tolerable sum-rate loss especially when the fronthaul resources is scarce, e.g., wireless implementation of fronthaul transmission. Also, it is shown that implementation of QCoF using even one nested lattice code outperforms CoF until moderately high SNR values.

In Section 4.2, we give network model, decomposition of network and communication model. In Section 4.3 and Section 4.4, we proceed the CoF and QCoF analysis for both clustering, respectively. In Section 4.5, we present the assignment algorithm for reducing the number of nested lattices and present the results.

4.2 Problem Definition

In this part, we reintroduce the M-CRAN and the communication model presented in Section 3.2 with some modifications.

4.2.1 Network Model

Consider the cellular network consisting of $N \gg 1$ hexagonal cells, each containing a BS equipped with 3 directional receive antennas. Every cell is divided into three sectors, where each sector is covered by 1 receive antenna². Usage of directional antennas, where side lobe radiation patterns are negligible, implies that communications in the three sectors of a cell do not interfere with each other. The model is restricted to a single mobile user per sector, which is convenient with current 4G standards that makes use of orthogonal multiple-access [54]. It is assumed that the signal from a mobile user attenuates rapidly enough so that it cannot cause interference to non-adjacent sectors. These assumptions lead to the interference graph in Figure 4.1, where each small circle depicts a mobile user and corresponding sector receive antenna. Solid black lines between any two circles represent symmetric interference between mobile user and sector antenna pairs of adjacent sectors. We assume that there are $K \gg 1$ base band unit pool (BBUP) in the network and each sector is connected to its associated BBUP through fronthaul link of its BS. For each sector of a BS, equal fronthaul rate C is allocated.

The users are given n channel uses to reliably communicate their messages. Each user $u \in \mathcal{T}$, $\mathcal{T} = \{1, \dots, 3N\}$, transmits a real signal $\mathbf{x}_u \in \mathbb{R}^{1 \times n}$ with average power constraint $\frac{1}{n}E\|\mathbf{X}_u\|^2 \leq P$. Let \mathcal{T}_u denote the index set of users whose transmit signals are observed by Rx u (including user u). The received signal at Rx u is

$$\mathbf{y}_u = \sum_{v \in \mathcal{T}_u} h_{uv} \mathbf{x}_v + \mathbf{z}_u \quad (4.1)$$

where each entry of $\mathbf{z}_u \in \mathbb{R}^{1 \times n}$ is an independent standard Gaussian and $h_{uv} \in \mathbb{R}$ denotes independent standard Gaussian channel coefficient from user v to sector u , which is constant during n channel uses. It is assumed that a channel coefficient is known by the corresponding sectors and the corresponding BBUP.

4.2.2 Decomposition to Identical Clusters and Communication Model

Consider the decomposed networks shown in Figure 4.2, where each I_h -cluster and WSC is comprised of 9 users/sectors whose interference pattern shown in solid black lines. Therefore, dashed lines refer to out-of-cluster interference pattern. We assume that there is an associated BBUP for each cluster.

Each mobile user $u \in \mathcal{T}$ chooses a message W_u uniformly distributed over the message set $\{1, \dots, 2^{nR_u}\}$ and encodes it to the vector \mathbf{x}_u for transmission. After observing receive signal at sector antennas, each BS quantizes each of its receive signals using at most with C bits and then sends the quantized messages only to the corresponding BBUP. Each BBUP is responsible to decode user messages of corresponding cluster by treating out-of-cluster as noise.

²Practically it is known that directional antenna systems are implemented by more than one antennas. However, for the sake of simplicity of the analysis, we assume that each sector has 1 antenna.

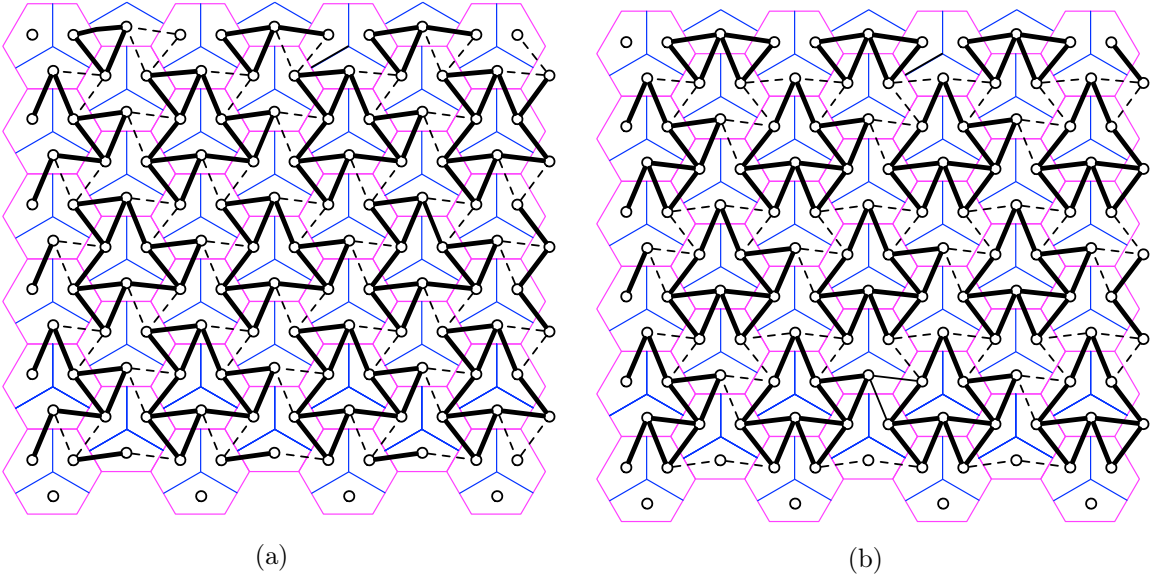


Figure 4.2: a-) Decomposition of cellular network into WSCs. b-) Decomposition of cellular network into I_h -clusters.

In view of the clustering regularity and without loss of generality, we focus only on one cluster of each clustering type with its out-of-cluster interferers, see Figure 4.3. Let the index set $\mathcal{N}^c := \{1, \dots, 9\}$ denote **in-cluster** sectors and the index set $\mathcal{N}^o := \{10, \dots, 18\}$ denotes **out-of-cluster** sectors. We define two types of index sets for each sector u :

$$\mathcal{T}_u^c := \{v: v \in \mathcal{N}^c, \text{sector antenna } u \text{ observes signal of user } v\}$$

and

$$\mathcal{T}_u^o := \{v: v \in \mathcal{N}^o, \text{sector antenna } u \text{ observes signal of user } v\}.$$

4.3 CoF for Decomposed Network

Consider Figure 4.3 and assume that the corresponding BBUP estimates the communication rate of each user before communication process starts and asks the **in-cluster** users, $u \in \mathcal{N}^c$, to employ one of n -dimensional nested lattices $\Lambda_s \subseteq \Lambda_1 \subseteq \dots \subseteq \Lambda_9$ to construct their codebooks, where Λ_s refers to the shaping lattice with $\sigma^2(\Lambda_s) = P$. Mapping from users to nesting order of lattices is given by $\phi: \mathcal{U} \mapsto \mathcal{V}$, s.t $\mathcal{U}, \mathcal{V} = \mathcal{N}^c$. Notice that we are not interested with nesting order of users $u \in \mathcal{N}^o$ since we treat out-of-cluster interference as noise. To perform encoding, as a first step each user $u \in \mathcal{N}^c$ maps its message \mathbf{w}_u to a lattice codeword $\mathbf{t}_u \in \Lambda_{\phi(u)} \cap \mathcal{V}(\Lambda_s)$, then, dithers its lattice point, takes mod Λ_s and transmits the signal

$$\mathbf{x}_u = [\mathbf{t}_u(\mathbf{w}_u) - \mathbf{d}_u] \bmod \Lambda_s \quad (4.2)$$

where the dither \mathbf{d}_u is independently and uniformly distributed over the voronoi region of $\mathcal{V}(\Lambda_s)$ and hence, by [46, Lemma 7], $E\|\mathbf{X}_u\|^2 = nP$. Each dither $\{\mathbf{d}_u\}_{u \in \mathcal{N}^c}$ is shared with

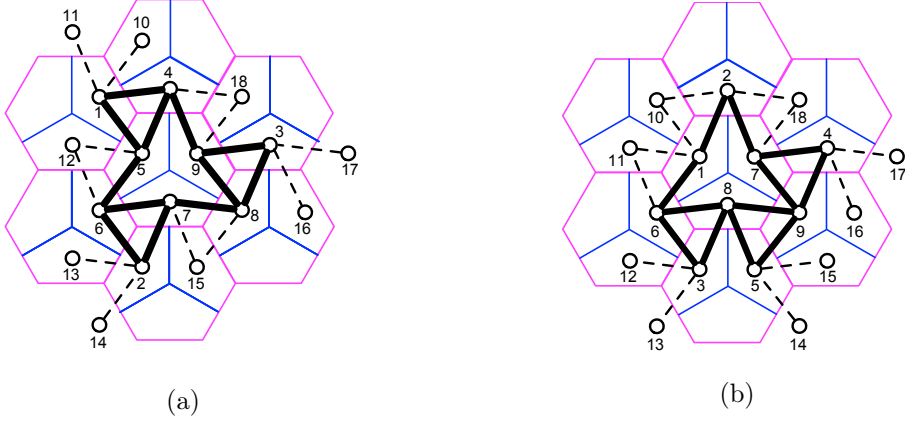


Figure 4.3: a-) A single WSC with out-of-cluster interferers. b-) A single I_n -cluster with out-of-cluster interferers.

the corresponding sectors and BBUP. In the similar manner, each user $u \in \mathcal{N}^o$ produces its transmission signal \mathbf{x}_u with $E\|\mathbf{X}_u\|^2 = nP$.

The channel output at Rx $u \in \mathcal{N}^c$ is

$$\mathbf{y}_u = \sum_{v \in \mathcal{T}_u^c} h_{uv} \mathbf{x}_v + \sum_{v \in \mathcal{T}_u^o} h_{uv} \mathbf{x}_v + \mathbf{z}_u, \quad u \in \mathcal{N}^c. \quad (4.3)$$

The objective of each sector u is to compute an integer combination of the transmitted lattice codewords by treating out-of-cluster interference as noise, that is

$$\mathbf{v}_u = \left[\sum_{v \in \mathcal{T}_u^c} a_{uv} \mathbf{t}_v \right] \bmod \Lambda_s, \quad u \in \mathcal{N}^c. \quad (4.4)$$

where $a_{uv} \in \mathbb{Z}$. Note that each sector u attempts to compute the equation that is a function of the lattice codewords $\{\mathbf{t}_v\}_{v \in \mathcal{T}_u^c}$. In order to do so, each sector u applies scaling to received signal, removes the dithers of corresponding in-cluster signals, and takes mod Λ_s , respectively, then obtains

$$\begin{aligned} \tilde{\mathbf{y}}_u &= \left[\alpha \mathbf{y}_u + \sum_{v \in \mathcal{T}_u^c} a_{uv} \mathbf{d}_v \right] \bmod \Lambda_s \\ &= \left[\mathbf{v}_u + \mathbf{z}_u^{\text{eff}} \right] \bmod \Lambda_s \end{aligned} \quad (4.5)$$

where

$$\mathbf{z}_u^{\text{eff}} = \sum_{v \in \mathcal{T}_u^c} (\alpha h_{uv} - a_{uv}) \mathbf{x}_v + \sum_{v \in \mathcal{T}_u^o} \alpha h_{uv} \mathbf{x}_v + \alpha \mathbf{z}_v \quad (4.6)$$

is the **effective noise** including noninteger in-cluster interference, out-of-cluster interference and Gaussian noise. Subsequently, as explained in detail in Appendix B.2, sector u applies quantization to $\tilde{\mathbf{y}}_u$ and computes $\hat{\mathbf{v}}_u$. Let $\mathbf{a}_u = [a_{l1}, \dots, a_{l9}]^T$ be the integer computation vector of sector u with $a_{uv} = 0$, if $v \notin \mathcal{T}_u^c$. Let $\mathbf{h}_u^c = [h_{l1}, \dots, h_{l9}]^T$ and $\mathbf{h}_u^o = [h_{l10}, \dots, h_{l18}]^T$ denote in-cluster and out-of-cluster channel vectors, respectively,

with $h_{uv} = 0$, if $v \notin \mathcal{T}_u^c \cup \mathcal{T}_u^o$. For instance, for user 1 of I_h -cluster, these vectors would be denoted as

$$\begin{aligned}\mathbf{a}_1 &= [a_{11}a_{12} \ 0 \ 0 \ 0 \ a_{16} \ 0 \ 0 \ 0]^T, \\ \mathbf{h}_1^c &= [h_{11}h_{12} \ 0 \ 0 \ 0 \ h_{16} \ 0 \ 0 \ 0]^T, \\ \mathbf{h}_1^o &= [h_{1,10}h_{1,11} \ 0 \ 0 \ 0 \ 0 \ 0 \ 0 \ 0]^T.\end{aligned}$$

Then, the variance of effective noise is given by

$$\begin{aligned}\sigma_{\text{eff}}^2(P, \mathbf{h}_u^c, \mathbf{h}_u^o; \alpha_u, \mathbf{a}_u) &= \frac{1}{n} E \|\mathbf{z}_u^{\text{eff}}\|^2 \\ &= P (\|\alpha_u \mathbf{h}_u^c - \mathbf{a}_u\|^2 + \|\alpha_u \mathbf{h}_u^o\|^2) + \|\alpha_u\|^2\end{aligned}\quad (4.7)$$

and, by [46], as $n \rightarrow \infty$, the computation rate at sector u is given by

$$\begin{aligned}\mathcal{R}_{\text{co}}(P, \mathbf{h}_u^c, \mathbf{h}_u^o; \mathbf{a}_u) &= \max_{\alpha} \frac{1}{2} \log^+ \left(\frac{P}{\sigma_{\text{eff}}^2(P, \mathbf{h}_u^c, \mathbf{h}_u^o; \alpha_u, \mathbf{a}_u)} \right) \\ &= \frac{1}{2} \log^+ \left(\frac{1 + P \|\mathbf{h}_u^c\|^2}{(1 + P (\|\mathbf{h}_u^c\|^2 + \|\mathbf{h}_u^o\|^2)) \|\mathbf{a}_u\|^2 - P (\mathbf{h}_u^{c,T} \mathbf{a}_u)^2} \right)\end{aligned}\quad (4.8)$$

where $\alpha_u = \frac{P \mathbf{h}_u^{c,T} \mathbf{a}_u}{1 + P (\|\mathbf{h}_u^c\|^2 + \|\mathbf{h}_u^o\|^2)}$ and $\log^+(x) = \max\{0, \log(x)\}$. We can now use the result of [46] that the computation error probability, $\Pr(\hat{\mathbf{v}}_u \neq \mathbf{v}_u)$, becomes vanishingly small as $n \rightarrow \infty$, if the communication rates of users whose lattice codewords are elements of \mathbf{v}_u , i.e., $\{R_v\}_{a_{uv} \neq 0 \text{ s.t. } v \in \mathcal{T}_u^c}$, is chosen smaller than the computation rate of the sector u :

$$\max_{v \in \mathcal{T}_u^c, a_{uv} \neq 0} R_v < \mathcal{R}_{\text{co}}(P, \mathbf{h}_u^c, \mathbf{h}_u^o; \mathbf{a}_u).\quad (4.9)$$

Note that $a_{uv} = 0$ by definition when $v \notin \mathcal{T}_u^c$, hence $\{R_v\}_{v \notin \mathcal{T}_u^c}$ is not constrained by $\mathcal{R}_{\text{co}}(P, \mathbf{a}_u; \mathbf{h}_u^c, \mathbf{h}_u^o)$. Then, by Lemma B.1, if we choose rate of user u as following

$$R_u < \min_{v \in \mathcal{T}_u^c, a_{vu} \neq 0} \mathcal{R}_{\text{co}}(P, \mathbf{h}_v^c, \mathbf{h}_v^o; \mathbf{a}_v),\quad (4.10)$$

the constraint (4.9) is met for all sectors.

After equation computation, the equation $\hat{\mathbf{v}}_u$ of sector u is forwarded by its BS through noise free fronthaul link of rate C . Due to the linear nature of nested lattice codes, all of the decoded equations are basically lattice codewords from one of the user codebooks. Therefore, forwarding operation is successful if

$$R_u < \min \left\{ C, \min_{v \in \mathcal{T}_u^c, a_{vu} \neq 0} \mathcal{R}_{\text{co}}(P, \mathbf{h}_v^c, \mathbf{h}_v^o; \mathbf{a}_v) \right\}.\quad (4.11)$$

Then, the BBUP decodes all of the messages $\{\mathbf{w}_u\}_{u \in \mathcal{N}^c}$ provided that $\mathbf{A} = [\mathbf{a}_1, \dots, \mathbf{a}_9]^T$ is full rank, see [46] for details.

4.4 QCoF for Decomposed Network

The difference between CoF and QCoF lies in the step after computing the equation $\hat{\mathbf{v}}_u$, $u \in \mathcal{N}^c$, see Appendix B.3 for details. To implement QCoF, each sector u remaps the computed equation $\hat{\mathbf{v}}_u$, which is a linear combination of **lattice** points, into a linear combination of **transmitted** signals using the same integer coefficients $a_{uv} \in \mathbb{Z}$, $v \in \mathcal{T}_u^c$:

$$\mathbf{s}_u = \sum_{v \in \mathcal{T}_u^c} a_{uv} \mathbf{x}_v, \quad u \in \mathcal{N}^c \quad (4.12)$$

with zero probability of error as long as $\mathcal{R}_{\text{co}}(P, \mathbf{a}_u; \mathbf{h}_u^c, \mathbf{h}_u^o) > 0$, [44, Lemma 1]. Then, each sector u compresses the remapped equation \mathbf{s}_u at rate C by using n -dimensional nested lattice pairs $\Lambda_{s,u}^c \subseteq \Lambda_u^c$, where $\Lambda_{s,u}^c$ is the shaping lattice and Λ_u^c is the coding lattice for compression. Note that all \mathbf{s}_u 's are functions of some \mathbf{x}_v 's leading to correlation between remapped equations. Hence, sectors exploit this correlation in quantization process as explained in the following. Let the mapping

$$\psi : \mathcal{U} \mapsto \mathcal{V} \quad u, v \in \mathcal{N}^c \quad (4.13)$$

define a **compression/decompression** order such that u is compressed/decompressed before v if $\psi(u) < \psi(v)$ and let $\psi_u = \{v : \psi(v) < \psi(u)\}$ denotes the indices of sectors whose remapped equation \mathbf{s}_v 's are compressed/decompressed before u . Also, let $\hat{\mathbf{S}}_{\psi_u} = [\hat{\mathbf{s}}_{\psi_u(1)}^T, \dots, \hat{\mathbf{s}}_{\psi_u(|\psi_u|)}^T]^T$ denote formerly decompressed equations from the first-to-last one, i.e., $\hat{\mathbf{s}}_{\psi_u(v)}$ is decompressed before $\hat{\mathbf{s}}_{\psi_u(v+1)}$. The Wyner-Ziv compression [75] at sector u is carried out by assuming that the correlation between \mathbf{s}_u and $\hat{\mathbf{S}}_{\psi_u}$ is used as side information through LMMSE estimation during the decompression process. Therefore, shaping and coding lattice variances for compression are chosen as

$$\sigma^2(\Lambda_{s,u}^c) = \nu(\mathbf{s}_u | \hat{\mathbf{S}}_{\psi_u}) + \sigma^2(\Lambda_u^c) \quad (4.14)$$

$$\sigma^2(\Lambda_u^c) = \frac{\nu(\mathbf{s}_u | \hat{\mathbf{S}}_{\psi_u})}{2^{2C} - 1}, \quad (4.15)$$

Here, $\nu(\mathbf{s}_u | \hat{\mathbf{S}}_{\psi_u})$ denotes the LMMSE obtained by estimating \mathbf{s}_u from $\hat{\mathbf{S}}_{\psi_u}$ and is given as

$$\nu(\mathbf{s}_u | \hat{\mathbf{S}}_{\psi_u}) = \mathbf{a}_u^T \left(P^{-1} \cdot \mathbf{I}_9 + \mathbf{A}_{\psi_u}^T \sum_{\psi_u}^{-1} \mathbf{A}_{\psi_u} \right)^{-1} \mathbf{a}_u \quad (4.16)$$

where $\mathbf{A}_{\psi_u} = [\mathbf{a}_{\psi_u(1)}, \dots, \mathbf{a}_{\psi_u(|\psi_u|)}]^T$ and

$$\sum_{\psi_u} = \begin{bmatrix} \sigma^2(\Lambda_{\psi_u(1)}^c) & & \\ & \ddots & \\ & & \sigma^2(\Lambda_{\psi_u(|\psi_u|)}^c) \end{bmatrix} \quad (4.17)$$

so that the rate constraint $C = \frac{1}{2} \log \frac{\sigma^2(\Lambda_{s,u}^c)}{\sigma^2(\Lambda_u^c)}$ is satisfied, and also, the minimum quantization noise for the backhaul rate constraint is obtained.

At the BBUP, as explained in detail in [5] and Appendix B.3, making choose of shaping and coding lattices for compression as in (4.14) and (4.15) and making use of the formerly reconstructed $\hat{\mathbf{s}}_v$, $v \in \psi_u$, as side information through an LMMSE estimation makes $\Pr(\hat{\mathbf{s}}_u \neq \mathbf{s}_u)$ vanishingly small as $n \rightarrow \infty$. After reconstruction of all $\{\hat{\mathbf{s}}_u\}_{u \in \mathcal{N}^c}$, the transmitted signals are again passed through LMMSE filter to estimate the transmitted signals. Let $\mathbf{X}_\psi = [\mathbf{x}_{\psi^{-1}(1)}^T, \dots, \mathbf{x}_{\psi^{-1}(9)}^T]^T$ and $\hat{\mathbf{S}}_\psi = [\hat{\mathbf{s}}_{\psi^{-1}(1)}^T, \dots, \hat{\mathbf{s}}_{\psi^{-1}(9)}^T]^T$ denote the transmitted signals and remapped equations according to the mapping ψ . The LMMSE estimation of \mathbf{X}_ψ is given as

$$\hat{\mathbf{X}}_\psi = \Gamma_{\text{LMMSE}} \hat{\mathbf{S}}_\psi, \quad (4.18)$$

where $\Gamma_{\text{LMMSE}} = P\mathbf{A}_\psi^T \left(P\mathbf{A}_\psi\mathbf{A}_\psi^T + \sum_\psi \right)^{-1}$ with $\mathbf{A}_\psi = [\mathbf{a}_{\psi^{-1}(1)}, \dots, \mathbf{a}_{\psi^{-1}(9)}]^T$ s.t. $\mathbf{a}_{\psi^{-1}(u)} = [\mathbf{a}_{\psi^{-1}(u), \psi^{-1}(1)}, \dots, \mathbf{a}_{\psi^{-1}(u), \psi^{-1}(9)}]^T$ for $u \in \mathcal{N}^c$, and

$$\sum_\psi = \begin{bmatrix} \sigma^2 \left(\Lambda_{\psi^{-1}(1)}^c \right) & & & \\ & \ddots & & \\ & & \sigma^2 \left(\Lambda_{\psi^{-1}(9)}^c \right) & \\ & & & \end{bmatrix}. \quad (4.19)$$

Then, lattice codewords $\{\mathbf{t}_u\}_{u \in \mathcal{N}^c}$ are estimated with lattice decoding and successive interference cancellation (SIC), at the same order with decompression, see Appendix B.3 for details. The resulting LMMSE covariance matrix obtained by applying SIC is given as

$$\mathbf{K}_{ee} = \left(P^{-1}\mathbf{I}_{9 \times 9} + \mathbf{A}_\psi^T \sum_\psi^{-1} \mathbf{A}_\psi \right)^{-1}, \quad (4.20)$$

which leads to the following unique Cholesky decomposition

$$\mathbf{G}\mathbf{G}^T = \left(\mathbf{I}_{9 \times 9} + P\mathbf{A}_\psi^T \sum_\psi^{-1} \mathbf{A}_\psi \right) \quad (4.21)$$

where \mathbf{G} is a lower triangular square matrix with strictly positive entries.

As a result of compression, decompression and SIC based lattice decoding operations, QCoF eliminates the full rank constraint on \mathbf{A}_ψ (equivalently on \mathbf{A}) imposed by CoF and, by Lemma B.2, puts forward another rate constraint for $\{R_u\}_{u \in \mathcal{N}^c}$ that takes into account effects of these operations:

$$R_u < \min \left\{ \min_{v \in \mathcal{T}_u^c, a_{vu} \neq 0} \mathcal{R}_{\text{Co}}(P, \mathbf{h}_v^c, \mathbf{h}_v^o; \mathbf{a}_v), \frac{1}{2} \log \left(g_{\psi(u), \psi(u)}^2 \right) \right\}, \quad (4.22)$$

where $g_{\psi(u), \psi(u)} = [\mathbf{G}]_{\psi(u), \psi(u)}$.

4.5 Simulation Results

In simulations, we run our algorithm over 10000 channel realizations, where each channel coefficient is independently drawn from a standard Gaussian. As a benchmark as well as to compare I_h -clustering with WSC in Gaussian coding, we compare average sum-rate

performance of QCoF and CoF in both clustering employing 9 nested lattices with average sum-rate obtained through cut-set argument. Figure 4.4a shows upper and lower bounds on the average sum-rate for both clustering schemes with $C = 5$ bits for each sector. It is seen that I_h -clustering outperforms WSC for Gaussian coding scheme. This is due to the fact that I_h -clustering provides higher mutual information than WSC.

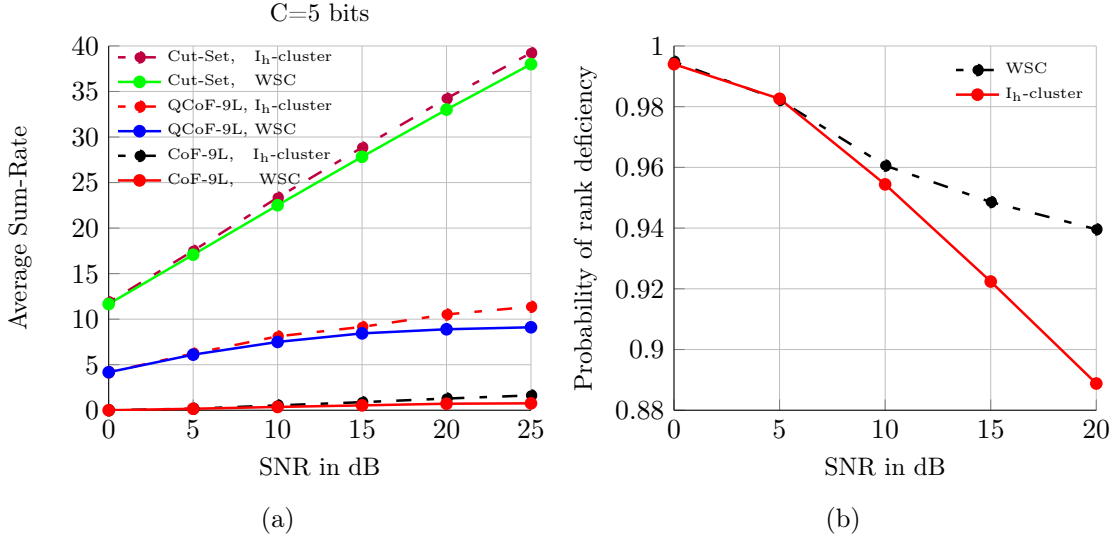


Figure 4.4: a-) Performance comparison of WSC and I_h -cluster for cut-set bound, QCoF and CoF coding schemes. b-) Rank deficiency probabilities of WSC and I_h -cluster for CoF with the selection of best integer vector at each sector.

We allow each sector to compute its equation with the **best integer** vector that gives the **highest** computation rate. As seen in Figure 4.4b, the probability of rank deficiency is very high for both the clusterings. The reason behind is that each sector computes a linear combination of codewords from its in-cluster interferences and at most 5 out of 9 users' signals are observed by a sector. For instance, the A matrix for I_h -clustering, say A_I , is given as:

$$A_I = \begin{bmatrix} a_{11} & a_{12} & 0 & 0 & 0 & a_{16} & 0 & 0 & 0 \\ a_{21} & a_{22} & 0 & 0 & 0 & 0 & a_{27} & 0 & 0 \\ 0 & 0 & a_{33} & 0 & 0 & a_{36} & 0 & a_{38} & 0 \\ 0 & 0 & 0 & a_{44} & 0 & 0 & a_{47} & 0 & a_{49} \\ 0 & 0 & 0 & 0 & a_{55} & 0 & 0 & a_{58} & a_{59} \\ a_{61} & 0 & a_{63} & 0 & 0 & a_{66} & 0 & a_{68} & 0 \\ 0 & a_{72} & 0 & a_{74} & 0 & 0 & a_{77} & 0 & a_{79} \\ 0 & 0 & 0 & a_{83} & 0 & a_{85} & a_{86} & a_{88} & a_{89} \\ 0 & 0 & 0 & a_{94} & a_{95} & 0 & a_{97} & a_{98} & a_{99} \end{bmatrix} \quad (4.23)$$

As seen, the A matrix is sparse, and therefore it is likely to have rank failure in both

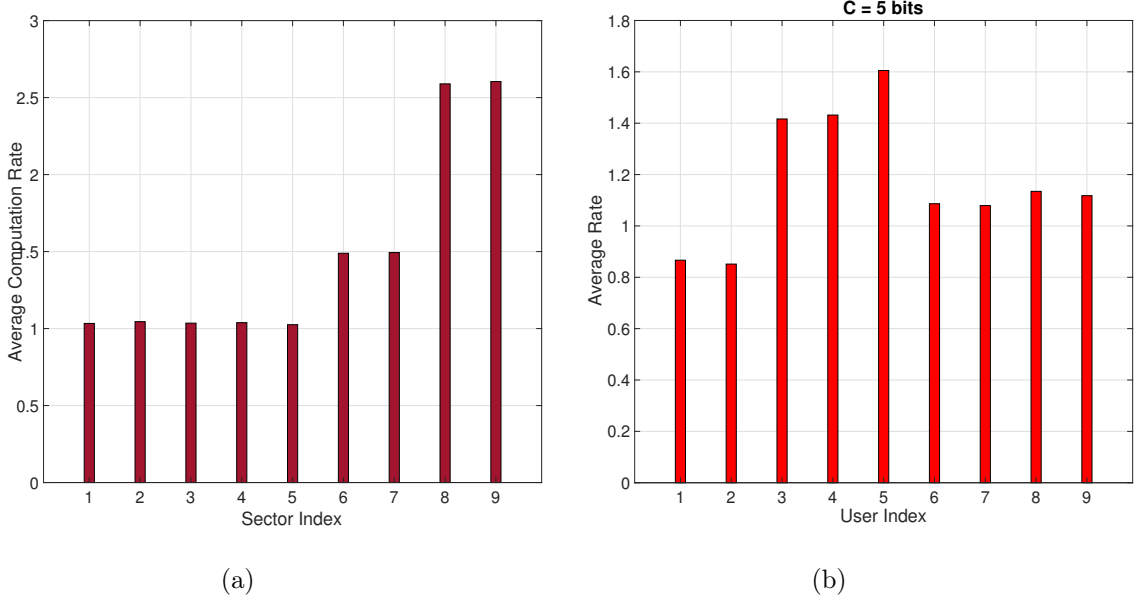


Figure 4.5: a-) Average computation rates for each sector of I_h -cluster at SNR= 20 dB. b-) Average rates for each user of I_h -cluster at SNR= 20 dB.

clustering due to computation at sectors with best integer vector. This condition implies very poor performance for the proposed CoF scheme, see Figure 4.4a. In the figure, we see also that I_h -clustering achieves higher average sum-rate than WS for CoF due to lower rank deficiency probability. However, since QCoF does not rely on full rank requirement due to SIC and lattice decoding, it outperforms CoF in both clustering at all SNR range. Notice that, for QCoF, I_h -clustering shows better performance than WSC at all SNR range and average sum-rate difference between two clusterings is around 2 bits at 25 dB SNR. In the rest, we investigate effect of reducing the number of nested lattices only for I_h -clustering for QCoF scheme since I_h -clustering provides higher rates than WSC for all coding schemes.

4.5.1 Reducing the Nested Lattice Number

Owing to complexity in generation of nested lattices, we study the impact of reducing number of nested lattices on the average sum-rate. For that, we **permanently** assign some nested lattice codebooks to more than one user during all channel realizations of simulation. We choose the rate of assigned lattice codebook as the **minimum** achievable rate of the assigned users for that realization obtained by Eq. (4.22). The procedure of assigning users to lattice codebooks is based on two observations. First, note that, in Figure 4.5b, average rates of users are not equal to each other. The rationale behind this is the following. The average computation rate of a sector $u \in \mathcal{N}^c$ depends on the number of out-of-cluster interferers. Therefore, the sectors 8 and 9, which have no out-of-cluster interferer, have highest average computation rate, see Figure 4.5a. The average

rate of user u is closely related to the average computation rates of sectors $v \in \mathcal{T}_u^c$, which constraints the achievable rate of user u by Eq. (4.22). For example, achievable rate of user 5 is constrained by sectors 5, 8 and 9, which have 2 and no out-of-cluster interferers, respectively. However, the achievable rate of user 2 is constrained by computation rate of sectors 1, 2 and 7, which have 2 and 1 out-of-cluster interferers, respectively. Therefore, average rate of user 5 is almost double of average rate of user 2, see Figure 4.5b. Respect to Figure 4.5b, we categorize the users of I_h -cluster into 4 different groups wrt average achievable rates, i.e., $\mathcal{J}_1 = \{1, 2\}$, $\mathcal{J}_2 = \{6, 7, 8, 9\}$, $\mathcal{J}_3 = \{3, 4\}$ and $\mathcal{J}_4 = \{5\}$. The second

Table 4.1: User grouping for assignment to lattice codes respect to number of nested lattices

# of Nested Lattices	Group#1	Group#2	Group#3	Group#4
8	(1, 2)	-	-	-
7	(1, 2)	(6, 9)	-	-
6	(1, 2)	(6, 9)	(7, 8)	-
5	(1, 2)	(6, 9)	(7, 8)	(3, 4)
4	(1, 2)	(6, 7, 9)	(4, 8)	(3, 5)
3	(1, 2, 8)	(6, 7, 9)	(3, 4, 5)	-
2	(1, 2, 6, 7, 8)	(3, 4, 5, 9)	-	-
1	(1, 2, 3, 4, 5, 6, 7, 8, 9)	-	-	-

observation is that it is likely that the more users are assigned to a lattice codebook the more rate differences between the maximum and the minimum rates of assigned users is obtained. Based on these facts, we have two criteria in assigning for lattice codebooks to users to get higher average sum rate:

- We group users in pairs as long as the number of nested lattices is enough, i.e. when more than 4 nested lattices is available we can group the users in pairs, and we assign a lattice codebook for each pair,
- We always group lowest available average rate users, e.g. for 8 nested lattices, we group users of \mathcal{J}_1 . For 5 nested lattices, we choose 4 pairs such that the first consists users of \mathcal{J}_1 , the second and third are pairs from \mathcal{J}_2 users, and the fourth consists users of \mathcal{J}_3 . See Table 4.1 for user grouping that we use in simulations respect to number of nested lattices.

In Figure 4.6, we plot the performance of QCoF and its reduced number of nested lattice implementations vs SNR with $C = 5$ bits. We see that the sum-rate differences between employing consecutive nesting numbers are not uniform since the average rates of grouped users change regarding the number of nested lattices. It is seen that the lowest marginal sum-rate difference is between 9 and 8 nested lattices employment since the \mathcal{J}_1 users have the lowest average rates. However, the marginal difference in reducing nested

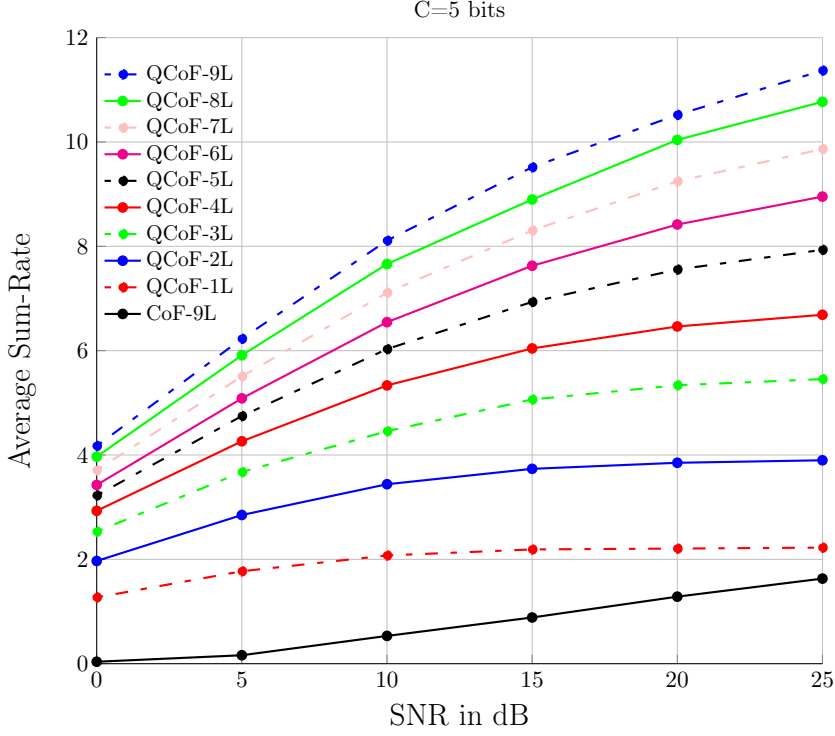


Figure 4.6: Average sum rate achieved in I_h -clusters respect to number of employed nested lattices versus SNR.

lattices from 8 to 7 is higher than in reducing from 9 to 8 nested lattices since the grouped user pair is from \mathcal{J}_2 , which is higher average user rate set, users in reducing from 8 to 7 lattice codes. Figure 4.6 shows that the proposed grouping for 4 nested lattice code achieves sum-rate of almost 7 bits on average at SNR of 25 dB. It is noteworthy that implementation of QCoF scheme even with single lattice code performs better than CoF with 9 nested lattices implementation until moderately high SNR values while the CoF scheme achieves almost zero rates at low SNR values due to rank deficiency problem.

Figure 4.7 depicts the performance of QCoF and its implementation with reduced number of nested lattices versus C at 20 dB SNR. The plot shows that the marginal sum-rate differences between consecutive number of nested lattice employments are not uniform and the marginal differences is quite low when fronthaul capacity is scarce. Therefore, it is evident that reducing nesting number is more efficient if the fronthaul capacity is limited, which is a common case when the fronthaul is a wireless connection rather than fiber-optics or microwave link. For instance, the achievable sum-rate almost saturates at $C = 5$ bits for 9 nested lattices implementation and we see that reducing the number of lattices provides less and less sum-rate degradation especially for $C < 2$. Also, we observe that implementation of QCoF with single lattice code outperforms CoF with 9 nested lattices implementation in all fronthaul capacity values.

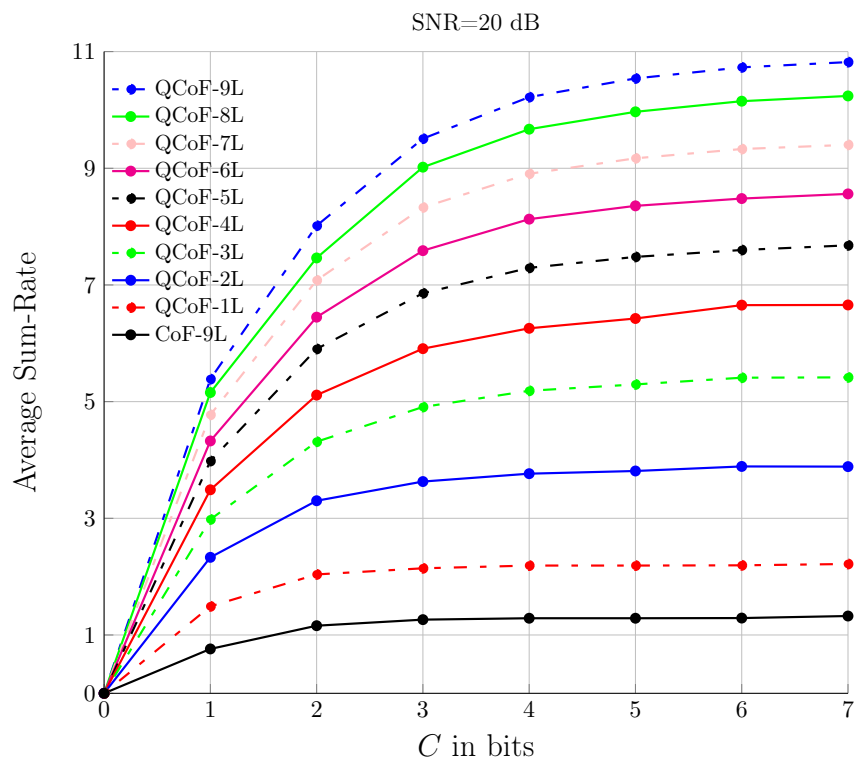


Figure 4.7: Average sum rate achieved in I_h -clusters respect to number of employed nested lattices versus fronthaul capacity C .

4.6 Summary

In this chapter, we study nested lattice code implementation in a M-CRAN and we essentially show the effectiveness of QCoF [5] implementation in exploiting interference for a network decomposed to regular clusters. In particular, we investigate the performance of the nested lattice codes for non-overlapping but interfering I_h -clustering of size $t = 1$, and we compare it with another hexagon-like non-overlapping but interfering clustering with same number of users called WSC. We show that the I_h -clustering performs better than WSC at all SNR range for Gaussian codes, QCoF and CoF coding schemes for the same number of users. Due to rank deficiency problem of CoF, we suggest to employ QCoF scheme, which shows highly favorable performance in terms of average sum-rate. However, as the generation of more than a few nested lattices are not feasible practically, for I_h -clustering, we study the impact of reducing the number of nested lattices for QCoF on the sum-rate. We conclude that reducing the number of lattice codes leads to lower sum-rate degradation if the fronthaul capacity is small, and that even single lattice code implementation of QCoF shows better performance than CoF in practical SNRs, particularly at low and moderate SNR values.

Chapter 5

Conclusion

In this thesis, we have studied the benefits of local MCP for interference management in sectorized cellular networks at uplink under different scenarios. The contributions of Chapters 2 and 3 are proposing schemes to determine which mobile users remain silent and which transmit their messages. In fact, these schemes exploit the sectorization of the cells and are done in a way that only a few users remain silent but the network still decomposes into non-interfering clusters. The decompositions guarantee that the interferences are not propagated across clusters and therefore exploit the local MCP. The main advantage of these two schemes arise at high SNRs for both weak and strong interference regimes. Also these schemes are advantageous at low and moderate SNRs, especially if the quantization rates are small. The contribution of Chapter 4 is a lattice codebook assignment method, that enables low complexity implementation of QCoF coding scheme in the I_h -clusters of size $t = 1$ with reasonable sum-rate degradation.

To elaborate, in Chapter 2, we have investigated largest the achievable DoF per-user and the average sum-rate with local MCP in a cooperative BS setting. The cooperation is limited by the number of interaction rounds that takes into account communication delay and computational complexity, and the cooperation is carried out by limited capacity but noise free backhaul links. We have proposed a lower and an upper bound on the achievable DoF, where both of them are characterized as a function of backhaul capacity and the number of cooperation rounds. The lower bound is based on silencing a particular subset of mobile users corresponding to the cooperation round, so that the network is decomposed into non-overlapping and non-interfering clusters. In each of these clusters every BS shares its received signal through point-to-point quantization with the master cell of the cluster, that performs joint decoding for all the users of the cluster. The obtained results show that limiting the number of cooperation rounds indeed limits the achievable DoF per-user. The upper bound presented in the same chapter is information-theoretic and allows for any coding scheme. The achievability gap gets smaller as the number of cooperation round increases if the backhaul capacity is large enough. Also, it is generally close to the obtained lower bounds for small backhaul link capacities. The finite SNR analysis shows that the

silencing strategy provides some advantages over I_h -clustering schemes at moderate and high SNR ranges, as well as at low-SNR values if the backhaul transmission resources is not scarce. The results found in this chapter provide information theoretic intuition about interference management capabilities of a cooperative sectored cellular network constrained by delay, complexity, and limited backhaul capacity.

In Chapter 3, we have investigated the largest DoF per-user and the average sum-rate with local MCP in M-CRAN. In the considered communication model, the number of BBUPs, their processing capacities, and fronthaul capacities are limited. We developed a lower bound on the achievable DoF by proposing two coding schemes, a parallelogram-like scheme and a hexagonal-like scheme. The upper bound is obtained through a cut-set argument. Both the lower and upper bounds are expressed as functions of BBUP-BS ratio, BBUP processing capacity, and fronthaul capacity. The results show that the lower and upper bounds match in several cases. For example, the cut-set bound at $\frac{5M}{6}$ DoF per-user is achieved with practical BBUP-BS ratios of $r_h = \frac{1}{12}$ and $r_p = \frac{1}{16}$. The achievability gap between the lower and upper bounds is proportional to the BBUP-BS ratio when the fronthaul capacity prelog $\mu_F \leq 2M$. It has been proved that if $\mu_F \leq 2M$, the parallelogram-like clustering performs at least as good as the hexagonal-like scheme irrespective of any choice of the other parameters. When $\mu_F > 2M$, hexagonal-like clustering has better interference management capability for high enough BBUP processing capacity due to the higher joint processing gain resulting from its specific geometry. Finite SNR analysis shows that non-interfering clustering achieves higher average sum-rate than interfering clustering except at low-SNR values. The results found in this chapter provides information theoretic intuition about interference management capability of a multi cloud sectored cellular network constrained by the number of available BBUPs, the limited processing complexity, and the limited fronthaul transmission resources.

In Chapter 4, we have investigated the average achievable sum-rate with local MCP in M-CRAN for a lattice code implementation. In the considered system model, the network is decomposed into interfering but non-overlapping I_h -clusters of size $t = 1$. The choice $t = 1$ is motivated by practical cluster sizes. There is a corresponding capacity unconstrained BBUP for each cluster. For such a clustering, it is observed that CoF scheme suffers from the rank deficiency problem due to the sparsity of the integer coefficient matrix. Instead, we propose to implement the rank independent scheme QCoF from [5]. It is shown that QCoF outperforms CoF for all SNRs. Due to the implementation complexity in constructing nested lattice codes, the effect of reducing the number of nested lattices is studied. An assignment algorithm suited to clustering shape is proposed, which is also independent of channel realization. We show by simulations that the performance degradation due to reducing the number of nested lattices is tolerable if the fronthaul capacity is scarce. We observe that even single lattice code implementation of QCoF achieves better performance than the CoF implementation. From a general perspective, the results show that CoF is not suitable for such a local interference network. On the other hand, due to the rank

independency, the QCoF scheme is implementable to larger cluster sizes or to single macro cells with many small cells. The proposed algorithm can be easily extended to more users.

We finally conclude this thesis by pointing out some possible future research directions. To improve average sum-rate in Chapter 3, the BSs can perform joint optimization of transmit beamforming and compression under fronthaul constraints instead of independent point-to-point compression. However, even under individual fronthaul constraints for each user, the complexity of joint optimization of these two phenomenon is non-polynomial (NP) hard [83]. In [83], the authors have proposed a low-complexity separate beamforming and compression design algorithm that gives near optimal results for high signal-to-quantization-ratio (SQNR). A practical separate beamforming and compression design algorithm that gives good trade-off for sum-rate and complexity under individual fronthaul constraints for BSs is an interesting problem for a future study.

The integer coefficient matrix \mathbf{A} of QCoF is likely to have zero column vector due to its sparsity and the employment of the best integer vector for each sector, which results in zero rate for the corresponding users. Exploring an integer vector assignment algorithm that solves the zero column problem and decreases the average sum-rate degradation due to employment of less nested codebook is an attractive but challenging problem for future research.

Appendices

Appendix A

A.1 Proof of Remark 3.1

By (3.27), any (t_1^*, t_2^*) pair that satisfies with $t_1^* t_2^* = \lceil \frac{1}{r} \rceil$ provides the maximum number of BBUP deployment for parallelogram clustering. By (3.37), $t^* = \lceil \sqrt{\frac{1}{3r}} \rceil$ is the minimum cluster size that can be created for the given r , and hence, provides the maximum possible number of BBUP deployment for hexagon clustering. Note that $t_1^* t_2^* \leq 3t^{*2}$ for $r \in (0, 1]$.

We now check the cases for $\mu_F \leq M$ and $M \leq \mu_F \leq 2M$.

A.1.1 Case 1: $\mu_F \leq M$

Proposition A.1. *From (3.16), the achievable DoF for **Parallelogram Scheme** can be written as:*

$$\text{DoF}_P(\mu_{\text{BBU}}, \mu_F, r) = \begin{cases} \frac{\mu_{\text{BBU}}}{3t_1^* t_2^*} & \text{if } \mu_{\text{BBU}} \leq \mu_F(t_1^* t_2^*) \\ \frac{\mu_F}{3} & \text{if } \mu_{\text{BBU}} \geq \mu_F(t_1^* t_2^*) \end{cases} \quad (\text{A.1})$$

and, from (3.17), the achievable DoF for **Hexagon Scheme** can be written as:

$$\text{DoF}_H(\mu_{\text{BBU}}, \mu_F, r) = \begin{cases} \frac{\mu_{\text{BBU}}}{3} \frac{1}{3t^{*2}}, & \text{if } \mu_{\text{BBU}} \leq \mu_F(3t^{*2} - 1) \\ \max \left\{ \mu_F \frac{3t'^2 - 1}{9t'^2}, \frac{\mu_{\text{BBU}}}{9(t' + 1)^2} \right\}, & \text{if } \mu_{\text{BBU}} \geq \mu_F(3t^{*2} - 1) \end{cases} \quad (\text{A.2})$$

for t' satisfying

$$\mu_F(3t'^2 - 1) \leq \mu_{\text{BBU}} \leq \mu_F(3(t' + 1)^2 - 1). \quad (\text{A.3})$$

Proof: The first part of the proposition, (A.1), is straightforward. For the second part, note that, for a given $\mu_{\text{BBU}} > 0$, there is a unique $t' \in \mathbb{Z}^+$ that satisfies (A.3) and the maximization term in (A.2) comes from the fact that, to implement the hexagonal scheme, we choose the design parameter t that gives the maximum DoF of among minimums found for satisfying $t \geq \lceil \sqrt{\frac{1}{3r}} \rceil$. From (3.17), we infer that the term $\frac{\mu_F(3t^2 - 1)}{9t^2}$ is active in

the minimization process for $t' \geq t \geq \left\lceil \sqrt{\frac{1}{3r}} \right\rceil$ since $\mu_{\text{BBU}} \geq \mu_{\text{F}}(3t'^2 - 1)$, and that the term $\frac{\mu_{\text{BBU}}}{9t'^2}$ is active in lower bound for $t > t'$ since $\mu_{\text{BBU}} \leq \mu_{\text{F}}(3(t' + 1)^2 - 1)$. Therefore, the achievable DoF by hexagon scheme is given by the second term of (A.2) if $\mu_{\text{BBU}} \geq \mu_{\text{F}}(3t^{*2} - 1)$.

We now check all possible intervals of μ_{BBU} regarding to (A.1) and (A.2).

$$\mathbf{A.1.1.1} \quad \mu_{\text{BBU}} \leq \min \left\{ \mu_{\text{F}}(3t_1^*t_2^*), \mu_{\text{F}}(3t^{*2} - 1) \right\}$$

The DoF is given as:

$$\begin{aligned} \text{DoF}(\mu_{\text{BBU}}, \mu_{\text{F}}, r) &\geq \max \left\{ \frac{\mu_{\text{BBU}}}{3t_1^*t_2^*}, \frac{\mu_{\text{BBU}}}{3} \frac{1}{3t^{*2}} \right\}, \\ &= \frac{\mu_{\text{BBU}}}{3t_1^*t_2^*}, \end{aligned} \quad (\text{A.4})$$

since $t_1^*t_2^* \leq 3t^{*2}$ for any $r \in (0, 1]$.

$$\mathbf{A.1.1.2} \quad \mu_{\text{F}}(3t^{*2} - 1) \leq \mu_{\text{BBU}} \leq \mu_{\text{F}}(3t_1^*t_2^*)$$

The DoF is given as:

$$\begin{aligned} \text{DoF}(\mu_{\text{BBU}}, \mu_{\text{F}}, r) &\geq \max \left\{ \frac{\mu_{\text{BBU}}}{3t_1^*t_2^*}, \max \left\{ \mu_{\text{F}} \frac{3t'^2 - 1}{9t'^2}, \frac{\mu_{\text{BBU}}}{9(t' + 1)^2} \right\} \right\} \\ &= \frac{\mu_{\text{BBU}}}{3t_1^*t_2^*} \end{aligned} \quad (\text{A.5})$$

Proof: Notice that the given condition on μ_{BBU} implies $t' = t^*$ and $t_1^*t_2^* = 3t^{*2}$, otherwise the imposed condition on μ_{BBU} is not possible. Also notice that, even for the $\max \mu_{\text{BBU}} = \mu_{\text{F}} 3t_1^*t_2^* = \mu_{\text{F}} 3t^{*2}$, the following inequality holds:

$$\mu_{\text{F}} \frac{(3t^{*2} - 1)}{9t^{*2}} \geq \frac{\mu_{\text{BBU}}}{9(t^* + 1)^2} \quad \forall t^* \in \mathbb{Z}^+, \quad (\text{A.6})$$

and therefore

$$\max \left\{ \mu_{\text{F}} \frac{3t^{*2} - 1}{9t^{*2}}, \frac{\mu_{\text{BBU}}}{9(t^* + 1)^2} \right\} = \mu_{\text{F}} \frac{3t^{*2} - 1}{9t^{*2}}. \quad (\text{A.7})$$

Then, we end up with:

$$\max \left\{ \frac{\mu_{\text{BBU}}}{3t_1^*t_2^*}, \mu_{\text{F}} \frac{(3t^{*2} - 1)}{9t^{*2}} \right\} = \frac{\mu_{\text{BBU}}}{3t_1^*t_2^*}, \quad (\text{A.8})$$

since $\min \mu_{\text{BBU}} = \mu_{\text{F}}(3t^{*2} - 1)$ and $t_1^*t_2^* = 3t^{*2}$.

$$\mathbf{A.1.1.3} \quad \mu_F (3t_1^* t_2^*) \leq \mu_{\text{BBU}} \leq \mu_F (3t^{*2} - 1)$$

The DoF is given as:

$$\begin{aligned} \text{DoF}(\mu_{\text{BBU}}, \mu_F, r) &\geq \max \left\{ \frac{\mu_{\text{BBU}}}{3} \frac{1}{3t^{*2}}, \frac{\mu_F}{3} \right\} \\ &= \frac{\mu_F}{3} \end{aligned} \quad (\text{A.9})$$

Proof: The condition $\mu_{\text{BBU}} \leq \mu_F (3t^{*2} - 1)$ implies $\mu_{\text{BBU}} < \mu_F (3t^{*2})$, then

$$\frac{\mu_F}{3} \geq \frac{\mu_{\text{BBU}}}{3} \frac{1}{3t^{*2}}. \quad (\text{A.10})$$

$$\mathbf{A.1.1.4} \quad \mu_{\text{BBU}} \geq \max \left\{ \mu_F (3t_1^* t_2^*), \mu_F (3t^{*2} - 1) \right\}$$

The DoF is given as:

$$\begin{aligned} \text{DoF}(\mu_{\text{BBU}}, \mu_F, r) &\geq \max \left\{ \frac{\mu_F}{3}, \max \left\{ \mu_F \frac{3t'^2 - 1}{9t'^2}, \frac{\mu_{\text{BBU}}}{9(t' + 1)^2} \right\} \right\} \\ &= \frac{\mu_F}{3}. \end{aligned} \quad (\text{A.11})$$

Proof: If $\mu_F \frac{3t'^2 - 1}{9t'^2}$ is active in the inner maximization, then

$$\frac{\mu_F}{3} > \mu_F \frac{3t'^2 - 1}{9t'^2} \quad \forall t' \in \mathbb{Z}^+. \quad (\text{A.12})$$

If $\frac{\mu_{\text{BBU}}}{9(t'+1)^2}$ is active in the inner maximization, we infer that the term $\frac{\mu_{\text{BBU}}}{9(t'+1)^2}$ is active in hexagon bound when the design parameter is chosen as $(t' + 1)$, which means

$$\frac{\mu_{\text{BBU}}}{9(t' + 1)^2} \leq \mu_F \frac{3(t' + 1)^2 - 1}{9(t' + 1)^2}. \quad (\text{A.13})$$

Therefore, the fact that

$$\frac{\mu_F}{3} > \mu_F \frac{3(t' + 1)^2 - 1}{9(t' + 1)^2} \quad \forall t' \in \mathbb{Z}^+ \quad (\text{A.14})$$

implies

$$\frac{\mu_F}{3} > \frac{\mu_{\text{BBU}}}{9(t' + 1)^2}. \quad (\text{A.15})$$

A.1.2 Case 2: $M \leq \mu_F \leq 2M$

Proposition A.2. From (3.16), the achievable DoF for Parallelogram Scheme can be written as:

$$\text{DoF}_P(\mu_{\text{BBU}}, \mu_F, r) = \begin{cases} \frac{\mu_{\text{BBU}}}{3t_1^* t_2^*}, & \text{if } \mu_{\text{BBU}} \leq M + \mu_F (t_1^* t_2^* - 1) \\ \max \left\{ \frac{M + \mu_F (t_1' t_2' - 1)}{3t_1' t_2'}, \frac{\mu_{\text{BBU}}}{3(t_1' t_2' + 1)} \right\}, & \text{if } \mu_{\text{BBU}} \geq M + \mu_F (t_1^* t_2^* - 1) \end{cases} \quad (\text{A.16})$$

for any pair (t'_1, t'_2) satisfying

$$M + \mu_F (t'_1 t'_2 - 1) \leq \mu_{\text{BBU}} \leq M + \mu_F (t'_1 t'_2), \quad (\text{A.17})$$

and, from (3.17), the achievable DoF for Hexagon Scheme can be written as:

$$\text{DoF}_{\text{H}}(\mu_{\text{BBU}}, \mu_F, r) = \begin{cases} \frac{\mu_{\text{BBU}}}{9t^{*2}}, & \text{if } \mu_{\text{BBU}} \leq \mu_F (3t^{*2} - 1) \\ \max \left\{ \mu_F \frac{3t'^2 - 1}{9t'^2}, \frac{\mu_{\text{BBU}}}{9(t' + 1)^2} \right\}, & \text{if } \mu_{\text{BBU}} \geq \mu_F (3t^{*2} - 1) \end{cases} \quad (\text{A.18})$$

for t' satisfying

$$\mu_F (3t'^2 - 1) \leq \mu_{\text{BBU}} \leq \mu_F (3(t' + 1)^2 - 1). \quad (\text{A.19})$$

Proof: For any given $\mu_{\text{BBU}} > 0$, there is a unique positive integer $c = t'_1 t'_2$ that satisfying (A.17). The maximization in (A.16) can be inferred from (3.16) by similar approach given for (A.2) in Section A.1.1. Note the DoF expression of hexagon case does not change for $M \leq \mu_F \leq 2M$.

We now check all possible intervals for μ_{BBU} regarding to Eq's (A.16) and (A.18)

$$\text{A.1.2.1} \quad \mu_{\text{BBU}} \leq \min \{ M + \mu_F (t_1^* t_2^* - 1), \mu_F (3t^{*2} - 1) \}$$

The DoF is given as:

$$\begin{aligned} \text{DoF}(\mu_{\text{BBU}}, \mu_F, r) &\geq \max \left\{ \frac{\mu_{\text{BBU}}}{3t_1^* t_2^*}, \frac{\mu_{\text{BBU}}}{9t^{*2}} \right\} \\ &= \frac{\mu_{\text{BBU}}}{3t_1^* t_2^*} \end{aligned} \quad (\text{A.20})$$

since $t_1^* t_2^* \leq 3t^{*2}$ for any $r \in (0, 1]$.

$$\text{A.1.2.2} \quad \mu_F (3t^{*2} - 1) \leq \mu_{\text{BBU}} \leq M + \mu_F (t_1^* t_2^* - 1)$$

The DoF is given as:

$$\begin{aligned} \text{DoF}(\mu_{\text{BBU}}, \mu_F, r) &\geq \max \left\{ \max \left\{ \mu_F \frac{3t'^2 - 1}{9t'^2}, \frac{\mu_{\text{BBU}}}{9(t' + 1)^2} \right\}, \frac{\mu_{\text{BBU}}}{3t_1^* t_2^*} \right\} \\ &= \frac{\mu_{\text{BBU}}}{3t_1^* t_2^*} \end{aligned} \quad (\text{A.21})$$

for t' satisfying (A.19).

Proof: Notice that the imposed condition on μ_{BBU} implies $t' = t^*$ since there is a unique

$t' \in \mathbb{Z}^+$ satisfying (A.19) and $\mu_{\text{BBU}} \geq \mu_{\text{F}}(3t^{*2} - 1)$ is already imposed. The rest is trivial. Since $\max t_1^* t_2^* = 3t^{*2}$,

$$\frac{\mu_{\text{BBU}}}{3t_1^* t_2^*} > \frac{\mu_{\text{BBU}}}{9(t^* + 1)^2} \quad (\text{A.22})$$

and since the condition requires $\mu_{\text{BBU}} \geq \mu_{\text{F}}(3t^{*2} - 1)$, then

$$\frac{\mu_{\text{BBU}}}{3t_1^* t_2^*} \geq \mu_{\text{F}} \frac{3t^{*2} - 1}{9t^{*2}}. \quad (\text{A.23})$$

$$\text{A.1.2.3} \quad M + \mu_{\text{F}}(t_1^* t_2^* - 1) \leq \mu_{\text{BBU}} \leq \mu_{\text{F}}(3t^{*2} - 1)$$

The DoF is given as:

$$\begin{aligned} \text{DoF}(\mu_{\text{BBU}}, \mu_{\text{F}}, r) &\geq \max \left\{ \frac{\mu_{\text{BBU}}}{9t^{*2}}, \max \left\{ \frac{M + \mu_{\text{F}}(t_1' t_2' - 1)}{3t_1' t_2'}, \frac{\mu_{\text{BBU}}}{3(t_1' t_2' + 1)} \right\} \right\} \\ &= \max \left\{ \frac{M + \mu_{\text{F}}(t_1' t_2' - 1)}{3t_1' t_2'}, \frac{\mu_{\text{BBU}}}{3(t_1' t_2' + 1)} \right\} \end{aligned} \quad (\text{A.24})$$

for (t_1', t_2') satisfying with (A.17).

Proof: Notice that, for any given $\mu_{\text{BBU}} > 0$, the (A.17) holds for a unique positive integer $c = t_1' t_2'$. The imposed condition implies

$$t_1' t_2' < 3t^{*2}, \quad (\text{A.25})$$

because assuming $t_1' t_2' \geq 3t^{*2}$ implies

$$\begin{aligned} M + \mu_{\text{F}}(t_1' t_2') \geq \mu_{\text{BBU}} &\geq M + \mu_{\text{F}}(t_1' t_2' - 1), \\ &\geq M + \mu_{\text{F}}(3t^{*2} - 1), \end{aligned} \quad (\text{A.26})$$

which is contrary to the imposed condition on $\mu_{\text{BBU}} \leq \mu_{\text{F}}(3t^{*2} - 1)$. Hence,

- If $\frac{\mu_{\text{BBU}}}{3(t_1' t_2' + 1)}$ is active in the inner maximization of (A.24),

$$\frac{\mu_{\text{BBU}}}{3(t_1' t_2' + 1)} \geq \frac{\mu_{\text{BBU}}}{9t^{*2}}. \quad (\text{A.27})$$

- If $\frac{M + \mu_{\text{F}}(t_1' t_2' - 1)}{3t_1' t_2'}$ is active in the inner maximization of (A.24), then

$$\frac{M + \mu_{\text{F}}(t_1' t_2')}{3t_1' t_2'} \geq \frac{\mu_{\text{BBU}}}{3(t_1' t_2' + 1)} \quad (\text{A.28})$$

which implies

$$\frac{M + \mu_{\text{F}}(t_1' t_2')}{3t_1' t_2'} \geq \frac{\mu_{\text{BBU}}}{9t^{*2}} \quad (\text{A.29})$$

by (A.27).

$$\mathbf{A.1.2.4} \quad \mu_{\text{BBU}} \geq \max \{ M + \mu_{\text{F}} (t_1^* t_2^* - 1), \mu_{\text{F}} (3t^{*2} - 1) \}$$

The DoF is given as:

$$\begin{aligned} \text{DoF}(\mu_{\text{BBU}}, \mu_{\text{F}}, r) &\geq \\ &\max \left\{ \max \left\{ \frac{M + \mu_{\text{F}} (t'_1 t'_2 - 1)}{3t'_1 t'_2}, \frac{\mu_{\text{BBU}}}{3(t'_1 t'_2 + 1)} \right\}, \max \left\{ \mu_{\text{F}} \frac{3t'^2 - 1}{9t'^2}, \frac{\mu_{\text{BBU}}}{9(t' + 1)^2} \right\} \right\} \\ &= \max \left\{ \frac{M + \mu_{\text{F}} (t'_1 t'_2 - 1)}{3t'_1 t'_2}, \frac{\mu_{\text{BBU}}}{3(t'_1 t'_2 + 1)} \right\} \end{aligned} \quad (\text{A.30})$$

for (t'_1, t'_2) satisfying with (A.17) and t' satisfying with (A.19).

Proof: Notice that for any given $\mu_{\text{BBU}} > 0$, Eq's (A.17) and (A.19) hold for a unique positive integer $c = t'_1 t'_2$ and a unique t' . For any given μ_{BBU} , Eq's (A.17) and (A.19) impose

$$M + \mu_{\text{F}} (t'_1 t'_2 - 1) \leq \mu_{\text{F}} \left(3(t' + 1)^2 - 1 \right), \quad (\text{A.31})$$

which implies

$$t'_1 t'_2 < 3(t' + 1)^2. \quad (\text{A.32})$$

The Eq's (A.17) and (A.19) also impose

$$\mu_{\text{F}} (3t'^2 - 1) \leq M + \mu_{\text{F}} (t'_1 t'_2), \quad (\text{A.33})$$

which implies

$$t'_1 t'_2 > 3t'^2. \quad (\text{A.34})$$

We now check the following cases:

- If $\frac{M + \mu_{\text{F}} (t'_1 t'_2 - 1)}{3t'_1 t'_2} \geq \frac{\mu_{\text{BBU}}}{3(t'_1 t'_2 + 1)}$ in the first inner maximization of (A.30), then

$$\frac{M + \mu_{\text{F}} (t'_1 t'_2 - 1)}{3t'_1 t'_2} \geq \frac{\mu_{\text{F}} (3t'^2 - 1)}{9t'^2} \quad (\text{A.35})$$

for any triplet $(t', t'_1, t'_2) \in \mathbb{Z}^+$ satisfying with (A.34), and also

$$\frac{M + \mu_{\text{F}} (t'_1 t'_2 - 1)}{3t'_1 t'_2} \geq \frac{\mu_{\text{BBU}}}{3(t'_1 t'_2 + 1)} \quad (\text{A.36})$$

$$\geq \frac{\mu_{\text{BBU}}}{9(t' + 1)^2} \quad (\text{A.37})$$

for any triplet $(t', t'_1, t'_2) \in \mathbb{Z}^+$ satisfying (A.32).

- If $\frac{\mu_{\text{BBU}}}{3(t'_1 t'_2 + 1)} \geq \frac{M + \mu_{\text{F}} (t'_1 t'_2 - 1)}{3t'_1 t'_2}$ in the first maximization of (A.30), then

$$\frac{\mu_{\text{BBU}}}{3(t'_1 t'_2 + 1)} \geq \frac{\mu_{\text{BBU}}}{9(t' + 1)^2} \quad (\text{A.38})$$

for any triplet $(t', t'_1, t'_2) \in \mathbb{Z}^+$ satisfying (A.32), and

$$\frac{\mu_{\text{BBU}}}{3(t'_1 t'_2 + 1)} \geq \frac{M + \mu_{\text{F}} (t'_1 t'_2 - 1)}{3t'_1 t'_2} \quad (\text{A.39})$$

$$\geq \frac{\mu_{\text{F}} (3t'^2 - 1)}{9t'^2} \quad (\text{A.40})$$

for any triplet $(t', t'_1, t'_2) \in \mathbb{Z}^+$ satisfying with (A.34).

This completes the proof for Remark 3.1.

A.2 Proof of Theorem 3.2

For the sake of simplicity in analysis, define $\mathbf{Y}_{\text{BBU}_k}$ as the received signal of BBUP k :

$$\mathbf{Y}_{\text{BBU}_k} = \left\{ \phi_{j,k}^{(n)} \left(\mathbf{Y}_{\text{B}_j}^{(3n)} \right) : j \in \mathcal{U}_k \right\}. \quad (\text{A.41})$$

We obtain the first two terms of the upper bound by choosing the cut set

$$\begin{aligned} \mathcal{S} &= \{\text{all base stations, } j = 1, \dots, N\} \\ \mathcal{S}^c &= \{\text{all BBUPs, } k = 1, \dots, K\} \end{aligned}$$

and defining

$$\begin{aligned} \mathbf{X}_{\mathcal{S}} &= \{\mathbf{X}_j : j \in \mathcal{S}\} \\ \mathbf{Y}_{\mathcal{S}^c} &= \{\mathbf{Y}_{\text{BBU}_k} : k \in \mathcal{S}^c\}. \end{aligned}$$

In that case, for any fixed BBUP to BS association for any given network, the total rate of all users is upper bounded by:

$$\begin{aligned} 3 \cdot N \cdot R_u &\leq I(\mathbf{X}_{\mathcal{S}}; \mathbf{Y}_{\mathcal{S}^c}) \\ &= H(\mathbf{Y}_{\mathcal{S}^c}) - H(\mathbf{Y}_{\mathcal{S}^c} | \mathbf{X}_{\mathcal{S}}) \\ &\leq \min\{K\mu_{\text{BBU}}, N\mu_{\text{F}}\} \cdot \frac{1}{2} \log P \end{aligned} \quad (\text{A.42})$$

where second inequality comes from applying Eq's (3.6) and (3.10) to received signals of BBUPs, which gives first two terms when we apply Def. B.6. Third term comes from the fact that, by [67], the DoF a $M \times M$ MIMO system is upper bounded by M .

A.3 Proof of Corollary 3.1

For the first item, the matching occurs when the term with μ_{F} is active in both lower and upper bounds. For the rest, the matchings occur the term with μ_{BBU} is active in both lower and upper bound. Due to the Remark 3.1, if $\mu_{\text{F}} \leq 2M$, showing the matching cases between parallelogram lower bound and cut-set upper bound is enough. For $\mu_{\text{F}} \geq 2M$, we show the matching cases between both lower bounds and cut-set bound.

For $\mu_{\text{F}} \leq M$, the term with μ_{F} is active in upper and lower bound if $\mu_{\text{F}} \leq \mu_{\text{BBU}} \cdot r$ and $\mu_{\text{F}} \leq \frac{\mu_{\text{BBU}}}{t_1 t_2}$, respectively. Since $t_1 t_2 \geq \lceil \frac{1}{r} \rceil$, choosing $\mu_{\text{F}} \leq \frac{\mu_{\text{BBU}}}{t_1 t_2}$ implies $\mu_{\text{F}} \leq \mu_{\text{BBU}} \cdot r$. The term with μ_{BBU} is active in upper and lower bound if $\mu_{\text{BBU}} \cdot r \leq \mu_{\text{F}}$ and $\frac{\mu_{\text{BBU}}}{t_1 t_2} \leq \mu_{\text{F}}$, respectively, where the matching requires $t_1 t_2 = \frac{1}{r}$.

For $M \leq \mu_{\text{F}} \leq 2M$, the term with μ_{BBU} is active in both upper and lower bound if $\mu_{\text{BBU}} \cdot r \leq \mu_{\text{F}}$ and $\mu_{\text{BBU}} \leq M + \mu_{\text{F}}(t_1 t_2 - 1)$, respectively, where the matching requires $t_1 t_2 = \frac{1}{r}$.

For $2M \leq \mu_{\text{F}} \leq 3M$, the term with μ_{BBU} is active in upper and parallelogram lower bound if $\mu_{\text{BBU}} \cdot r \leq \mu_{\text{F}}$ and $\mu_{\text{BBU}} \leq M(2t_1 + 2t_2 - 3) + \mu_{\text{F}}(t_1 t_2 - t_1 - t_2 - 1)$, respectively,

where matching requires $t_1 t_2 = \frac{1}{r}$. If $\frac{1}{r} \in \mathbb{Z}^+$, there is at least one (t_1, t_2) pair that results in $t_1 t_2 = \frac{1}{r}$. However, unless $\mu_{\text{BBU}} \leq \max_{t_1, t_2} M(2t_1 + 2t_2 - 3) + \mu_{\text{F}}(t_1 t_2 - t_1 - t_2 - 1)$, the term with μ_{BBU} can not be active in lower bound. This imposes to choose the pair (t_1, t_2) that minimizes $t_1 + t_2$. The term with μ_{BBU} is active in upper and hexagon lower bound if $\mu_{\text{BBU}} \cdot r \leq \mu_{\text{F}}$ and $\mu_{\text{BBU}} \leq M(6t - 6) + \mu_{\text{F}}(3t^2 - 3t - 2)$, where matching requires $t = \sqrt{\frac{1}{3r}}$.

For $3M \leq \mu_{\text{F}}$, the matching cases can be found by applying similar procedures as in the $2M \leq \mu_{\text{F}} \leq 3M$ case.

A.4 Proof of Theorem 3.3

Due to the Remark 3.1, we do the achievability gap analysis only for parallelogram clustering. We do analysis for one of the cases which leads to the maximum achievability gap. For other cases, a similar procedure can be applied.

- If $\mu_{\text{F}} \leq M$, the maximum gap occurs when $\frac{\mu_{\text{F}}}{3}$ and $\frac{\mu_{\text{BBU}}}{3t_1 t_2}$ is active in upper and lower bound, respectively. Note that this assumption imposes $\frac{\mu_{\text{F}}}{r} \leq \mu_{\text{BBU}} \leq \mu_{\text{F}} \cdot t_1 \cdot t_2$.

$$\begin{aligned}
 \Delta(\mu_{\text{BBU}}, \mu_{\text{F}}, r) &= \frac{\mu_{\text{F}}}{3} - \frac{\mu_{\text{BBU}}}{3 \cdot t_1 \cdot t_2} \\
 &\stackrel{a}{\leq} \frac{\mu_{\text{F}}}{3} - \frac{\mu_{\text{F}} \cdot \frac{1}{r}}{3 \cdot t_1 \cdot t_2} \\
 &\stackrel{b}{\leq} \frac{\mu_{\text{F}}}{3} - \frac{\mu_{\text{F}} \cdot \frac{1}{r}}{3 \cdot \lceil \frac{1}{r} \rceil} \\
 &= \frac{\mu_{\text{F}} \lceil \frac{1}{r} \rceil - \frac{1}{r}}{3 \lceil \frac{1}{r} \rceil} \\
 &< \frac{\mu_{\text{F}}}{3 \cdot \lceil \frac{1}{r} \rceil}
 \end{aligned} \tag{A.43}$$

where (a) is due to $\max \mu_{\text{BBU}} = \mu_{\text{F}} \cdot \frac{1}{r}$ and (b) is due to $\min t_1 \cdot t_2 = \lceil \frac{1}{r} \rceil$ by (3.27).

- If $M \leq \mu_{\text{F}} \leq 2M$, the maximum gap occurs when $\frac{\mu_{\text{BBU}}}{3} \cdot r$ and $\frac{\mu_{\text{BBU}}}{3 \cdot t_1 \cdot t_2}$ is active in upper and lower bound, respectively. Notice that this assumption imposes $\mu_{\text{BBU}} \leq$

$$\min \left\{ \mu_F \cdot \frac{1}{r}, M + \mu_F (t_1 t_2 - 1) \right\}.$$

$$\begin{aligned} \Delta(\mu_{\text{BBU}}, \mu_F, r) &= \frac{\mu_{\text{BBU}} \cdot r}{3} - \frac{\mu_{\text{BBU}}}{3 \cdot t_1 \cdot t_2} \\ &\stackrel{a}{\leq} \frac{\mu_{\text{BBU}}}{3} \left(r - \frac{1}{\lceil \frac{1}{r} \rceil} \right) \\ &\leq \frac{\min \left\{ \mu_F \cdot \frac{1}{r}, M + \mu_F (\lceil \frac{1}{r} \rceil - 1) \right\}}{3} \left(r - \frac{1}{\lceil \frac{1}{r} \rceil} \right) \\ &\stackrel{b}{\leq} \frac{\mu_F}{3} \cdot \frac{1}{r} \left(r - \frac{1}{\lceil \frac{1}{r} \rceil} \right) \\ &< \frac{\mu_F}{3 \cdot \lceil \frac{1}{r} \rceil} \end{aligned} \tag{A.44}$$

where (a) is due to $\min t_1 \cdot t_2 = \lceil \frac{1}{r} \rceil$ by (3.27), and (b) is due the fact that if $\mu_F \cdot \frac{1}{r} \leq M + \mu_F (\lceil \frac{1}{r} \rceil - 1)$ there is equality, if $M + \mu_F (\lceil \frac{1}{r} \rceil - 1) \leq \mu_F \cdot \frac{1}{r}$, there is strict inequality.

Appendix B

B.1 Preliminaries for Lattices

Definition B.1 (Lattice). *A n -dimensional lattice, Λ , is a discrete subgroup in \mathbb{R}^n such that if $\mathbf{t}_1, \mathbf{t}_2 \in \Lambda$, then $\mathbf{t}_1 + \mathbf{t}_2 \in \Lambda$ and if $\mathbf{t}_1 \in \Lambda$, then $-\mathbf{t}_1 \in \Lambda$. Every lattice can be expressed by a generator matrix $\mathbf{F} \in \mathbb{R}^{n \times n}$:*

$$\Lambda = \{\mathbf{t} = \mathbf{F}\mathbf{c} : \mathbf{c} \in \mathbb{Z}^n\}. \quad (\text{B.1})$$

Definition B.2 (Lattice Quantizer). *The lattice quantizer Q_Λ is a mapping from \mathbb{R}^n to the nearest lattice point in Euclidean distance: :*

$$Q_\Lambda(\mathbf{x}) = \arg \min_{\mathbf{t} \in \Lambda} \|\mathbf{x} - \mathbf{t}\|. \quad (\text{B.2})$$

Definition B.3 (Fundamental Voronoi Region). *The fundamental Voronoi region of a lattice, \mathcal{V}_Λ , is the set of points that are closer to the zero vector than any other lattice points, i.e., $\mathcal{V}_\Lambda = \{\mathbf{x} \in \mathbb{R}^n : Q_\Lambda(\mathbf{x}) = \mathbf{0}\}$.*

Definition B.4 (Second Moment). *The second moment of Λ , which quantifies the average power per dimension in \mathcal{V}_Λ , is given by*

$$\sigma^2(\Lambda) = \frac{1}{n \text{Vol}(\mathcal{V}_\Lambda)} \int_{\mathcal{V}_\Lambda} \|\mathbf{x}\|^2 d\mathbf{x} \quad (\text{B.3})$$

where $\text{Vol}(\mathcal{V}_\Lambda)$ denotes the volume of the Voronoi region, $\text{Vol}(\mathcal{V}_\Lambda) = \det \sqrt{\mathbf{F}\mathbf{F}^T}$.

The **normalized** second moment of Λ is given by

$$G(\Lambda) = \frac{\sigma^2(\Lambda)}{(n \text{Vol}(\mathcal{V}_\Lambda))^{2/n}}. \quad (\text{B.4})$$

Definition B.5 (Nested Lattices). *The lattice Λ_1 is nesting the lattice Λ_s if $\Lambda_s \subseteq \Lambda_1$ and, Λ_1 and Λ_s are referred to the fine and coarse(shaping) lattice, respectively. In general, the lattice sequence $\Lambda_s, \Lambda_1, \dots, \Lambda_L$ is nested if $\Lambda_s \subseteq \Lambda_1 \subseteq \dots \subseteq \Lambda_L$. We assume that nested lattices are generated by construction A as in [22, 39].*

Definition B.6 (Modulo Operation). *The modulo operation for the point $\mathbf{x} \in \mathbb{R}^n$ gives the quantization error respect to lattice Λ :*

$$[\mathbf{x}] \bmod \Lambda = \mathbf{x} - Q_\Lambda(\mathbf{x}). \quad (\text{B.5})$$

For all $\mathbf{t}_1, \mathbf{t}_2 \in \mathbb{R}^n$ and any $\Lambda_s \subseteq \Lambda$, the mod Λ_s operation satisfies

$$[\mathbf{t}_1 + \mathbf{t}_2] \bmod \Lambda_s = [[\mathbf{t}_1] \bmod \Lambda_s + \mathbf{t}_2] \bmod \Lambda_s \quad (\text{B.6})$$

$$[Q_\Lambda(\mathbf{t}_1)] \bmod \Lambda_s = [Q_\Lambda([\mathbf{t}_1] \bmod \Lambda_s)] \bmod \Lambda_s \quad (\text{B.7})$$

$$[a\mathbf{t}_1] \bmod \Lambda_s = [a[\mathbf{t}_1] \bmod \Lambda_s] \bmod \Lambda_s \quad \forall a \in \mathbb{Z} \quad (\text{B.8})$$

$$\beta[\mathbf{t}_1] \bmod \Lambda_s = [\beta\mathbf{t}_1] \bmod \beta\Lambda_s \quad \forall \beta \in \mathbb{R} \quad (\text{B.9})$$

Definition B.7 (Nested Lattice Codebook). *A nested lattice codebook \mathcal{C}_u for a shaping lattice Λ_s and a nesting lattice Λ_u is given as: $\mathcal{C}_u = \Lambda_u \cap \mathcal{V}_\Lambda$. The rate R_u of the lattice codebook \mathcal{C}_u is given as:*

$$R_u = \frac{1}{n} \log_2 \frac{\text{Vol}(\mathcal{V}_{\Lambda_s})}{\text{Vol}(\mathcal{V}_{\Lambda_u})} = \frac{1}{2} \log_2 \frac{\sigma^2(\Lambda_s)}{\sigma^2(\Lambda_u)}. \quad (\text{B.10})$$

Let $\mathcal{B}(r) \triangleq \{\mathbf{t} : \|\mathbf{t}\| \leq r, \mathbf{t} \in \mathbb{R}^n\}$ define a n -dimensional ball of radius $r \in \mathbb{R}$, and $\text{Vol}(\mathcal{B}(r))$ denote its volume.

Definition B.8 (Covering Radius). *The **covering radius** of n -dimensional lattice Λ is defined as the smallest $r_{\text{cov},n} \in \mathbb{R}$ such that*

$$\mathbb{R}^n \subseteq \Lambda + \mathcal{B}(r_{\text{cov},n}(\Lambda)) \quad (\text{B.11})$$

Definition B.9 (Effective Radius). *The **effective radius** of n -dimensional lattice Λ is defined as the real number $r_{\text{eff},n}$ such that*

$$\text{Vol}(\mathcal{B}(r_{\text{eff},n}(\Lambda))) = \text{Vol}(\mathcal{V}_\Lambda). \quad (\text{B.12})$$

Definition B.10 (Covering Goodness). *A sequences of lattices $\Lambda \subset \mathbb{R}^n$ is good for covering if:*

$$\lim_{n \rightarrow \infty} \frac{r_{\text{cov},n}(\Lambda)}{r_{\text{eff},n}(\Lambda)} = 1. \quad (\text{B.13})$$

Definition B.11 (Quantization Goodness). *A n -dimensional lattices $\Lambda \subset \mathbb{R}^n$ is good for mean-squared error quantization if:*

$$\lim_{n \rightarrow \infty} G(\Lambda) = \frac{1}{2\pi e}. \quad (\text{B.14})$$

Definition B.12 (AWGN Goodness). *Let \mathbf{z} denote an n -dimensional random vector generated according to the Gaussian distribution $\mathcal{N}(0, \sigma_z^2 \mathbf{I}_n)$. The volume-to-noise ratio of a lattice is given by*

$$\mu(\Lambda, P_e) = \frac{(\text{Vol}(\mathcal{V}_\Lambda))^{\frac{2}{n}}}{\sigma_z^2} \quad (\text{B.15})$$

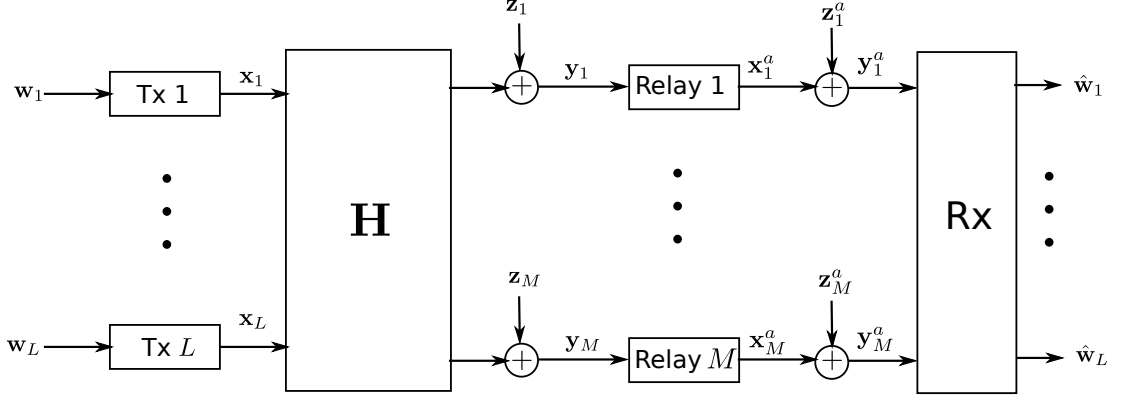


Figure B.1: A general AWGN relay network that CoF can be beneficial.

The variance σ_z^2 is selected such that $\Pr(\mathbf{z} \notin \mathcal{V}_\Lambda) = P_e$. A sequence of lattices Λ is AWGN good if:

$$\lim_{n \rightarrow \infty} \mu(\Lambda, P_e) = 2\pi e \quad \forall P_e \in (0, 1). \quad (\text{B.16})$$

For more details and detailed analysis on this topic, we refer readers to [22, 16].

B.2 Basic Compute and Forward (CoF) in Real Valued Channels

The compute-and-forward (CoF) is essentially a relaying strategy that is applicable to any configuration of sources, relays and destinations that are linked through linear channels with additive white Gaussian noise (AWGN) [46]. Here, we will focus on how to transmit signals and deliver the equations to a receiver (Rx).

Consider a network that consists of L users, M relays and a Rx, see Figure B.1. Each user $l \in \mathcal{L}, \mathcal{L} = \{1, \dots, L\}$, generates its transmitted signal $\mathbf{x}_l \in \mathbb{R}^{1 \times n}$ by using the n -dimensional nested lattice Λ_l , for the given nesting order $\Lambda_s \subseteq \Lambda_1 \subseteq \dots \subseteq \Lambda_L$, as follows.

By [45, Lemma 2], we choose an n -dimensional shaping lattice Λ_s with $\sigma^2(\Lambda_s) = P$, which is simultaneously good for covering, AWGN and quantization. We construct nested lattices by construction A [22, 39]. Then, the lattice codebooks $\{\mathcal{C}_l = \mathcal{V}_{\Lambda_s} \cap \Lambda_l\}_{l \in \mathcal{L}}$ are constructed.

Each user $l \in \mathcal{L}$ attempts to communicate a length- k_l message vector \mathbf{w}_l which is drawn independently and uniformly over a prime size finite field $\mathbb{F}_p^{1 \times k_l}$. Due to the nesting order, the message rates are decreasing order which requires $k_1 \leq k_2 \leq \dots \leq k_L$. Since, we are interested with functions of these message vectors we zero pad them to a common length, $k = \max_l k_l$. The message rate R_l of each user is the length of its message (except zero padded part) normalized by the number of channel use

$$R_l = \frac{k_l}{n} \log p, \quad (\text{B.17})$$

where k_l is chosen satisfying with (B.10). Then, each user l applies the same one-to-one mapping from finite field messages to the elements of lattice codebooks, \mathcal{C}_l :

$$\begin{aligned}\phi : \mathbb{F}_p^{1 \times k_l} &\mapsto \mathbb{R}^{1 \times n}, \\ \phi(\mathbf{w}_l) &= \mathbf{t}_l.\end{aligned}\tag{B.18}$$

Subsequently, each user l adds dither to the resulting lattice point and takes mod Λ_s :

$$\mathbf{x}_l = [\mathbf{t}_l + \mathbf{d}_l] \bmod \Lambda_s,\tag{B.19}$$

where \mathbf{d}_l is uniformly distributed over \mathcal{V}_{Λ_s} and, therefore, $E\|\mathbf{x}_l\|^2 = nP$ by [21]. The expectation is taken over the dithers and each dither \mathbf{d}_l is shared with all relays. The output of relay $m \in \mathcal{M}$, $\mathcal{M} = \{1, \dots, M\}$, is given as

$$\mathbf{y}_m = \sum_{l=1}^L h_{ml} \mathbf{x}_l.\tag{B.20}$$

The objective of each relay m is to decode an integer combination of transmitted lattice codewords:

$$\mathbf{v}_m = \left[\sum_{l=1}^L a_{ml} \mathbf{t}_l \right] \bmod \Lambda_s,\tag{B.21}$$

where $a_{ml} \in \mathbb{Z}$. In order to do so, relay m applies scaling, non-dithering to corresponding received signal and takes mod Λ_s , respectively, and obtains

$$\begin{aligned}\tilde{\mathbf{y}}_m &= \left[\alpha_m \mathbf{y}_m - \sum_{l=1}^L a_{ml} \mathbf{d}_l \right] \bmod \Lambda_s \\ &= \left[\sum_{l=1}^L a_{ml} (\mathbf{x}_l - \mathbf{d}_l) + \sum_{l=1}^L (\alpha_m h_{ml} - a_{ml}) \mathbf{x}_l + \alpha_m \mathbf{z}_m \right] \bmod \Lambda_s\end{aligned}\tag{B.22}$$

$$\stackrel{a}{=} \left[\left[\sum_{l=1}^L a_{ml} (\mathbf{x}_l - \mathbf{d}_l) \right] \bmod \Lambda_s + \mathbf{z}_m^{\text{eff}} \right] \bmod \Lambda_s\tag{B.23}$$

$$\stackrel{b}{=} [\mathbf{v}_m + \mathbf{z}_m^{\text{eff}}] \bmod \Lambda_s\tag{B.24}$$

where a and b is due to (B.7) and (B.8), and

$$\mathbf{z}_m^{\text{eff}} = \sum_{l=1}^L (\alpha_m h_{ml} - a_{ml}) \mathbf{x}_l + \alpha_m \mathbf{z}_m\tag{B.25}$$

is the *effective noise* including noninteger interference and Gaussian noise. The variance of the effective noise is given by

$$\sigma_{\text{eff}}^2(P, \mathbf{h}_m; \alpha_m, \mathbf{a}_m) = \frac{1}{n} E \|\mathbf{z}_m^{\text{eff}}\|^2\tag{B.26}$$

$$= P (\|\alpha_m \mathbf{h}_m - \mathbf{a}_m\|^2) + \|\alpha_m\|^2,\tag{B.27}$$

where $\mathbf{a}_m = [a_{m1}, \dots, a_{mL}]^T$ and $\mathbf{h}_m = [h_{m1}, \dots, h_{mL}]^T$.

Let $\Lambda_{l^*(m)}$ be finest lattice regarding the lattice equation \mathbf{v}_m with coefficients \mathbf{a}_m , where $l^*(m) = \max\{l : a_{ml} \neq 0\}$. Note that $\mathbf{v}_m \in \mathcal{V}_{\Lambda_s} \cap \Lambda_{l^*(m)}$ due to the linear nature of nested lattices and $\mathbf{a}_m \in \mathbb{Z}^L$. Then, the relay m produces an estimation of \mathbf{v}_m by quantizing $\tilde{\mathbf{y}}_m$ with the lattice quantizer $Q_{\Lambda_{l^*(m)}}$ and taking mod Λ_s :

$$\hat{\mathbf{v}}_m = \left[Q_{\Lambda_{l^*(m)}}(\tilde{\mathbf{y}}_m) \right] \bmod \Lambda_s, \quad (\text{B.28})$$

$$= \left[Q_{\Lambda_{l^*(m)}}([\mathbf{v}_m + \mathbf{z}_m^{\text{eff}}] \bmod \Lambda_s) \right] \bmod \Lambda_s, \quad (\text{B.29})$$

$$\stackrel{(a)}{=} \left[Q_{\Lambda_{l^*(m)}}(\mathbf{v}_m + \mathbf{z}_m^{\text{eff}}) \right] \bmod \Lambda_s, \quad (\text{B.30})$$

where (a) is due to (B.7).

An error occurs in computation if the effective noise leaves the Voronoi region surrounding \mathbf{v}_m , $\Pr(\mathbf{z}_m^{\text{eff}} \notin \mathcal{V}_{\Lambda_{l^*(m)}})$. By [45], since $\{\Lambda_l\}_{l \in \mathcal{L}}$ is AWGN good, it can be shown that P_e goes to zero exponentially with sufficiently large n , if the volume of $\mathcal{V}_{\Lambda_{l^*(m)}}$ is chosen as

$$\frac{\left(\text{Vol}(\mathcal{V}_{\Lambda_{l^*(m)}}) \right)^{\frac{2}{n}}}{\sigma_{\text{eff}}^2(P, \mathbf{h}_m; \alpha_m, \mathbf{a}_m)} > 2\pi e. \quad (\text{B.31})$$

Then, if the volume of Voronoi region of each Λ_l is chosen as

$$\text{Vol}(\mathcal{V}_{\Lambda_l}) > (2\pi e \max_{m: a_{ml} \neq 0} \sigma_{\text{eff}}^2(P, \mathbf{h}_m; \alpha_m, \mathbf{a}_m))^{\frac{n}{2}}, \quad (\text{B.32})$$

the computation error probability at each relay goes to zero. Since Λ_s is quantization good, by (B.10), the following lemma can be stated:

Lemma B.1. [46, Theorem 5] *For any $\epsilon > 0$ and n large enough, there exist nested lattice codes $\Lambda_s \subseteq \Lambda_1 \subseteq \dots \subseteq \Lambda_L$ with rates $\{R_l\}_{l=1}^L$ such that for all channel vectors $\{\mathbf{h}_m \in \mathbb{R}^L\}_{m=1}^M$ and integer coefficient vectors $\{\mathbf{a}_m \in \mathbb{Z}^L\}_{m=1}^M$, relay m can compute the lattice equation*

$$\mathbf{v}_m = \left[\sum_{l=1}^L a_{ml} \mathbf{t}_l \right] \bmod \Lambda_s, \quad (\text{B.33})$$

of transmitted lattice points $\mathbf{t}_l \in \mathcal{C}_l$ with the average probability of error ϵ as long as

$$R_l < \min_{m: a_{ml} \neq 0} \frac{1}{2} \log^+ \left(\frac{P}{\sigma_{\text{eff}}^2(P, \mathbf{h}_m; \alpha_m, \mathbf{a}_m)} \right), \quad (\text{B.34})$$

for some choice of $\{\alpha_m \in \mathbb{R}\}_{m=1}^M$.

In (B.34), the right side of the equation is defined as **computation rate**:

$$\mathcal{R}_{\text{co}}(P, \mathbf{h}_m; \alpha_m, \mathbf{a}_m) = \frac{1}{2} \log^+ \left(\frac{P}{\sigma_{\text{eff}}^2(P, \mathbf{h}_m; \alpha_m, \mathbf{a}_m)} \right), \quad (\text{B.35})$$

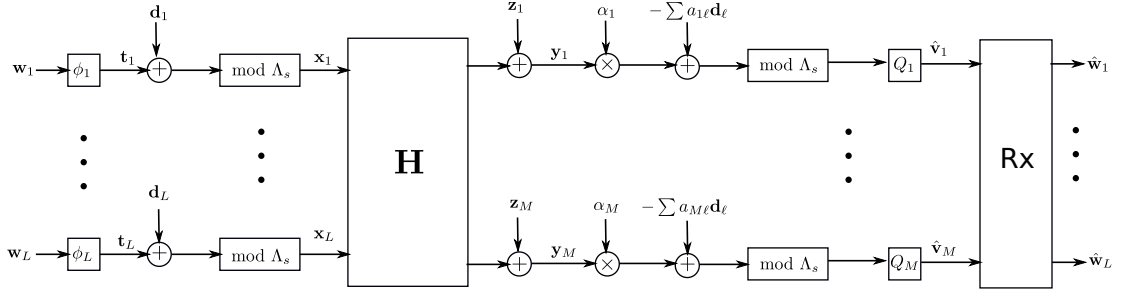


Figure B.2: System diagram of CoF.

and is maximized by choosing

$$\alpha_m = \frac{P \mathbf{h}_m^T \mathbf{a}_m}{1 + P \|\mathbf{h}_m\|^2}. \quad (\text{B.36})$$

In that case, it is given by

$$\mathcal{R}_{\text{co}}(P, \mathbf{h}_m; \mathbf{a}_m) = \frac{1}{2} \log^+ \left(\frac{P}{\mathbf{a}_m^T (P^{-1} \mathbf{I}_L + \mathbf{h}_m \mathbf{h}_m^T)^{-1} \mathbf{a}_m} \right). \quad (\text{B.37})$$

After computation of equations, each relay m sends $\hat{\mathbf{v}}_m$ to the Rx and it decodes the messages $\{\mathbf{w}_l\}_{l \in \mathcal{L}}$ given $\mathbf{A} = [\mathbf{a}_1, \dots, \mathbf{a}_M]^T$ is full rank, by applying basic finite field algebraic filter as explained in [45] with detail. Figure B.2 summarizes the explained operations.

B.3 Basic Quantized Compute and Forward (QCoF) in Real Valued Channels

The quantized CoF (QCoF) scheme is a relaying strategy that is variant of CoF. As mentioned above, the conventional CoF scheme requires full rank integer vector matrix, which leads to performance degradation in the following cases:

- **When $L > M$,**
It is implemented by allowing some relays to compute more than one equations that the latter ones are with lower computation rates.
- **When $L \leq M$,**
The requirement of full rank matrix imposes to compute the equations with lower computation rates in case there is linear dependency between computation vectors of relays.

The main idea of QCoF is to eliminate full rank requirement of CoF by employing the following procedures:

- **At the relay side:** The computed equations, which are functions of lattice codewords, are remapped to the equations of transmitted codewords. Then, they are quantized with Wyner-Ziv (WZ) compression instead of directly forwarding or point-to-point quantization,

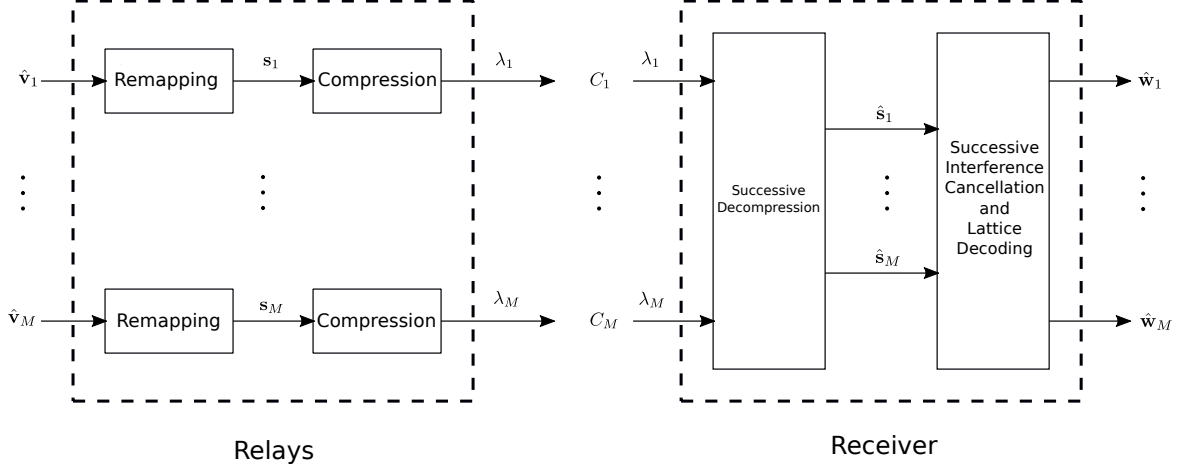


Figure B.3: System diagram of QCoF.

- **At the Rx side:** The decompression is implemented by using the formerly decompressed signals as side information. Then, the decoding is performed with successive interference cancellation (SIC) based lattice decoding.

As stated above, the differentiation between CoF and QCoF starts after computing $\hat{\mathbf{v}}_m$, $m \in \mathcal{M}$. Figure B.3 shows these steps starting from relay side. In the following, we will explain them:

1) **Equation Remapping:** Let $\mathbf{X} = [\mathbf{x}_1, \dots, \mathbf{x}_L]^T$. Each relay $m \in \mathcal{M}$ remaps the computed equation $\hat{\mathbf{v}}_m$, which is a linear combination of *lattice* points, into a linear combination of *transmitted* signals $\mathbf{s}_m = \mathbf{a}_m^T \mathbf{X}$ with zero probability of error as long as $\mathcal{R}_{\text{co}}(P, \mathbf{a}_m; \mathbf{h}_m) > 0$ [44, Lemma 1], by implementing following equation:

$$\mathbf{s}_m = \mathcal{Q}_{\Lambda_s}(\alpha_m \mathbf{y}_m - \boldsymbol{\theta}_m), \text{ where} \quad (\text{B.38})$$

$$\boldsymbol{\theta}_m = \left[\hat{\mathbf{v}}_m + \sum_{l=1}^L a_{ml} \mathbf{d}_l \right] \text{ mod } \Lambda_s. \quad (\text{B.39})$$

2) **Lossy Compression at Relay m :** Relay m compresses \mathbf{s}_m at rate C_m , which is the capacity of the channel between relay m and the Rx. Compression is implemented via nested lattice pair $\Lambda_{s,m}^c \subseteq \Lambda_m^c$, where $\Lambda_{s,m}^c$ and Λ_m^c are AWGN and quantization good respectively, as follows: signal \mathbf{s}_m is added a dither \mathbf{d}_m^c , which is uniform over $\mathcal{V}_{\Lambda_{s,m}^c}$ and quantized to the nearest fine lattice point Λ_m^c , after which modulo reduction is implemented via shaping lattice $\Lambda_{s,m}^c$:

$$\boldsymbol{\lambda}_m = \mathcal{Q}_{\Lambda_{s,m}^c}(\mathbf{s}_m + \mathbf{d}_m^c) \text{ mod } \Lambda_{s,m}^c \quad (\text{B.40})$$

$$= (\mathbf{s}_m + \mathbf{d}_m^c - \mathbf{z}_{\text{eff},m}^c) \text{ mod } \Lambda_{s,m}^c, \quad (\text{B.41})$$

where $\mathbf{z}_{\text{eff},m}^c = (\mathbf{s}_m + \mathbf{d}_m^c) \text{ mod } \Lambda_m^c$ is the quantization noise with variance $\sigma^2(\Lambda_m^c)$. By [21], the $\mathbf{z}_{\text{eff},m}^c$ is uniform over $\mathcal{V}_{\Lambda_m^c}$ and independent of \mathbf{s}_m .

Since there is a correlation between remapped equations, note that all \mathbf{s}_m 's are functions of some \mathbf{x}_l 's, relays exploit this in quantization process as explained in the following. Let $\hat{\mathbf{S}}_{m-1} = [\hat{\mathbf{s}}_1^T, \dots, \hat{\mathbf{s}}_{m-1}^T]^T$ denote formerly decompressed equations. The compression process at relay m is implemented by assuming that the correlation between \mathbf{s}_m and $\hat{\mathbf{S}}_{m-1}$ is exploited during the decompression process via LMMSE estimation. Therefore, shaping and fine lattice variances for compression are chosen as

$$\sigma^2(\Lambda_{s,m}^c) = \nu(\mathbf{s}_m | \hat{\mathbf{S}}_{m-1}) + \sigma^2(\Lambda_m^c) \quad (\text{B.42})$$

$$\sigma^2(\Lambda_m^c) = \frac{\nu(\mathbf{s}_m | \hat{\mathbf{S}}_{m-1})}{2^{2C_m} - 1}, \quad (\text{B.43})$$

Here, $\nu(\mathbf{s}_m | \hat{\mathbf{S}}_{m-1})$ denotes the LMMSE error obtained by estimating \mathbf{s}_l from $\hat{\mathbf{S}}_{m-1}$ and is given as

$$\nu(\mathbf{s}_m | \hat{\mathbf{S}}_{m-1}) = \mathbf{a}_m^T \left(P^{-1} \cdot \mathbf{I}_m + \mathbf{A}_{m-1}^T \sum_{m-1}^{-1} \mathbf{A}_{m-1} \right)^{-1} \mathbf{a}_m \quad (\text{B.44})$$

where

$$\mathbf{A}_m = [\mathbf{a}_1, \dots, \mathbf{a}_m]^T, \quad (\text{B.45})$$

and

$$\sum_m = \text{diag}[\sigma^2(\Lambda_1^c), \dots, \sigma^2(\Lambda_m^c)]. \quad (\text{B.46})$$

Therefore, the rate constraint $C_m = \frac{1}{2} \log \frac{\sigma^2(\Lambda_{s,m}^c)}{\sigma^2(\Lambda_m^c)}$ is satisfied and the minimum quantization noise is obtained.

3) Successive Decompression at Receiver: After observing the compression lattice points $(\boldsymbol{\lambda}_1, \dots, \boldsymbol{\lambda}_M)$, the Rx attempts to reconstruct $\hat{\mathbf{S}}_M = [\hat{\mathbf{s}}_1^T, \dots, \hat{\mathbf{s}}_M^T]^T$ successively, starting from $\hat{\mathbf{s}}_1$. Assume $\hat{\mathbf{S}}_{m-1}$ has already been reconstructed. Then, Rx computes $\hat{\mathbf{s}}_m$, which is LMMSE estimate of \mathbf{s}_m :

$$\tilde{\mathbf{s}}_m = \boldsymbol{\gamma}_m \hat{\mathbf{S}}_{m-1} \quad (\text{B.47})$$

$$= \boldsymbol{\gamma}_m (\mathbf{A}_{m-1} \mathbf{X} + \mathbf{Z}_{\text{eff},m-1}^c) \quad (\text{B.48})$$

where

$$\boldsymbol{\gamma}_m = P \mathbf{a}_m^T \left(P \mathbf{A}_{m-1}^T \mathbf{A}_{m-1} + \mathbf{I}_{m-1} + \sum_{m-1} \right)^{-1} \quad (\text{B.49})$$

and $\mathbf{Z}_{\text{eff},m}^c = [\mathbf{z}_{\text{eff},1}^{c,T}, \dots, \mathbf{z}_{\text{eff},m}^{c,T}]^T$ with covariance matrix \sum_m .

The Rx reconstructs $\hat{\mathbf{s}}_m$ with $\boldsymbol{\lambda}_m$ and $\tilde{\mathbf{s}}_m$ by computing:

$$\hat{\mathbf{s}}_m = [\boldsymbol{\lambda}_m - \mathbf{d}_m^c - \tilde{\mathbf{s}}_m] \bmod \Lambda_{s,m}^c + \tilde{\mathbf{s}}_m \quad (\text{B.50})$$

$$= [\mathbf{s}_m - \mathbf{z}_{\text{eff},m}^c - \tilde{\mathbf{s}}_m] \bmod \Lambda_{s,m}^c + \tilde{\mathbf{s}}_m \quad (\text{B.51})$$

$$\stackrel{\text{c.d}}{=} \mathbf{s}_m + \mathbf{z}_{\text{eff},m}^c \quad (\text{B.52})$$

where (c.d) holds if the decompression is correct. An error in decompression $\Pr(\hat{\mathbf{s}}_m \neq \mathbf{s}_m + \mathbf{z}_{\text{eff},m}^c)$ occurs if $\bar{\mathbf{s}}_m = (\mathbf{s}_m - \tilde{\mathbf{s}}_m) - \mathbf{z}_{\text{eff},m}^c$ leaves the fundamental Voronoi region $\mathcal{V}_{\Lambda_{s,m}^c}$. By [45, Lemma 8], we know that the pdf of $\bar{\mathbf{s}}_m$ is upper bounded by a constant times the pdf of i.i.d. zero-mean Gaussian vector $\bar{\mathbf{s}}_m^*$ whose variance $\sigma_{\bar{\mathbf{s}}_m^*}^2$ approaches $\sigma_{\bar{\mathbf{s}}_m}^2$ as $n \rightarrow \infty$. Since $\Lambda_{s,m}^c$ and Λ_m^c are AWGN and quantization good respectively, if

$$\sigma^2(\Lambda_{s,m}^c) = \sigma_{\bar{\mathbf{s}}_m}^2 \quad (\text{B.53})$$

$$= \mathbf{a}_m^T \left(P^{-1} \cdot \mathbf{I}_m + \mathbf{A}_{m-1}^T \sum_{m-1}^{-1} \mathbf{A}_m \right)^{-1} \mathbf{a}_m + \sigma^2(\Lambda_m^c) \quad (\text{B.54})$$

the $\Pr(\hat{\mathbf{s}}_m \neq \mathbf{s}_m + \mathbf{z}_{\text{eff},m}^c) \rightarrow 0$ exponentially with n , hence the decompression is succesful.

4) Lattice Decoding with Successive Ineterference Cancellation at Receiver:

After reconstruction of all $\{\hat{\mathbf{s}}_m\}_{m \in M}$, the transmitted signals are again passed through LMMSE filter to estimate the transmitted signals. The LMMSE of \mathbf{X} is given as

$$\hat{\mathbf{X}} = \Gamma_L \hat{\mathbf{S}}_M \quad (\text{B.55})$$

$$= \Gamma_L (\mathbf{A}_M \mathbf{X} + \mathbf{Z}_{\text{eff},M}^c) \quad (\text{B.56})$$

where $\Gamma_L = P \mathbf{A}_M^T (P \mathbf{A}_M \mathbf{A}_M^T + \sum_M)^{-1}$. The resulting LMMSE error covariance matrix is given as

$$\mathbf{K}_{\text{ee}} = \left(P^{-1} \mathbf{I}_M + \mathbf{A}_M^T \sum_M^{-1} \mathbf{A}_M \right)^{-1} \quad (\text{B.57})$$

which leads to the following unique Cholesky decomposition, $\mathbf{K}_{\text{ee}} = P (\mathbf{G}\mathbf{G}^T)^{-1}$, where

$$\mathbf{G}\mathbf{G}^T = \mathbf{I}_M + P \mathbf{A}_M^T \sum_M^{-1} \mathbf{A}_M \quad (\text{B.58})$$

and $\mathbf{G} = [\mathbf{g}_1, \dots, \mathbf{g}_M]$ is a lower triangular square matrix with strictly positive entries. The estimated symbols are distributed as

$$\hat{\mathbf{X}} = \mathbf{X} + \sqrt{P} \mathbf{G}^{-1} \mathbf{N}, \quad (\text{B.59})$$

where $\mathbf{N} = [\mathbf{n}_1, \dots, \mathbf{n}_L]^T$ is equivalent white noise with covariance $\frac{1}{n} E[\mathbf{N}\mathbf{N}^T] = \mathbf{I}_L$.

The lattice points $\{\mathbf{t}_l(\mathbf{w}_l)\}_{l \in \mathcal{L}}$ are decoded starting from $\mathbf{t}_1(\mathbf{w}_1)$. To estimate $\mathbf{t}_1(\mathbf{w}_1)$, the Rx obtains an estimate of \mathbf{x}_1 with the first column of Γ_L , $\hat{\mathbf{x}}_1 = \Gamma_L^{1,T} \hat{\mathbf{S}}_M$ and computes

$$\hat{\mathbf{t}}_1(\mathbf{w}_1) = \mathcal{Q}_{\Lambda_1} \left(\left[\Gamma_L^{1,T} \hat{\mathbf{S}}_M - \mathbf{d}_1 \right] \right) \text{ mod } \Lambda_s \quad (\text{B.60})$$

$$= \mathcal{Q}_{\Lambda_1} \left(\mathbf{t}_1(\mathbf{w}_1) + \sqrt{P} g_{11}^{-1} \mathbf{n}_1 \right) \text{ mod } \Lambda_s. \quad (\text{B.61})$$

The decoding is performed with error if the effective noise of LMMSE estimation leaves the fundamental Voronoi region \mathcal{V}_{Λ_1} . By using similar arguments proposed above, if $\sigma_{\Lambda_1}^2 > \sigma_{\text{eff},1}^{2,L} = \frac{1}{n} E \|\sqrt{P} g_{11}^{-1} \mathbf{n}_1\|^2 = \sqrt{P} g_{11}^{-1}$, the probability of error decreases exponentially in n , that is, if

$$R_1 < \frac{1}{2} \log \frac{P}{\sigma_{\text{eff},1}^{2,L}} \quad (\text{B.62})$$

$$= \frac{1}{2} \log g_{11}^2. \quad (\text{B.63})$$

Given that $\mathbf{t}_1(\mathbf{w}_1)$ is successfully decoded the Rx estimates \mathbf{n}_1 almost surely. Then, the Rx discards \mathbf{n}_1 and recovers $\mathbf{t}_2(\mathbf{w}_2)$ similarly to $\mathbf{t}_1(\mathbf{w}_1)$:

$$\hat{\mathbf{t}}_2(\mathbf{w}_2) = \mathcal{Q}_{\Lambda_2} \left(\left[\Gamma_L^2 \hat{\mathbf{S}}_M - g_{12}^{-1} \hat{\mathbf{n}}_1 + \mathbf{d}_2 \right] \right) \bmod \Lambda_s \quad (\text{B.64})$$

$$= \mathcal{Q}_{\Lambda_2} \left(\mathbf{t}_2(\mathbf{w}_2) + \sqrt{P} g_{22}^{-1} \mathbf{n}_2 \right) \bmod \Lambda_s. \quad (\text{B.65})$$

By iterating this process, the effective noise of LMMSE is obtained as $\sigma_{\text{eff},l}^{2,L} = \frac{1}{n} E \|\sqrt{P} g_{ll}^{-1} \mathbf{n}_1\|^2 = \sqrt{P} g_{ll}^{-1}$, therefore as long as

$$\begin{aligned} R_l &< \frac{1}{2} \log \frac{P}{\sigma_{\text{eff},l}^{2,L}} \\ &= \frac{1}{2} \log g_{ll}^2 \end{aligned} \quad (\text{B.66})$$

is satisfied, each $\mathbf{t}_l(\mathbf{w}_l)$ can be decoded successfully. After $\{\mathbf{t}_l(\mathbf{w}_l)\}_{l \in \mathcal{L}}$ is decoded, the messages $\{\mathbf{w}_l\}_{l \in \mathcal{L}}$ are recovered by $\mathbf{w}_l = \phi_l^{-1}(\mathbf{t}_l)$.

By Lemma B.1, (B.36) and (B.66), we can state the following lemma:

Lemma B.2. [5, Theorem 1] For a set of integer valued vectors $\mathbf{A}_M = [\mathbf{a}_1, \dots, \mathbf{a}_M]^T$, not necessarily full rank, the rate tuple $\{R_l\}_{l \in \mathcal{L}}$ is achievable so long as

$$R_l < \min \left\{ \min_{m: a_{ml} \neq 0} \frac{1}{2} \log^+ \left(\frac{P}{\mathbf{a}_m^T (P^{-1} \mathbf{I}_L + \mathbf{h}_m \mathbf{h}_m^T)^{-1} \mathbf{a}_m} \right), \frac{1}{2} \log g_{ll}^2 \right\}. \quad (\text{B.67})$$

such that g_{ll} are diagonal terms of the unique lower triangular matrix G determined by

$$\mathbf{G}\mathbf{G}^T = \mathbf{I}_M + P \mathbf{A}_M^T \sum_M^{-1} \mathbf{A}_M \quad (\text{B.68})$$

with $\sum_M = \text{diag}[\sigma_1^2, \dots, \sigma_M^2]$ and

$$\sigma_m^2 = \frac{\mathbf{a}_m^T \left(P^{-1} \cdot \mathbf{I}_m + \mathbf{A}_{m-1}^T \sum_{m-1}^{-1} \mathbf{A}_{m-1} \right)^{-1} \mathbf{a}_m}{2^{2C_m} - 1}, \quad (\text{B.69})$$

where $\sum_m = \text{diag}[\sigma_1^2, \dots, \sigma_m^2]$ and $\mathbf{A}_m = [\mathbf{a}_1, \dots, \mathbf{a}_m]^T$.

Appendix C

C.1 Appendix for Chapter 4

In the following, for Gaussian inputs generated independently and satisfying power constraint P , we will prove that I_h -clustering outperforms WSC on the average sum-rate by showing that the ergodic sum-rate capacity of I_h -clustering is upper bounded by a higher value than WSCs capacity.

Let $X^u = (X_1, \dots, X_u)$ and $Y^u = (Y_1, \dots, Y_u)$ denote vectors of random variables indexed from 1 to u . For given channel realizations $\{\mathbf{h}_u\}_{u \in \mathcal{N}^c}$, the single letter characterization of the sum-rate capacity of I_h -clustering is given as:

$$R_{I_h} = I(X^9; Y^9) \quad (\text{C.1})$$

$$= h(Y^9) - h(Y^9|X^9) \quad (\text{C.2})$$

$$= h(Y^9) - \sum_{u=1}^9 h(Y_u|X^9, Y^{u-1}) \quad (\text{C.3})$$

$$\leq h(Y^9) - \sum_{u=1}^9 h(Y_u|X^9) \quad (\text{C.4})$$

$$\leq \sum_{u=1}^9 h(Y_u) - h(Y_u|X^9) \quad (\text{C.5})$$

The ergodic sum-rate of I_h -clustering is given as:

$$R_{I_h}^{\text{erg}} = E_{\{\mathbf{H}_u\}_{u \in \mathcal{N}^c}} [I(X^9; Y^9)] \quad (\text{C.6})$$

$$\leq E_{\{\mathbf{H}_u\}_{u \in \mathcal{N}^c}} \left[\sum_{u=1}^9 h(Y_u) \right] - E_{\{\mathbf{H}_u\}_{u \in \mathcal{N}^c}} \left[\sum_{u=1}^9 h(Y_u|X^9) \right] \quad (\text{C.7})$$

$$= C - \sum_{u=1}^9 E_{\mathbf{H}_u} [h(Y_u|X^9)] \quad (\text{C.8})$$

$$= C - \frac{5}{2} \log(1 + 2P) - \log(1 + P), \quad (\text{C.9})$$

where $C = E_{\{\mathbf{H}_u\}_{u \in \mathcal{N}^c}} \left[\sum_{u=1}^9 h(Y_u) \right]$ is a constant. The result comes by applying inverse

Jensen's inequality [19, Chapter 2] to the terms $\{E_{\mathbf{H}_u}[h(Y_u|X^9)]\}_{u \in \mathcal{N}^c}$ and, then applying Chi-square expectation.

By similar arguments, the ergodic sum-rate of WSC is obtained as

$$R_{\text{WS}}^{\text{erg}} \leq C - \frac{3}{2} \log(1 + 2P) - 3 \log(1 + P). \quad (\text{C.10})$$

One can easily show that the right hand side of Eq. (C.9) is greater than right hand side of Eq. (C.10) for $P > 0$.

Bibliography

- [1] “C-ran the road towards green ran,” China Mobile Research Institute, Beijing, China, Tech. Rep., October 2011. Cited page 8
 - [2] 3GPP-TR-36.814, “Further advancement for e-utra physical layer aspects,” Release 9, v. 9.0, Tech. Rep., March 2010. Cited page 8
 - [3] 3GPP-TR-36.932, “Scenarios and requirements for small cell enhancements for e-utra and e-utran (release 12),” December 2012. Cited page 1
 - [4] M. Agiwal, A. Roy, and N. Saxena, “Next generation 5g wireless networks: A comprehensive survey,” **IEEE Communications Surveys Tutorials**, vol. 18, no. 3, pp. 1617–1655, thirdquarter 2016. Cited page 4
 - [5] I. E. Aguerri and A. Zaidi, “Lossy compression for compute-and-forward in limited backhaul uplink multicell processing,” **IEEE Transactions on Communications**, vol. 64, no. 12, pp. 5227–5238, Dec 2016. Cited pages 3, 10, 71, 78, 84, 86, and 110
 - [6] E. Aktas, J. Evans, and S. Hanly, “Distributed decoding in a cellular multiple-access channel,” **IEEE Transactions on Wireless Communications**, vol. 7, no. 1, pp. 241–250, Jan 2008. Cited page 2
 - [7] H. Al-Raweshidy and S. Komaki, **Radio over Fiber Technologies**. Artech House. Cited page 8
 - [8] H. Al-Shatri and A. Klein, “Hierarchical beamforming for downlink fog ran,” in **2017 International Symposium on Wireless Communication Systems (ISWCS)**, Aug 2017, pp. 199–204. Cited page 1
 - [9] G. C. Alexandropoulos, P. Ferrand, J. Gorce, and C. B. Papadias, “Advanced coordinated beamforming for the downlink of future lte cellular networks,” **IEEE Communications Magazine**, vol. 54, no. 7, pp. 54–60, July 2016. Cited page 1
 - [10] E. Atsan, R. Knopp, S. Diggavi, and C. Fragouli, “Towards integrating quantize-map-forward relaying into LTE,” in **Proc. 2012 IEEE Inform. Theory Workshop (ITW)**, Sep. 2012, pp. 212–216. Cited page 2
 - [11] M. N. Bacha, J. S. Evans, and S. Hanly., “On the capacity of mimo cellular networks with macro-diversity,” in **Proc. Australian Communication Theory Workshop**, Australia, February 2006, pp. 105–109. Cited pages 2 and 3
 - [12] S. I. Bross, A. Lapidoth, and M. A. Wigger, “The gaussian mac with conferencing encoders,” in **2008 IEEE International Symposium on Information Theory**, July 2008, pp. 2702–2706. Cited page 2
-

-
- [13] V. R. Cadambe and S. A. Jafar, "Interference alignment and degrees of freedom of the k -user interference channel," **IEEE Transactions on Information Theory**, vol. 54, no. 8, pp. 3425–3441, Aug 2008. Cited page 2
- [14] A. Checko, H. L. Christiansen, Y. Yan, L. Scolari, G. Kardaras, M. S. Berger, and L. Dittmann, "Cloud ran for mobile networks? a technology overview," **IEEE Communications Surveys Tutorials**, vol. 17, no. 1, pp. 405–426, Firstquarter 2015. Cited pages 7 and 8
- [15] J. Chen, U. Mitra, and D. Gesbert, "Optimal UAV relay placement for single user capacity maximization over terrain with obstacles," in **Proc. 2019 IEEE 20th International Workshop on Signal Processing Advances in Wireless Communications (SPAWC)**, July 2019, pp. 1–5. Cited page 2
- [16] J. H. Conway and N. J. A. Sloane, **Sphere-packings, lattices, and groups**. New York, NY, USA: Springer. Cited page 103
- [17] M. Costa, "Writing on dirty paper (corresp.)," **IEEE Transactions on Information Theory**, vol. 29, no. 3, pp. 439–441, May 1983. Cited page 2
- [18] T. Cover and A. E. Gamal, "Capacity theorems for the relay channel," **IEEE Transactions on Information Theory**, vol. 25, no. 5, pp. 572–584, Sep. 1979. Cited pages 2 and 3
- [19] T. M. Cover and J. A. Thomas, **Elements of information theory**. Wiley-Interscience, 2006. Cited page 112
- [20] O. Dhif-Allah, H. Dahrouj, T. Y. Al-Naffouri, and M. Alouini, "Distributed robust power minimization for the downlink of multi-cloud radio access networks," **IEEE Transactions on Green Communications and Networking**, vol. 2, no. 2, pp. 327–335, June 2018. Cited page 4
- [21] U. Erez and R. Zamir, "Achieving $1/2 \log(1+\text{snr})$ on the awgn channel with lattice encoding and decoding," **IEEE Transactions on Information Theory**, vol. 50, no. 10, pp. 2293–2314, Oct 2004. Cited pages 104 and 107
- [22] U. Erez, S. Litsyn, and R. Zamir, "Lattices which are good for (almost) everything," **IEEE Transactions on Information Theory**, vol. 51, no. 10, pp. 3401–3416, Oct 2005. Cited pages 101 and 103
- [23] C. Feng, D. Silva, and F. R. Kschischang, "An algebraic approach to physical-layer network coding," **IEEE Transactions on Information Theory**, vol. 59, no. 11, pp. 7576–7596, Nov 2013. Cited page 3
- [24] G. Foschini and M. Gans, "On limits of wireless communications in a fading environment when using multiple antennas," **Wireless Personal Communications**, vol. 6, no. 3, pp. 311–335, Mar 1998. [Online]. Available: <https://doi.org/10.1023/A:1008889222784> Cited pages 6 and 7
- [25] D. Gesbert, S. Hanly, H. Huang, S. Shamai Shitz, O. Simeone, and W. Yu, "Multi-cell mimo cooperative networks: A new look at interference," **IEEE Journal on Selected Areas in Communications**, vol. 28, no. 9, pp. 1380–1408, December 2010. Cited pages 1 and 2
- [26] K. Gomadam, V. R. Cadambe, and S. A. Jafar, "A distributed numerical approach to interference alignment and applications to wireless interference networks," **IEEE Transactions on Information Theory**, vol. 57, no. 6, pp. 3309–3322, June 2011. Cited page 2
-

-
- [27] S. V. Hanly and P. Whiting, "Information-theoretic capacity of multi-receiver networks," **Telecommunication Systems**, vol. 1, no. 1, pp. 1–42, Dec 1993. [Online]. Available: <https://doi.org/10.1007/BF02136153> Cited page 2
- [28] S. Hong and G. Caire, "Compute-and-forward strategies for cooperative distributed antenna systems," **IEEE Transactions on Information Theory**, vol. 59, no. 9, pp. 5227–5243, Sep. 2013. Cited page 3
- [29] G. Katz, B. M. Zaidel, and S. Shamai (Shitz), "On layered transmission in clustered cooperative cellular architectures," in **Proc. 2013 IEEE Int. Symp. Inf. Theory (ISIT'13)**, Istanbul, Turkey, Jul. 7–12, 2013, pp. 1162–1166. Cited pages 2, 13, and 43
- [30] M. N. Khormuji and E. G. Larsson, "Improving collaborative transmit diversity by using constellation rearrangement," in **Proc. 2007 IEEE Wireless Communications and Networking Conference**, March 2007, pp. 803–807. Cited page 2
- [31] S.-J. Kim, S. Jain, and G. B. Giannakis, "Backhaul-constrained multi-cell cooperation using compressive sensing and spectral clustering," in **Proc. 2012 SPAWC**, Cesme, Turkey, June 17–20 2012, pp. 65–69. Cited pages 2, 13, and 43
- [32] G. Kramer, "Outer bounds on the capacity of gaussian interference channels," **IEEE Transactions on Information Theory**, vol. 50, no. 3, pp. 581–586, March 2004. Cited page 25
- [33] G. Kramer, I. Marić, and R. D. Yates, "Cooperative communications," **Foundations and Trends® in Networking**, vol. 1, no. 3–4, pp. 271–425, 2007. [Online]. Available: <http://dx.doi.org/10.1561/1300000004> Cited page 2
- [34] J. N. Laneman, G. W. Wornell, and D. N. C. Tse, "An efficient protocol for realizing cooperative diversity in wireless networks," in **Proc. 2001 IEEE International Symposium on Information Theory (IEEE Cat. No.01CH37252)**, June 2001, pp. 294–. Cited page 2
- [35] A. Lapidoth, **A Foundation in Digital Communication**, 2nd ed. Cambridge University Press, 2017. Cited page 6
- [36] A. Lapidoth, N. Levy, S. Shamai, and M. A. Wigger, "Cognitive wyner networks with clustered decoding," **IEEE Transactions on Information Theory**, vol. 60, pp. 6342–6367, October 2014. Cited page 25
- [37] N. Levy and S. Shamai, "Clustered local decoding for wyner-type cellular models," **IEEE Transactions on Information Theory**, vol. 55, no. 11, pp. 4967–4985, November 2009. Cited pages 2 and 3
- [38] Lizhong Zheng and D. N. C. Tse, "Diversity and multiplexing: a fundamental tradeoff in multiple-antenna channels," **IEEE Transactions on Information Theory**, vol. 49, no. 5, pp. 1073–1096, May 2003. Cited page 7
- [39] H. . Loeliger, "Averaging bounds for lattices and linear codes," **IEEE Transactions on Information Theory**, vol. 43, no. 6, pp. 1767–1773, Nov 1997. Cited pages 101 and 103
- [40] M. A. Maddah-Ali, A. S. Motahari, and A. K. Khandani, "Communication over mimo x channels: Interference alignment, decomposition, and performance analysis," **IEEE Transactions on Information Theory**, vol. 54, no. 8, pp. 3457–3470, Aug 2008. Cited page 2
- [41] A. F. Molisch, **Wireless Communications**. New York, NY, USA: Wiley. Cited pages 4 and 44
-

-
- [42] A. S. Motahari, S. Oveis-Gharan, M. Maddah-Ali, and A. K. Khandani, "Real interference alignment: Exploiting the potential of single antenna systems," **IEEE Transactions on Information Theory**, vol. 60, no. 8, pp. 4799–4810, Aug 2014. Cited page 2
- [43] R. Narasimhan, "Finite-snr diversity-multiplexing tradeoff for correlated rayleigh and rician mimo channels," **IEEE Transactions on Information Theory**, vol. 52, no. 9, pp. 3965–3979, September 2006. Cited pages 7 and 64
- [44] B. Nazer, "Two-sample testing can be as hard as structure learning in ising models: Minimax lower bounds," in **Int. Zurich Seminar Commun. (IZS)**, March 2012, pp. 103–106. Cited pages 77 and 107
- [45] B. Nazer and M. Gastpar, "Compute-and-forward: Harnessing interference through structured codes," **IEEE Transactions on Information Theory**, vol. 57, no. 10, pp. 6463–6486, Oct 2011. Cited pages 103, 105, 106, and 109
- [46] B. Nazer and M. Gastpar, "Compute-and-forward: Harnessing interference with structured codes," in **2008 IEEE International Symposium on Information Theory**, Jul. 2008, pp. 772–776. Cited pages 2, 3, 71, 74, 76, 103, and 105
- [47] B. Nazer, A. Sanderovich, M. Gastpar, and S. Shamai, "Structured superposition for backhaul constrained cellular uplink," in **2009 IEEE International Symposium on Information Theory**, June 2009, pp. 1530–1534. Cited page 3
- [48] B. Nazer, M. Gastpar, S. A. Jafar, and S. Vishwanath, "Ergodic interference alignment," **IEEE Transactions on Information Theory**, vol. 58, no. 10, pp. 6355–6371, Oct 2012. Cited page 2
- [49] S. Park, O. Simeone, O. Sahin, and S. Shamai, "Inter-cluster design of precoding and fronthaul compression for cloud radio access networks," **IEEE Wireless Communications Letters**, vol. 3, no. 4, pp. 369–372, Aug 2014. Cited page 4
- [50] S. W. Peters and R. W. Heath, "Cooperative algorithms for mimo interference channels," **IEEE Transactions on Vehicular Technology**, vol. 60, no. 1, pp. 206–218, Jan 2011. Cited page 2
- [51] D. M. Pozar, **Microwave and RF Design of Wireless Systems**. John Wiley and Sons. Cited page 8
- [52] T. Rappaport, S. Sun, R. Mayzus, H. Zhao, Y. Azar, K. Wang, G. Wong, J. Schulz, M. Samimi, and F. Gutierrez, "Millimeter wave mobile communications for 5g cellular: It will work!" **IEEE Access**, vol. 1, pp. 335–349, 2013. Cited page 8
- [53] M. Razaviyayn, G. Lyubeznik, and Z. Luo, "On the degrees of freedom achievable through interference alignment in a mimo interference channel," **IEEE Transactions on Signal Processing**, vol. 60, no. 2, pp. 812–821, Feb 2012. Cited page 2
- [54] I. T. S. Sesia and M. Baker, **LTE The UMTS Long Term Evolution: From Theory to Practice**. New York, NY, USA: Wiley. Cited pages 4, 44, and 73
- [55] A. Sanderovich, S. Shamai, Y. Steinberg, and G. Kramer, "Communication via decentralized processing," **IEEE Transactions on Information Theory**, vol. 54, no. 7, pp. 3008–3023, July 2008. Cited page 2
- [56] A. Sanderovich, S. Shamai, and Y. Steinberg, "Distributed mimo receiver: Achievable rates and upper bounds," **IEEE Transactions on Information Theory**, vol. 55, no. 10, pp. 4419–4438, Oct 2009. Cited page 2
-

-
- [57] A. Sanderovich, O. Somekh, H. V. Poor, and S. Shamai, "Uplink macro diversity of limited backhaul cellular network," **IEEE Transactions on Information Theory**, vol. 55, no. 8, pp. 3457–3478, Aug 2009. Cited page 2
- [58] A. Sanderovich, O. Somekh, H. V. Poor, and S. S. (Shitz), "Uplink macro diversity of limited backhaul cellular network," **IEEE Transactions on Information Theory**, vol. 55, no. 8, pp. 3457–3478, August 2009. Cited page 2
- [59] H. Sato, "The capacity of the gaussian interference channel under strong interference (corresp.)," **IEEE Transactions on Information Theory**, vol. 27, no. 6, pp. 786–788, November 1981. Cited page 25
- [60] A. Sendonaris, E. Erkip, and B. Aazhang, "User cooperation diversity. part i. system description," **IEEE Transactions on Communications**, vol. 51, no. 11, pp. 1927–1938, Nov 2003. Cited page 2
- [61] —, "User cooperation diversity. part ii. implementation aspects and performance analysis," **IEEE Transactions on Communications**, vol. 51, no. 11, pp. 1939–1948, Nov 2003. Cited page 2
- [62] S. Shamai and B. M. Zaidel, "Enhancing the cellular downlink capacity via co-processing at the transmitting end," in **IEEE VTS 53rd Vehicular Technology Conference, Spring 2001. Proceedings (Cat. No.01CH37202)**, vol. 3, May 2001, pp. 1745–1749 vol.3. Cited page 2
- [63] O. Simeone, H. V. P. O. Somekh, and S. S. (Shitz), "Local base station cooperation via finite-capacity links for the uplink of linear cellular networks," **IEEE Transactions on Information Theory**, vol. 55, no. 1, pp. 190–204, January 2009. Cited pages 2 and 3
- [64] O. Simeone, O. Somekh, H. V. Poor, and S. Shamai (Shitz), "Downlink multicell processing with limited-backhaul capacity," **EURASIP Journal on Advances in Signal Processing**, vol. 2009, no. 1, p. 840814, Jun 2009. [Online]. Available: <https://doi.org/10.1155/2009/840814> Cited page 2
- [65] O. Simeone, N. Levy, A. Sanderovich, O. Somekh, B. M. Zaidel, H. V. Poor, and S. Shamai (Shitz), "Cooperative wireless cellular systems: An information-theoretic view," **Foundations and Trends in Communications and Information Theory**, Now Publishers Inc., Hanover MA, vol. 8, no. 1–2, pp. 1–177, 2012. Cited page 2
- [66] G. Sridharan and W. Yu, "Degrees of freedom of mimo cellular networks: Decomposition and linear beamforming design," **IEEE Transactions on Information Theory**, vol. 61, no. 6, pp. 3339–3364, June 2015. Cited page 2
- [67] I. E. Telatar, "Capacity of multi-antenna gaussian channels," **EUROPEAN TRANSACTIONS ON TELECOMMUNICATIONS**, vol. 10, pp. 585–595, 1999. Cited pages 7, 52, and 97
- [68] V. Tralli, R. Veronesi, and M. Zorzi, "Power-shaped advanced resource assignment (psara) for fixed broadband wireless access systems," **IEEE Transactions on Wireless Communications**, vol. 3, no. 6, pp. 2207–2220, Nov 2004. Cited page 1
- [69] D. Tse and P. Viswanath, **Fundamentals of Wireless Communication**. Cambridge, UK: Cambridge University Press. Cited page 6
- [70] L. Venturino, N. Prasad, and X. Wang, "Coordinated scheduling and power allocation in downlink multicell ofdma networks," **IEEE Transactions on Vehicular Technology**, vol. 58, no. 6, pp. 2835–2848, July 2009. Cited page 1
-

-
- [71] M. Wigger, R. Timo, and S. Shamai (Shitz), “Conferencing in Wyner’s asymmetric interference network: Effect of number of rounds,” **IEEE Transactions on Information Theory**, vol. 63, Mar. 2017. Cited pages 2, 3, and 25
- [72] M. A. Wigger and G. Kramer, “Three-user mimo macs with cooperation,” in **2009 IEEE Information Theory Workshop on Networking and Information Theory**, June 2009, pp. 221–225. Cited page 2
- [73] F. Willems, “The discrete memoryless multiple access channel with partially cooperating encoders (corresp.),” **IEEE Transactions on Information Theory**, vol. 29, no. 3, pp. 441–445, May 1983. Cited page 2
- [74] A. Wyner and J. Ziv, “The rate-distortion function for source coding with side information at the decoder,” **IEEE Transactions on Information Theory**, vol. 22, no. 1, pp. 1–10, January 1976. Cited page 3
- [75] —, “The rate-distortion function for source coding with side information at the decoder,” **IEEE Transactions on Information Theory**, vol. 22, no. 1, pp. 1–10, January 1976. Cited page 77
- [76] A. D. Wyner, “Shannon-theoretic approach to a gaussian cellular multiple-access channel,” **IEEE Transactions on Information Theory**, vol. 40, no. 6, pp. 1713–1727, November 1994. Cited pages 2, 3, and 4
- [77] C. M. Yetis, T. Gou, S. A. Jafar, and A. H. Kayran, “On feasibility of interference alignment in mimo interference networks,” **IEEE Transactions on Signal Processing**, vol. 58, no. 9, pp. 4771–4782, Sep. 2010. Cited page 2
- [78] W. Yu, Taesoo Kwon, and Changyong Shin, “Joint scheduling and dynamic power spectrum optimization for wireless multicell networks,” in **2010 44th Annual Conference on Information Sciences and Systems (CISS)**, March 2010, pp. 1–6. Cited page 1
- [79] R. Zakhour and D. Gesbert, “Distributed multicell-miso precoding using the layered virtual sinr framework,” **IEEE Transactions on Wireless Communications**, vol. 9, no. 8, pp. 2444–2448, August 2010. Cited page 1
- [80] H. Zhang, L. Venturino, N. Prasad, P. Li, S. Rangarajan, and X. Wang, “Weighted sum-rate maximization in multi-cell networks via coordinated scheduling and discrete power control,” **IEEE Journal on Selected Areas in Communications**, vol. 29, no. 6, pp. 1214–1224, June 2011. Cited page 1
- [81] R. Zhang and S. Cui, “Cooperative interference management with miso beamforming,” **IEEE Transactions on Signal Processing**, vol. 58, no. 10, pp. 5450–5458, Oct 2010. Cited page 1
- [82] Y. Zhou, “Fronthaul-constrained uplink cloud radio-access networks: Capacity analysis and algorithm design,” Ph.D. dissertation, University of Toronto, 2016. Cited page 8
- [83] Y. Zhou and W. Yu, “Fronthaul compression and transmit beamforming optimization for multi-antenna uplink c-ran,” **IEEE Transactions on Signal Processing**, vol. 64, no. 16, pp. 4138–4151, Aug 2016. Cited page 87
-

Titre : Gestion des interférences dans les réseaux cellulaires hexagonaux sectoriels avec traitement multicellulaire local

Mots clés : Gestion des interférences, systèmes cellulaires sectoriels, réseaux cellulaires coopératifs, réseaux d'accès radio en nuage, calcul et transfert

Résumé : L'exigence de débit de données dans les communications sans fil due à l'emploi de smartphones, d'ordinateurs portables, de tablettes et de capteurs augmente considérablement. Cela pose directement des demandes extraordinaires sur de précieuses ressources spectrales. Pour satisfaire la saturation attendue sur les bandes actuellement utilisées, les systèmes de communication modernes permettent une réutilisation très fréquente des fréquences spatiales et évoluent vers des réseaux hétérogènes de stations de base (BS) couvrant des zones plus petites (petites cellules). De toute évidence, un tel système souffre des conditions d'interférence intercellulaires préjudiciables, en particulier aux bords des cellules. Par conséquent, il est clairement convaincant que la gestion des interférences est un goulot d'étranglement pour les réseaux sans fil actuels et futurs. Les schémas de traitement multicellulaire (MCP) ont été principalement utilisés pour fournir aux BS des versions quantifiées des signaux d'émission / réception d'autres BS via des liaisons de liaison (permettant le décodage en cluster. Il est alors possible que les données utilisateur soient traitées conjointement par plusieurs BS) à la fois en liaison montante et en liaison descendante, imitant ainsi les avantages du MIMO virtuel. Cependant, la mise en œuvre de MCP pour toutes les BS du réseau est assez difficile en pratique en raison de la grande complexité de calcul et des retards excessifs, même pour les grands réseaux modérés. Cependant, diviser le réseau en plusieurs clusters et les laisser coopérer au sein de chaque cluster plutôt que sur l'ensemble du réseau apporte également certains avantages du

MCP en ne nécessitant que les signaux reçus locaux et le CSI local. Nous appelons ce cadre MCP local, ce qui améliore également la robustesse du réseau aux échecs de connexion et l'évolutivité. Dans cette thèse, nous avons étudié les avantages de MCP local dans la gestion des interférences pour modèle de réseau hexagonal sectorisé sous trois scénarios différents. Dans le premier, nous avons supposé que le BS peut coopérer par le biais de liaisons à capacité limitée pour un nombre donné de cycles de coopération. Nous avons proposé un nouveau schéma de regroupement pratique qui adapte la façon dont les BS coopèrent à la sectorisation des cellules. Plus haut et plus bas et limites supérieures des degrés de liberté par utilisateur (DoF) en fonction de la coopération de nombres et la capacité de raccordement a été dérivée et une analyse SNR finie a été effectuée. Dans le deuxième scénario, nous supposé un système cellulaire multi-cloud, où chaque processeur central (CP) a une puissance de traitement limitée. UNE un schéma de clustering a été proposé qui adapte l'association entre BS et CP à la sectorisation. Limite inférieure du DoF par utilisateur en fonction de la capacité de liaison, de la capacité de CP et du rapport du nombre de Le CP en nombre de BS a été dérivé. Dans le dernier scénario, nous avons supposé à nouveau un cellulaire basé sur plusieurs nuages et appliqué des systèmes de calcul et de transfert (CoF) et de CoF quantifiés au clustering proposé. Pour CoF quantifié, nous avons proposé une méthode pour réduire le nombre de codes de réseau imbriqués pour réduire la mise en œuvre complexité tout en conservant une dégradation raisonnable des performances.

Title : Interference Management in Sectorized Hexagonal Cellular Networks with Local Multi-Cell Processing

Keywords : Interference Management, Sectorized Cellular Systems, Cooperative Cellular Networks, Cloud Radio Access Networks, Compute-and-Forward

Abstract : The data rate requirement in wireless communication due to employment of smartphones, laptops, tablets and sensors is increasing drastically. This directly poses extra-ordinary demands on precious spectral resources. To satisfy with the expected saturation on the currently used bands, modern communication systems are allowing very aggressive spatial frequency reuse and moving towards heterogeneous networks of base stations (BS) covering smaller areas (small cells). Evidently, such systems suffer from the detrimental inter-cell interference conditions, particularly at cell edges. Therefore, it is clearly convincing that interference management is a bottleneck for current and future wireless networks. Multi-cell processing (MCP) schemes have mostly been used to provide BSs with quantized versions of the transmit/receive signals of other BSs via backhaul/fronthaul links (allowing for clustered decoding). It is then possible for user data to be jointly processed by several BSs at both uplink and downlink, hence imitating the benefits of virtual MIMO. However, the implementation of MCP for all the BSs of the network is quite challenging in practice due to large computational complexity and excessive delays even for moderately large networks. However, dividing the network into several clusters and letting them to cooperate within each cluster rather than the entire network also brings some benefit of MCP by requiring only local received signals and local CSI. We name this framework as local MCP,

which also improves the robustness of the network to connection failures and scalability. In this thesis, we have investigated the benefits of local MCP in interference management for sectorized hexagonal network model under three different scenarios. In the first one, we assumed that the BS can cooperate through limited capacity links for a given number of cooperation rounds. We proposed a new practical clustering scheme that adapts the way BSs cooperate to cells sectorization. Upper and lower bounds on the per-user degrees-of-freedom (DoF) as a function of number of cooperation rounds and backhaul capacity have been derived, and finite SNR analysis has been done. In the second scenario, we assumed a multi-cloud cellular system, where each central processor (CP) has a limited processing power. A clustering scheme has been proposed that adapts the association between BSs and CPs to the sectorization. Lower bound on the per-user DoF as a function of fronthaul capacity, CP capacity and the ratio of number of CP to number of BS has been derived. In the last scenario, we assumed again a multi-cloud based cellular system, and applied compute-and-forward (CoF) and Quantized CoF schemes to the proposed clustering. For Quantized CoF, we proposed a method for reducing the number of nested lattice codes to lower the implementation complexity while keeping reasonable performance degradation.